HYBRID MATERIALS FROM COVALENT ORGANIC FRAMEWORKS AND IONIC LIQUIDS

Miss Ranida Maliyaem

จุฬาลงกรณ์มหาวิทยาลัย
CHULALONGKORN UNIVERSITY

A Thesis Submitted in Partial Fulfillment of the Requirements
for the Degree of Master of Science in Chemistry
Department of Chemistry
Faculty of Science
Chulalongkorn University
Academic Year 2018
Copyright of Chulalongkorn University

วัสดุไฮบริดจากโครงข่ายอินทรีย์โคเวเลนต์และของเหลวไอออนิก

น.ส.รณิดา มะลิแย้ม

วิทยานิพนธ์นี้เป็นส่วนหนึ่งของการศึกษาตามหลักสูตรปริญญาวิทยาศาสตรมหาบัณฑิต
สาขาวิชาเคมี ภาควิชาเคมี
คณะวิทยาศาสตร์ จุฬาลงกรณ์มหาวิทยาลัย
ปีการศึกษา 2561
ลิขสิทธิ์ของจุฬาลงกรณ์มหาวิทยาลัย

Thesis Title   HYBRID MATERIALS FROM COVALENT
                      ORGANIC FRAMEWORKS AND IONIC LIQUIDS
By   Miss Ranida Maliyaem
Field of Study   Chemistry
Thesis Advisor   Professor THAWATCHAI TUNTULANI, Ph.D.
Co Advisor   Junjuda Unruangsri, Ph.D.

        Accepted by the Faculty of Science, Chulalongkorn University in Partial
Fulfillment of the Requirement for the Master of Science

                                          Dean of the Faculty of Science
            (Professor POLKIT SANGVANICH, Ph.D.)

THESIS COMMITTEE
                                          Chairman
            (Associate Professor Vudhichai Parasuk, Ph.D.)
                                          Advisor
            (Professor THAWATCHAI TUNTULANI, Ph.D.)
                                          Co-Advisor
            (Junjuda Unruangsri, Ph.D.)
                                          Examiner
            (Numpon Insin, Ph.D.)
                                          External Examiner
            (Gamolwan Tumcharern, Ph.D.)

จุฬาลงกรณ์มหาวิทยาลัย

CHULALONGKORN UNIVERSITY

รณิดา มะลิแย้ม : วัสดุไฮบริดจากโครงข่ายอินทรีย์โคเวเลนต์และของเหลวไอออนิก. (HYBRID MATERIALS FROM COVALENT ORGANIC FRAMEWORKS AND IONIC LIQUIDS) อ.ที่ปรึกษาหลัก : ศ. ดร.ธวัชชัย ตันฑุลานิ, อ.ที่ปรึกษาร่วม : ดร.จัญจุดา อุ่นเรืองศรี

โครงข่ายอินทรีย์โคเวเลนต์ (COFs) เป็นวัสดุรูพรุนชนิดหนึ่งที่มีสมบัติโดดเด่น เช่น พื้นที่ผิวสูง, ความหนาแน่นต่ำ, มีความเสถียรสูงและสามารถออกแบบได้ ปัจจุบันมีการออกแบบและพัฒนาวัสดุรูพรุนชนิดนี้ให้มีความหลากหลายและตอบสนองต่อการใช้งานมากยิ่งขึ้น ในงานวิจัยนี้ผู้วิจัยจึงมีความประสงค์ที่จะนำเอาวัสดุโครงข่ายอินทรีย์โคเวเลนต์นี้มาพัฒนาเป็นวัสดุไฮบริดชนิดใหม่ระหว่างโครงข่ายอินทรีย์โคเวเลนต์และของเหลวไอออนิก (ionic liquids) เพื่อใช้สำหรับเป็นตัวเร่งปฏิกิริยาในปฏิกิริยา cycloaddition สำหรับก๊าซคาร์บอนไดออกไซด์และสารอีพอกไซด์ โดยจะเริ่มจากการสังเคราะห์วัสดุโครงข่ายอินทรีย์โคเวเลนต์ที่มีชื่อว่า COF-5 ผ่านปฏิกิริยาควบแน่นระหว่าง hexahydroxyltriphenylene และ phenyldiboronic acid ด้วยการให้ความร้อนที่ 90 องศาเซลเซียส เป็นเวลา 24 ชั่วโมง สารผลิตภัณฑ์ที่ได้รับจะถูกวิเคราะห์ด้วยเทคนิคต่างๆ เช่น PXRD, FT-IR, TGA และ BET เป็นต้น จากผลการวิเคราะห์พบว่าวัสดุ COF-5 มีลักษณะรูพรุนเป็นแบบท่อยาวตรงใน 1 มิติ ซึ่งเกิดจากการซ้อนทับกันของแผ่น 2 มิติจำนวนมากผ่านแรงกระทำแบบ π-π stacking โดยสามารถให้ค่าพื้นที่ผิวสูงถึง 1700 $m^2 g^{-1}$ จากนั้นนำวัสดุรูพรุนนี้มาใส่ด้วยโมเลกุลของของเหลวไอออนิกที่มีชื่อว่า 1-vinyl-3-ethylimidazolium bromide (VEIM[Br]) และ 1-vinyl-3-ethylimidazolium bis(trifluoromethanesulfonyl)imide (VEIM[NTf$_2$]) ผ่านกระบวนการลดความดัน (vacuum infiltration method) โดยเปรียบเทียบความสามารถในการใส่ของเหลวไอออนิกเข้าสู่วัสดุรูพรุนด้วยการใช้วัสดุรูพรุนต่างชนิดได้แก่ SBA-15 และ imine-1 ซึ่งผลจากการวิเคราะห์วัสดุไฮบริดที่มีชื่อว่า VEIM[Br]@COF-5 พบว่า พื้นที่ผิวของวัสดุชนิดนี้มีค่าเท่ากับ 170 $m^2 g^{-1}$ ซึ่งลดลงอย่างเห็นได้ชัดเมื่อเทียบกับวัสดุตั้งต้น ประกอบกับผลที่ได้จาก PXRD และ TGA แสดงให้เห็นว่ามีปริมาณของของเหลวไอออนิก VEIM[Br] อยู่ภายในวัสดุรูพรุน COF-5 ประมาณ 20 %โดยน้ำหนัก ซึ่งการอยู่ร่วมกันระหว่างวัสดุสองชนิดนี้ไม่ก่อให้เกิดความเสียหายของโครงสร้างของวัสดุทั้งสองชนิด และจากการศึกษาการพอลิเมอไรเซชันของ VEIM[Br] ขณะบรรจุอยู่ในวัสดุรูพรุน COF-5 ในสภาวะที่ไม่มีตัวทำละลาย ได้เป็น polyVEIM[Br]@COF-5 โดยผลการวิเคราะห์ผลิตภัณฑ์นี้พบว่า มีพื้นที่ผิวเพิ่มมากขึ้นกว่าตัวอย่าง VEIM[Br]@COF-5 ถึง 3 เท่า (518 $m^2 g^{-1}$) รวมไปถึงมีความเข้มของสัญญาณอัตลักษณ์เพิ่มมากขึ้นที่ 2θ = 3.5 องศา แสดงให้เห็นถึงความเป็นระเบียบของสายพอลิเมอร์ที่เรียงตัวตามแนวยาวของท่อ 1 มิติของวัสดุรูพรุนที่มากกว่าตัวอย่างที่ไม่ได้ทำพอลิเมอร์ไรซ์ นอกจากนี้ในงานวิจัยนี้ได้ศึกษาการนำเอาวัสดุไฮบริด VEIM[Br]@COF-5 มาใช้เป็นตัวเร่งปฏิกิริยาสำหรับปฏิกิริยาการเพิ่มโมเลกุลคาร์บอนไดออกไซด์ในโมเลกุลของโพลีนออกไซด์ ซึ่งผลจากเทคนิค ^{1}H-NMR พบว่าสามารถเร่งปฏิกิริยาการเกิดผลผลิตของไซคลิกคาร์บอเนตได้ร้อยละ 4 คิดเป็น Turnover number (TON) = 64 ภายใน 20 ชั่วโมงและ Turnover frequency (TOF) = 3.2 ต่อชั่วโมง

สาขาวิชา	เคมี	ลายมือชื่อนิสิต ....
ปีการศึกษา	2561	ลายมือชื่อ อ.ที่ปรึกษาหลัก ....
		ลายมือชื่อ อ.ที่ปรึกษาร่วม ....

5872029223 : MAJOR CHEMISTRY

Ranida Maliyaem : HYBRID MATERIALS FROM COVALENT ORGANIC FRAMEWORKS AND IONIC LIQUIDS. Advisor: Prof. THAWATCHAI TUNTULANI, Ph.D., Junjuda Unruangsri, Ph.D.

Covalent organic frameworks (COFs) are new type material, whereby their wide range of properties derived from the chemistry of frameworks and their regular porosity. Here in, we reported the successful syntheses of the novel hybrid materials between porous COF material and ionic liquids (ILs). The crystalline porous powder of boroxine-based COF, so called COF-5, is reproducible *via* a condensation reaction between hexahydroxyltriphenylene and phenyldiboronic acid under a mild condition using a conventional heating method. The as-synthesized COF-5 was characterized with PXRD, FT-IR, TGA and BET techniques, showing that the material contained 1D regular channels caused by π-π stacking of the gauze sheets with a surface area of 1700 m^2 g^{-1}. Ionic liquid, namely 1-vinyl-3-ethylimidazolium bromide (VEIM[Br]) and 1-vinyl-3-ethylimidazolium bis(trifluoromethanesulfonyl)imide (VEIM[NTf_2]), were infiltrated into the pores of COF-5 comparing with a silica porous material SBA-15 and imine-based COF, named imine-1, using a vacuum infiltration method. The BET analysis of VEIM[Br]@COF-5 shows a decrease in surface area of 170 m^2 g^{-1} along with the PXRD and TGA profile shows that 20 % of infiltrated IL are occupied in pore cavities without a disruption on the host structure. The *in-situ* polymerization of VEIM[Br] in porous material was carried out using thermal radical initiator in solvent-free condition under an inert atmosphere of nitrogen yielding a polyVEIM[Br]@COF-5. The BET surface area of 518 m^2 g^{-1} implies the higher ordered-alignment of polymer of VEIM[Br] along the 1D-channel of COF-5. Moreover, the new hybrid material, VEIM[Br]@COF-5 was attempted to use as a heterogeneous catalyst in a cycloaddition of CO_2 with propylene oxide. The result shows a turnover number (TON) of 64 within 20 hours and turnover frequency (TOF) of 3.2, which calculated from the measured conversions by ^{1}H-NMR technique. Even through, the hybrid material is not yet be a high effective catalyst, but it has shed some light on the further development of new hybrid materials.

Field of Study:	Chemistry	Student's Signature	....
Academic Year:	2018	Advisor's Signature	....
		Co-advisor's Signature	....

ACKNOWLEDGEMENTS

Ranida Maliyaem

TABLE OF CONTENTS

LIST OF FIGURES

Page

จุฬาลงกรณ์มหาวิทยาลัย

CHULALONGKORN UNIVERSITY

LIST OF TABLES

Page

จุฬาลงกรณ์มหาวิทยาลัย

CHULALONGKORN UNIVERSITY

CHAPTER 1

Introduction and literature reviews

Porous materials are outstanding materials used in catalysis, gas storage, separation and molecular sensor. They have a regular porosity possessing 0.2 to 0.95 of total volume of the materials.[1] They can be classified into 3 types in term of pore sizes: microporous materials with pore size smaller than 2 nm, mesoporous materials with pore size between 2-50 nm and macroporous materials with pore size larger than 50 nm.[2] In the past 20 years, several kinds of the porous materials have been developed such as zeolites,[3, 4] metal-organic frameworks (MOFs)[5] and covalent organic frameworks (COFs)[6] (Figure 1.1). Each type possesses unique nature and properties due to their compositional elements and types of bonding, for instance zeolites are microporous aluminosilicate minerals, which mainly compose of silicon, aluminum and oxygen atoms with $SiO_{4/2}$ or $AlO_{4/2}$ in tetrahedral structure.[4] Zeolites are typically found in both forms of crystal and amorphous with limited pore sizes ranging from 0.4 to 1.3 nm. However, due to their high thermal stability, zeolites have great potential as adsorbents, molecular sieves and also catalysts. Whilst, MOFs are typically high in crystallinity, but their stability depends on their structures.[1] MOFs are more structurally diverse than zeolite since their compositions, metal ions and organic ligands are varied. As some metal ions in MOFs structure are toxic and unfriendly to the environment, COFs are an interesting alternative materials, which have recently been developed.
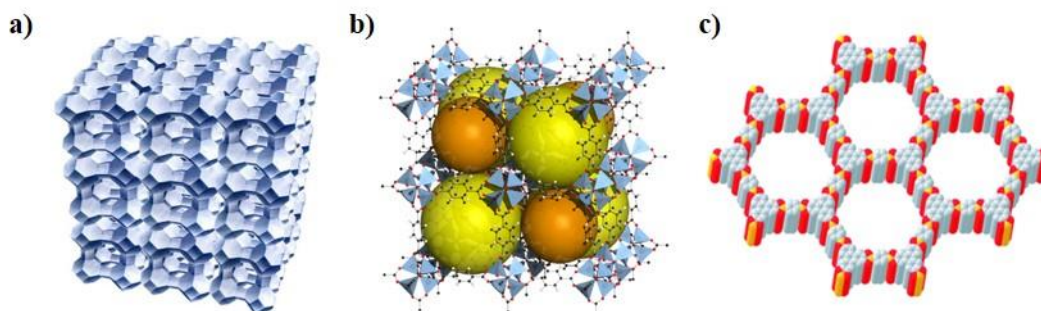
Figure 1.1 Examples of porous materials a) zeolite, b) metal organic frameworks (MOFs) and c) covalent organic frameworks (COFs).

1.1 Covalent organic frameworks (COFs)

Over the past 10 years, covalent organic frameworks (COFs) have been an emerging field of studies since Yaghi and co-workers successfully synthesized the first COF in 2005.[7] COFs are constructed *via* strong covalent bonds between rigid organic building block units which consist of light elements namely carbon, hydrogen, nitrogen, oxygen, boron, sulfur, and *etc.* Owning to the light components in COFs, the materials are less dense compared to the MOFs, zeolites or coordination polymers. Moreover, a variety of structural and component designs, and environmental friendliness are the superior features of COFs over the others. In fact, COFs material can be considered as organic zeolites with their potent properties, such as high surface area, thermal and chemical stability and tunability, as well as designable chemical structures. Therefore, COF materials are applied in extensive fields, for example, gas storage,[8] catalyst,[9-11] adsorbent and sensor for heavy metals,[12] separators[13] and electronic applications.[14]

To design the structural and porosity of COF materials, the suitable organic building units should be selected based on their geometry and functionality. 2-dimesional COFs (2D-COFs) were constructed from 1D or 2D-building units forming single gauze layers stacked or assembled by interlayer non-covalent bond such as π-π interactions of conjugations in their structures. The stacking model of 2D-COFs provides remarkable characteristic – 1D channel, which is fundamental for this 2D-structural design. This is reflected through the article of Jiang *et al.* in 2009, whereby the polypyrene sheets containing extensive π-conjugations stacked to form PPy-COF, was reported. (Figure 1.2a, b) PPy-COF was synthesized from pyrenediboronic acid (PDBA) *via* a self-condensation reaction to give a pale-yellow solid. The eclipse of self-condensation layers was found leading to the generation of the internal channels in its structure, which can be confirmed using high resolution transmission electron microscopy (HRTEM) and X-ray powder diffraction (PXRD) techniques. PPy-COF showed a highly blue luminescent response at 484 nm under the fluorescence microscope which is higher than a monomer of PDBA emission (421 nm). This result indicates that the blue-shine is derived from an excimer of PDBA, through the pyrene close-packing *via* π-π interaction. Current-voltage profile of

electrical conductivity measurement indicated the switching on off properties of PPy-COF with a high current responding on and off upon the voltage applying many times resulting from a high molecular order of its structure. (Figure 1.2c) The interposed layers encourage the transportation and migration of exciton in the structure not only along the plane but also across the pile layers due to the single energy gap of a one component. Therefore, PPy-COF was examined by casting onto an aluminum electrode as a thin film prior to a conductivity measurement. The result showed a quick respond to photon movement and a large reversible on-off ratio of photocurrent generation, which could be developed into optoelectronic or photovoltaic devices.[15]
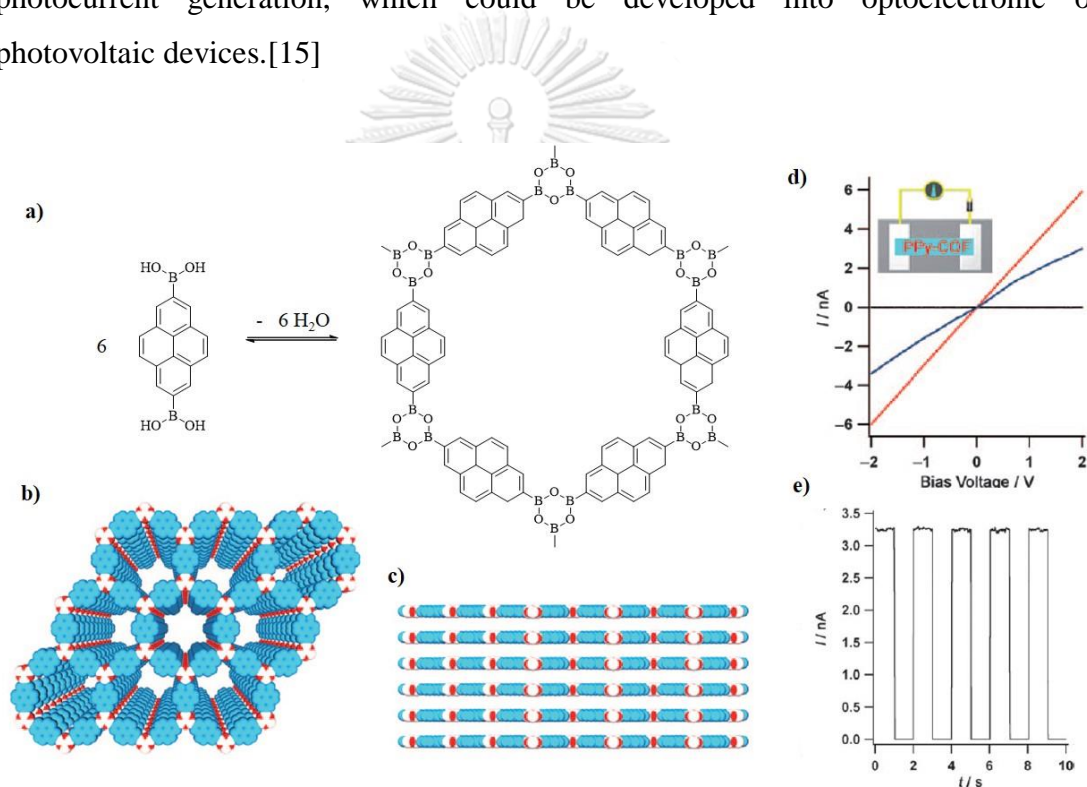
Figure 1.2 a) The condensation reaction of the PPy-COF synthesis, b) top-view and c) side-view of PPy-COF structure, d) I–V profile of PPy-COF between the Pt electrodes (black line: without PPy-COF; blue line: with PPy-COF; red line: with iodine-doped PPy-COF) and e) electric current upon the 2 V bias voltage was turned on or off.

However, aside from the 2D-COFs, 3-dimensional forms (3D-COFs) are also known, normally with extended skeleton network and ordered pores through 3D-building units, such as tetrahedral-structural building block units. Mostly, 3D-COFs are constructed *via* an expansion through a tetrahedral-skeleton unit combined with, triangular, square or tetrahedral fabric unit.[14] For instance, in 2007, Yaghi *et al.* reported the syntheses of the 3D-COF, namely COF-102, COF-103, COF-105 and COF-108 as shown in Figure 1.3. The COF-102 and COF-103 were synthesized *via* a self-condensation reaction of tetetrahedral-tetra(4-dihydroxyborylphenyl) methane (TBPM) and tetra(4-dihydroxyborylphenyl) silane (TBPS), respectively. Whilst, the co-condensation reaction was used in the cases of COF-105 and COF-108 by TBPM or TBPS with a triangular 2,3,6,7,10,11-hexahydroxytriphenylene (HHTP).[16]
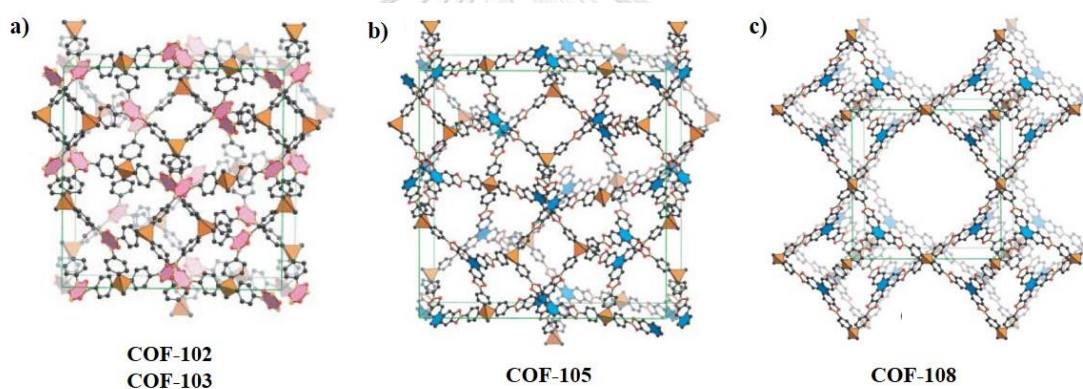
Figure 1.3 The graphical representation of atomic structures of the crystalline products of a) COF-102 and COF-103, b) COF-105 and c) COF-108. (gray: carbon, orange: boron, red: hydrogen. In the case of COF-103, the gray dots mean silicon atoms.)

Two years after the first publication, the successful syntheses of 3D-COFs were repeated by the same research group, whereby imine-based 3D-COF named COF-300 with a pore diameter of 7.2 Å was demonstrated. They were constructed *via* a solvothermolysis reaction of tetrahedral tetra(4-anilyl)methane and linear terephthaldehyde. COF-300 showed high porosity with a surface area of 1360 m^2 g^{-1} (Figure 1.4).[17]
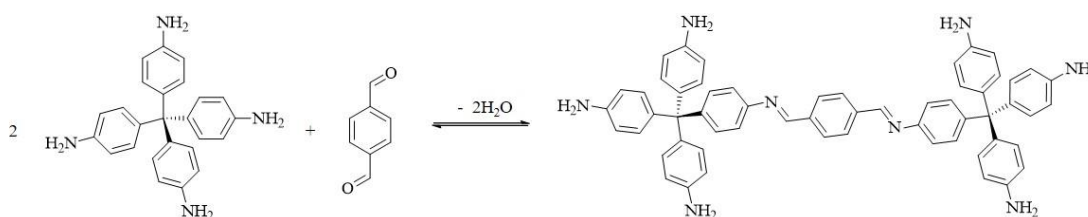
Figure 1.4 The condensation reaction of COF-300.

According to the observation in porous organic polymers, the strong covalent bonds mostly leads to the production of the distort ordered products. It is generally believed that the crystalline COF formation is produced *via* a reversible reaction as obtained in the zeolite syntheses.[18] Thus, this enables thermodynamically driven regularity found in COFs, which is a key to the structural design and synthesis. The examples of the successfully reactions of COF formation can be divided into three types based on the covalent linkages between building block units.[18] (Figure 1.5):

Boron-containing COFs: Boron-containing COFs are constructed though the formation of boronate anhydride linkages or boronate ester linkages. Boronate anhydrides are formed *via* a reversible self-condensation reaction of boronic acids whilst the boronate esters are created *via* a co-condensation reaction of boronic acids and catechols such as COF-1 and COF-5.[7]

Imine-based COFs: In general, imine-based COFs are synthesized *via* a Schiff base co-condensation reaction resulting in a C=N formation. Furthermore, precedent literature also shows hydrazone-linkages, which are formed *via* a co-condensation reaction of hydrazide and aldehyde unit such as COF-300 [17]and COF-LZU1.[19]

Triazine-based COFs: The triazine-based COFs are formed *via* a cyclotrimerization of nitrile units resulting in a triazine-ring formation, for example CTF-1 and CTF-2.[20]
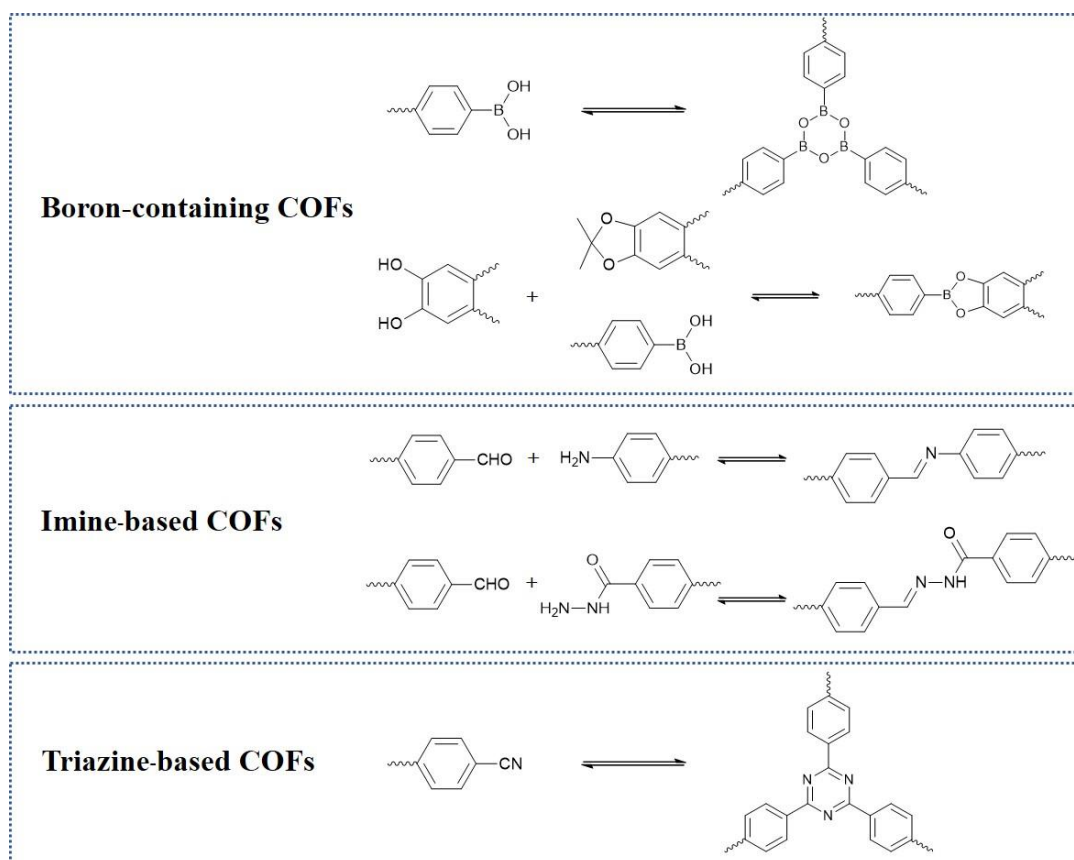
Figure 1.5 The examples of the successfully reactions of COFs formations.

Due to the difference in chemistry of the aforementioned linkages, each COF materials exhibits their own unique properties including their surplus advantages and some drawbacks. For example, boronate ester-based COFs usually illustrate high crystallinity, but exhibit some chemical and thermal instability as the structural sp^2 boron atoms contain vacant orbitals which provoke a nucleophile attack.[21] On the other hand, better chemical and thermal stability is provided in the case of imine-based COFs, nevertheless, their crystallinity is low.

The functionalization of COF structures is executed through a post synthesis and a bottom up approach.[18] For the post-synthesis approach, the COF skeleton is synthesized prior to an introduction of functional groups into the COF networks. This approach enables the control of the composition and density of the functional groups. For example, the subsequent modification of COF was successfully demonstrated by Jiang *et al.* in 2011. They used functionalized azide-adhered phenylene building block units to synthesize the COF skeleton, N_3-COF-5, since the tunability of quantity of

azide units on the walls was possible. Two-component system was used to construct a 100% of azide-uploaded on the wall, as 100% N_3-COF-5 (Figure 1.6), through the addition of a corner block (2,3,6,7,10,11-hexahydroxytriphenylene, HHTP) and an azide adhered phenylene unit (2,5-bis(azidomethyl)benzene-1,4-diboronic acid, N_3-BDBA) as a wall. Moreover, 5%, 25%, 50% and 75% N_3-COF-5 were also synthesized *via* a three-component system including a naked phenylene (BDBA). After the condensation reaction, the azide-adhered COF-5 products were converted to a triazole linkage *via* a quantitative click reaction of various alkyne groups. All the products of an alkyne-functionalization were affirmed using infrared spectroscopy (IR), X-ray diffraction (XRD), thermogravimetric analysis (TGA) and nitrogen sorption techniques.[22]
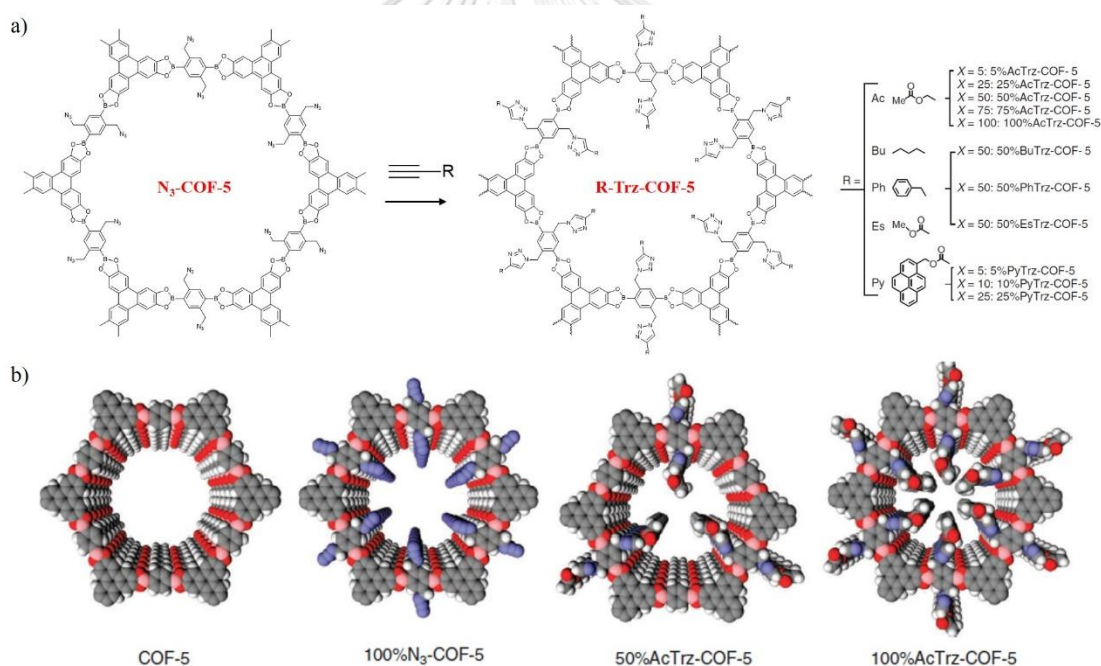
Figure 1.6 a) The post-modification of alkyne groups *via* a click reaction of N_3-COF-5 samples, b) the graphical representation of COF-5, 100%N_3-COF-5, 50%AcTrz-COF-5 and 100%AcTrz-COF-5.

Besides, Dichtel *et al.* reported the tandem truncation-functionalization strategy on 3D-COF named COF-12 in 2013. The COF-12-allyl were synthesized prior to the thiol-ene reaction of propanethiol to anchor the thiol groups within the COF-12 pores so called COF-12-SPr, which can be confirmed by ^{1}H-NMR, PXRD and nitrogen adsorption techniques. In the case of COF-12-SPr, ^{1}H-NMR showed no resonances at the chemical shifts of 3.41, 4.91 and 5.52 ppm corresponding to an allylic proton and the two vinylic protons, respectively and also showed the new resonances at the chemical shifts of 0.84, 1.42 and 2.38 ppm correlating to the thiopropyl chains. These results indicated the entirely modified allyl groups after the thiol-ene reaction. In addition, PXRD data of COF-12-SPr showed the peaks at 2θ of 7.9 (211), 9.2 (220), 12.1 (321), 13.0 (400), 14.5 (420), 15.2 (332), and 16.01 (422) degrees signifying the finger print pattern of COF-102. The slight broadening of the parent peak was observed indicating the lessening crystallinity which could be due to either the change of the components in the crystalline structure or the possible hydrolysis during the manipulation process.[23]
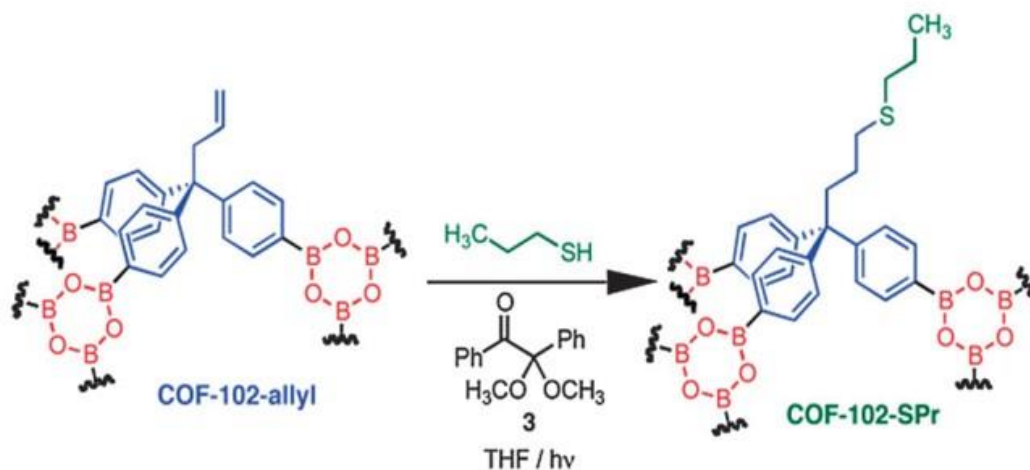
Figure 1.7 The thiol-ene reaction of COF-102-SPr.

In the case of a bottom-up approach, the functional group was placed on designed building block units ahead of a COF assembly process, which can improve a homogeneity of distribution of functional groups. In 2013, Jiang *et al*. revealed the designed triazine-based COF namely CS-COF, which was synthesized by the condensation reaction of triphenylene hexamine (TPHA) and tert butylpyrene tetraone (PT) under solvothermal condition. (Figure 1.8) The tert-butyl groups were anchored to pyrene rings prior to the COFs synthesis to control the distribution of tert-butyl groups on the network and also to increase the solubility of monomer in the reaction. In this work, CS-COF was found to be useful for a high on-off ratio photoswitches and photovoltaic cells due to the extended π conjugation in COF network which enabling electron delocalization in three dimensions.[24]
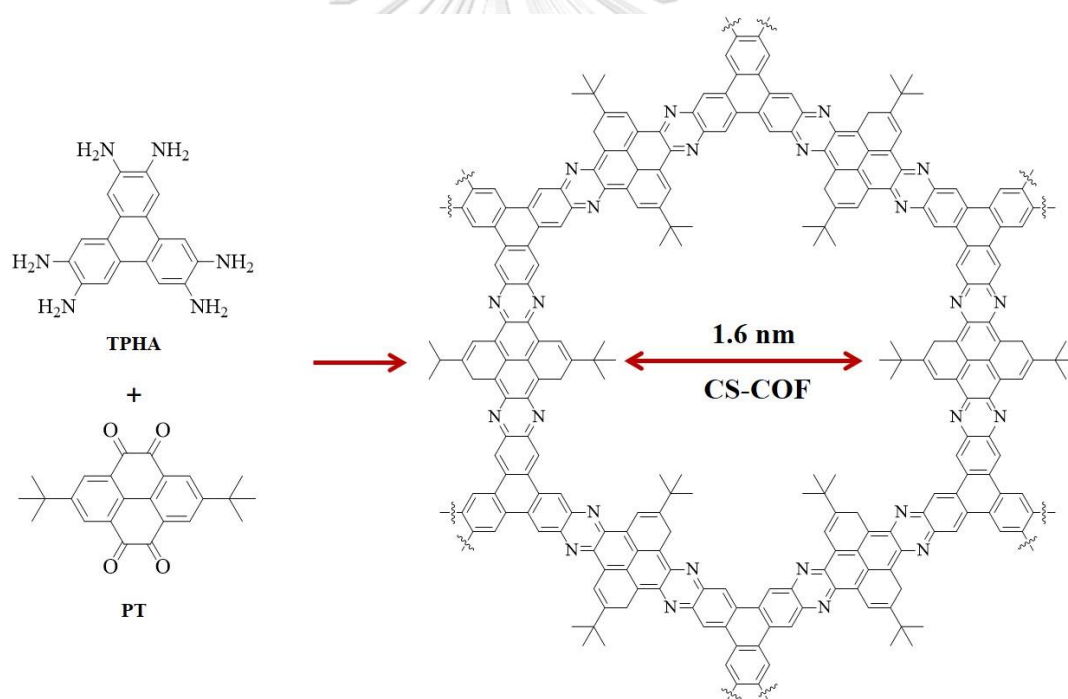
Figure 1.8 The condensation reaction of CS-COF.

In 2016, Wang *et al*. reported the extended π-conjugated hydrazone-linked COF framework, COF-LZU8, which was constructed from 2,5-Bis(3-(ethylthio)propoxy) terephthalohydrazide (an anchored thioether side chains to diethyl 2,5-dihydroxy terephthalate) and 1,3,5-trisformyl benzene under solvothermal conditions. (Figure 1.9) The rigid building block units were used as a fluorophore and the thioether side chain as an ionophore for metal ions. COF-LZU8 material exhibited the excellent selective sensing performance for Hg^{2+} in water through the noticeable change in fluorescent signals. Upon the addition of 33.3 µM of Hg^{2+}, the fluorescent signal was obviously quenched for 83 %, which was more efficiently than previous reports.[12]

Figure 1.9 a) The synthesis pathway of COF-LZU8 and b) the significant change in the fluorescent emission before (left) and after (right) the adsorption of Hg^{2+}.
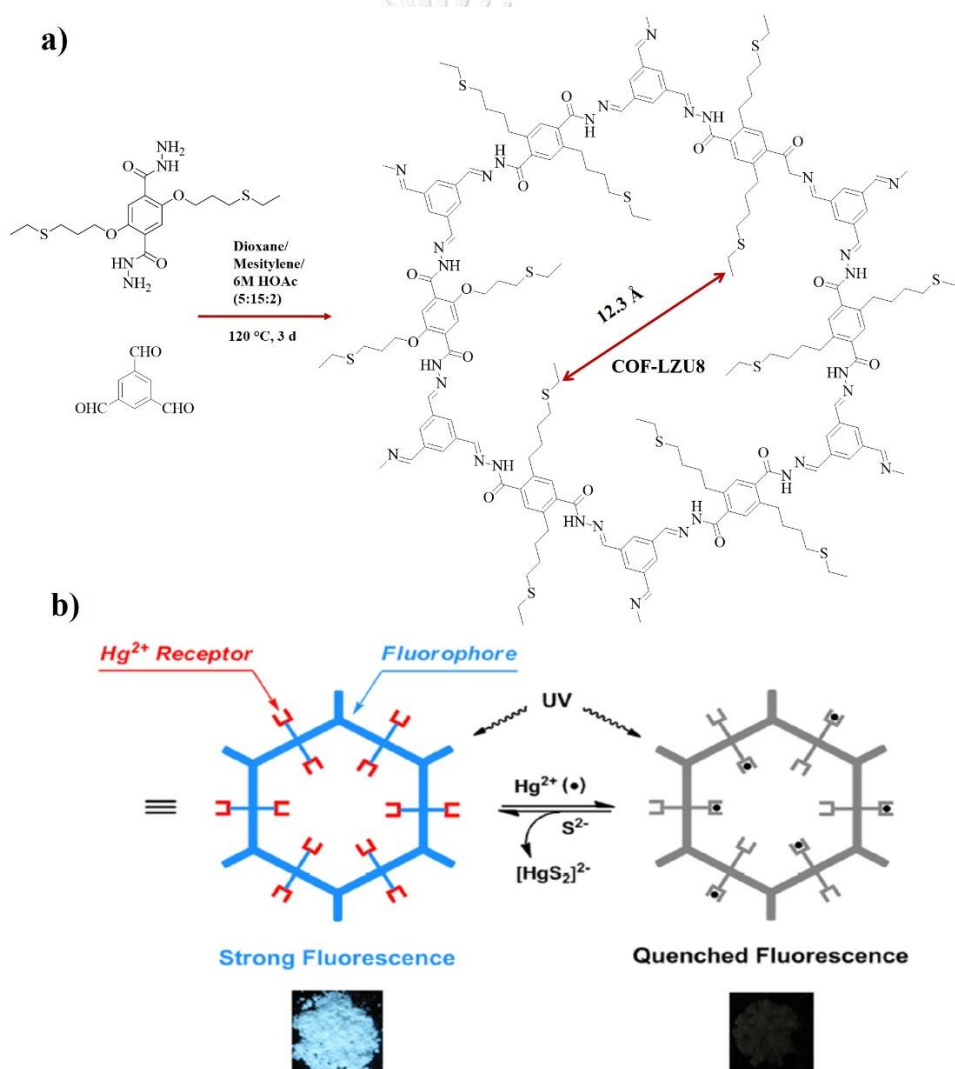
From previous literature reports, the desired properties of COF materials can be primarily obtained from the chemistry of their building units and linkages as well as the infiltration of the guest molecules enabling the specific properties for desired applications. Therefore, the applications of COF materials stem from two means: isolated structural and host-guest application. For isolated structural applications, the suitable properties of the materials derive from their structures as illustrated by the work of Wan *et al.* in 2008. The work illustrated the successful synthesis of COF material, termed TP-COF, which is a mesoporous material with hexagonal skeleton. TP-COF was constructed from triphenylene connected to pyrene through boronated linkages *via* a condensation reaction. TP-COF showed broad luminescent signal due to the energy transfer within their structure from triphenylene to pyrene moiety. Moreover, TP-COF also showed the semiconducting properties due to the presence of numerous π-conjugation in each COF sheets stacked through π-π interactions. The electron movement within the COF structure also affects the conductivity and the on off current switching signal.[25]
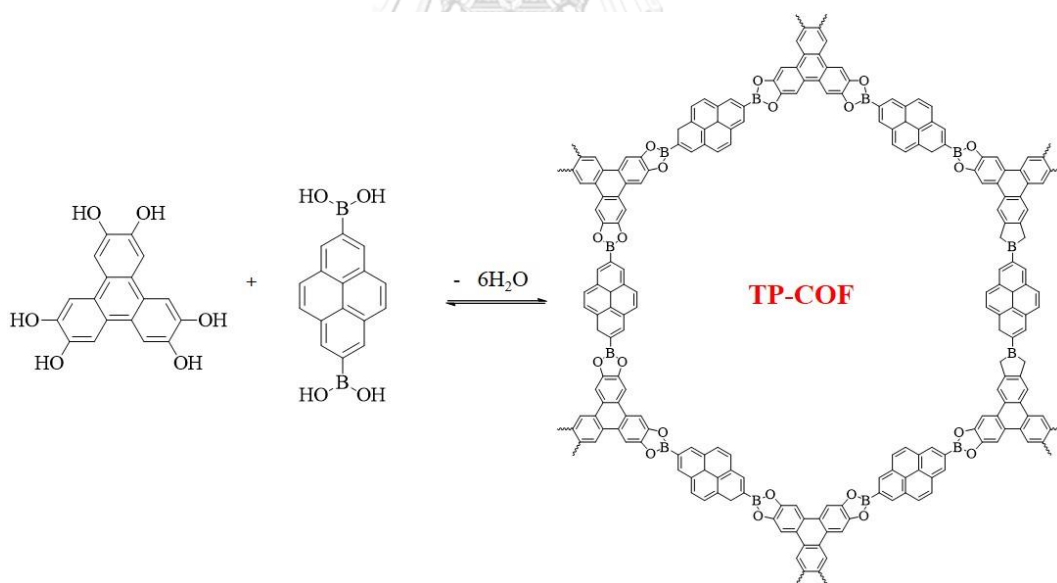
Figure 1.10 The condensation reaction of TP-COF.

The latter is a host-guest application, which the regular porosity of COF material is employed as a host for the incoming guests. The guest molecules can alter the properties of the whole COF materials shown in the work of Dogru *et al.* in 2013. The intercalation of a fullerene electron acceptor, [6,6]-phenyl-C_{61}-butyric acid methyl

ester (PCBM), into the COF named TT-COF was feasible. PCBM is well-known as an electron acceptor while the TT-COF structure itself can act as electron donor. Thus, when the material is stimulated by light, the electron from the TT-COF structure moves to the PCBM guest molecule. The potent finding was claimed to be a starting point for the development of efficient photovoltaic cells.[26]
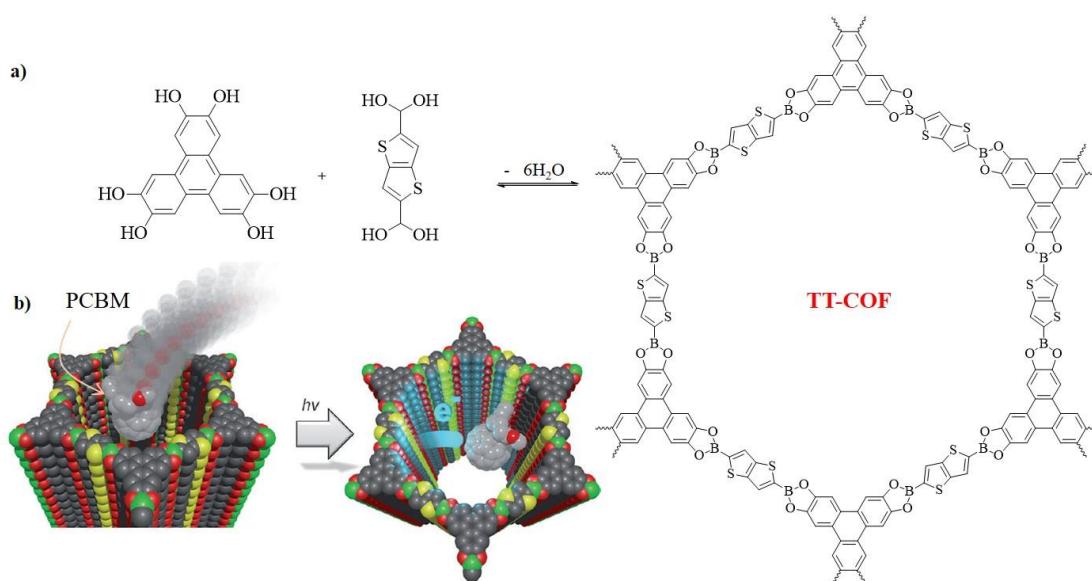
Figure 1.11 a) The synthesis pathway of TT-COF and b) graphical representation of the fullerene (PCBM) intercalation into a TT-COF channel. (C grey, O red, B green and S yellow).

In the term of catalysis properties of COF materials, triazine-based COF-JLU6 and COF-JLU8 were reported as catalysts in a cycloaddition of carbon dioxide (CO_2) to epoxide generating a cyclic carbonate. The characterization data of COF materials show that both of them are mesoporous materials with high crystallinity, high specific surface area, good thermal and chemical stability as well as containing a large number of hydroxy groups in the wall. The catalytic results showed that the COF-JLU7 is more effective than the analogue COF-JLU6 due to its ability of CO_2 adsorption capacity.
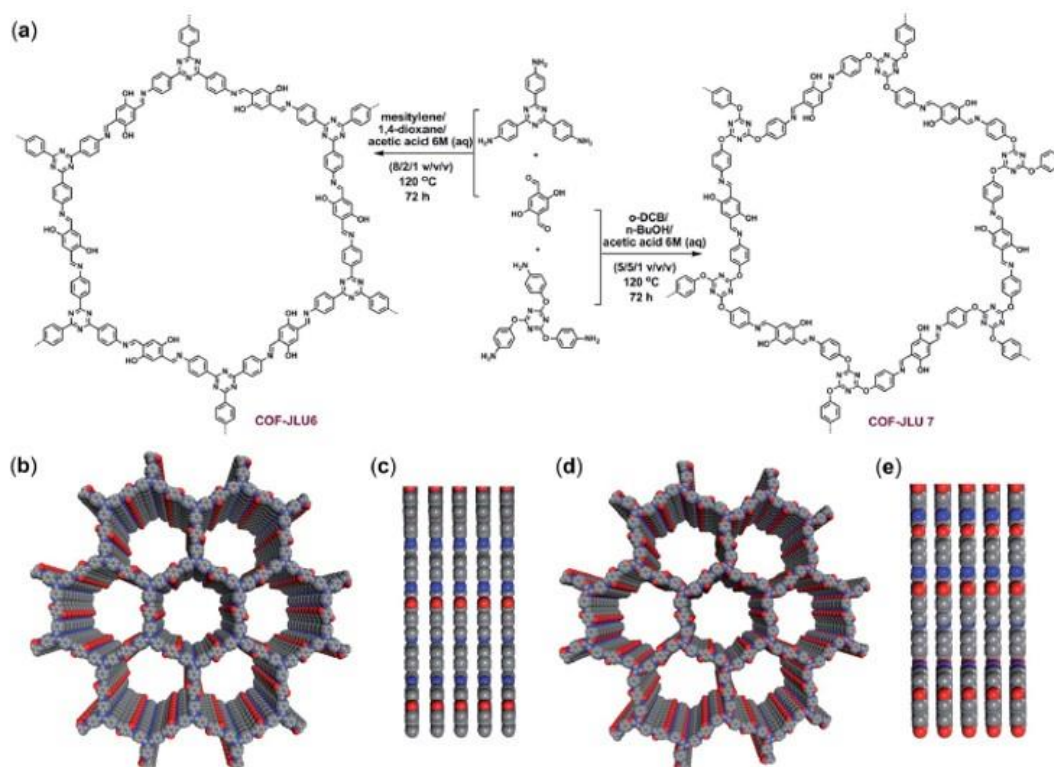
Figure 1.12 a) Schematic representation of the syntheses of COF-JLU6 and COF-JLU7 *via* Schiff-base condensation under solvothermal conditions, b) top view and c) side view of COF-JLU6, d) top view and e) side view of COF-JLU7 (red, oxygen; blue, nitrogen; gray, carbon).

Furthermore, the four different co-catalysts, tetra-*n*-butylammonium bromide (TBAB), tetra-*n*-butylammonium chloride (TBAC) and tetra-*n*-butylammonium iodide (TBAI), were employed. The order of co-catalyst activity is TBAI, TBAB and TBAC, described by the synergistic effects of nucleophilicity and leaving ability of anions. The COF-JLU7 catalyst can be recovered and reused for five times with the identical catalytic efficiency.[27]

1.2 Ionic liquids (ILs)

Ionic liquids (ILs) are room temperature molten organic salts which are mostly in liquid state at room temperature or the temperature lower than 100 °C. ILs generally consist of organic cations which are asymmetric and flexible with delocalized electrostatic charges (i.e., imidazolium, pyridinium, alkylammonium, guanidinium and pyrrolidinium) and organic or inorganic anions (i.e., halides, nitrate, acetate, tetrafluoroborate and hexafluorophosphate).[28] The characters of obtained ILs in the terms of chemical and physical properties such as state of IL under ambient conditions, hydrophobicity, solubility, conductive activity, *etc.*, are designable by pairing the different anions, cations and also alkyl substituted groups on the cations (Figure 1.13a).[29] A coulombic, hydrogen bonding and van der Waals interaction between cation and anion mainly determine the ILs behavior especially their ionicity, which affects the cohesive energy between the ions.[30] In 2010, Watanabe *et al.* reviewed the relationship between an ionic structures and physicochemical properties. They divided the salt combination into four groups (Figure 1.13b): a strongly Lewis-acidic cation and a strongly Lewis-basic anion (type I), a weakly Lewis-acidic cation and a strongly Lewis-basic anion (type II), a strongly Lewis-acidic cation and a weakly Lewis-basic anion (type III) and a weakly Lewis-acidic cation and a weakly Lewis-basic anion (type IV). They found that type I salts are of the ionic crystal forms, which are not typical ILs whilst the type II and III are still liquid at room temperature but their ionicity are quite lower than type IV. Moreover, type II and III salts showed poorer ionicity than type IV due to a degree of dissociation properties. The ionic dissociation of type IV is no need a strong coordination of solvent molecules around each ion, which are the typical polarity scale for the ILs reported to date, so called solvate ions.[31]
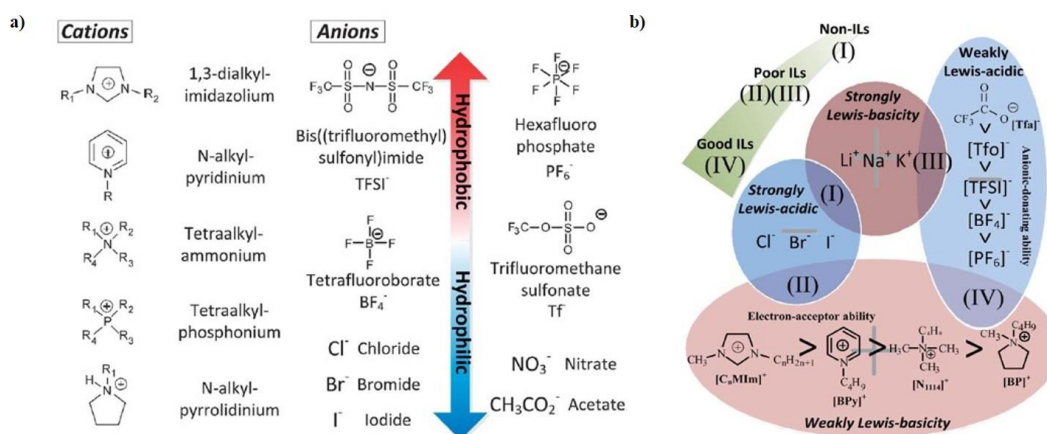
Figure 1.13 Examples of cations and anions used in the formation of ILs and b) various combinations of salts composed of cations and anions.

In general, ILs exhibit remarkable properties such as environmentally friendly, nonflammable, negligible vapor pressure, highly temperature and chemical stability and high ionic conductivity. ILs are good media with viscosity and density higher than some general solvents and are also reusable. Deriving from their properties, ILs are therefore the one of attractive materials used in many fields, such as an exchange media,[29, 32] catalysis[29] and electrical applications.[33-35] Attempt to use ILs as conducting materials was recently shown by Ven and coworker in 2013. The researchers report a composite membrane by doping a conductive filler ionic liquid named 1-H-3-methylimidazolium bis(trifluoromethanesulfonyl)imide ([h-min][NTf$_2$]) into the porous polymeric polybenzimidazole (PBI). The proton conductivity of 1.86 mS/cm was harvested at 190 °C, which are superior to the Nafion 117 at temperature above 90 °C. Even so the power density of 0.039 w cm^{-2} is obtained at 150 °C with H$_2$/O$_2$.[36]

Catalytic activity in the organic syntheses of ILs is the one of their major applications. For instance, Zhimin *et al.* reported the use of 1-alkyl-3-methyl imidazolium-based ionic liquids as a catalyst for the *N*-formylation reaction of an amine with a carbon dioxide and phenylsilane under a metal-free and mild condition. The formylamide products were obtained in high yields in the presence of ILs indicating the bifunctional catalytic behavior of ILs to activate the Si-H bond in the phenylsilane and to bind with a CO$_2$ molecule to form a formoxysilane intermediate. Meanwhile,

the cation simultaneously activates a substrate molecule *via* hydrogen bond making the insertion of CO_2 to the substrate more feasible to form the product. (Figure 1.14) These results indicate the excellent synergistic effect between cation and anion in ILs molecule.[37]
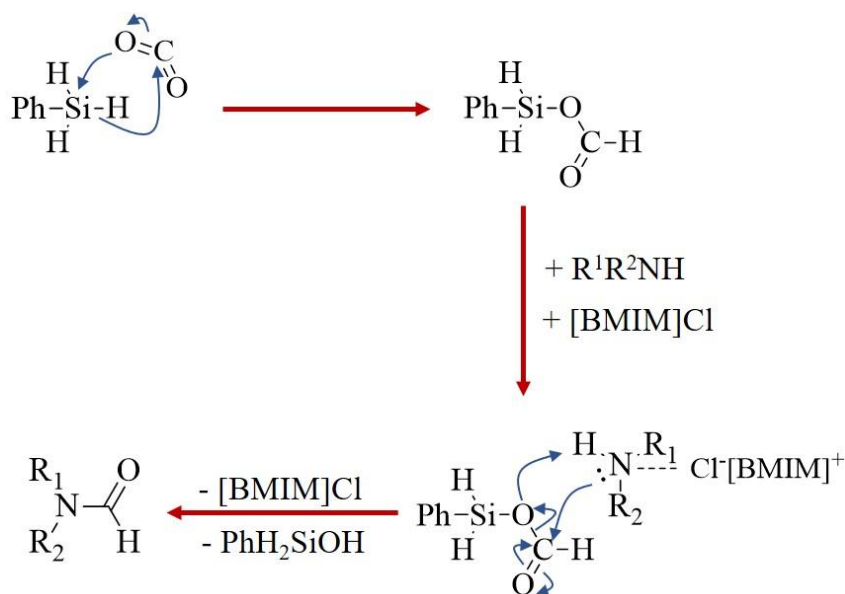
Figure 1.14 The schematic pathway of the possible reaction mechanism of the insertion of CO_2 to *N*-formylation.

Moreover, the polymeric ionic liquids (PILs) are commonly prepared *via* a free radical polymerization of vinyl functionalized ionic liquid molecules. In general, the free radical is generated from the activation of vinyl of solely monomeric IL molecule, so-called a homopolymerization. In some cases, copolymerization with vinyl benzene derivatives could be more facile than the homopolymerization.[38] It is generally known that the PILs do not only show the combination of the unique properties of component ILs in monomeric state but also demonstrate the new properties and function of synthesized PILs. The PILs are more stable, processable, durable and spatially control than the counterpart ILs, and mostly are in solid state.[38] PILs are attended in the various applications due to their tunable properties such as ionic conductors for energy storage, membranes, dispersants, gas sorbents and separators, carbon precursors and also catalysts.[38-40] In 2013, Paul *et al.* reported the heterogeneous catalysis of 1,3-bis(4-vinylbenzyl)imidazolium chloride

([bvbim]Cl) for the cycloaddition of carbon dioxide to epoxide derivatives. The monomeric ILs was polymerized using an initiator, 2,2'-azobisisobutyronitrile (AIBN). After the characterization, the ILs and PILs were examined the catalytic activity in the cycloaddition reaction using epichlorohydrin as an initially substrate to optimize the reaction condition. The results showed that both reactions catalyzed by [bvbim]Cl and poly[bvbim]Cl yielding higher than 98 % conversion at 5 MPa and 140 °C indicating the both of discrete and polymeric form are equally effective in catalytic activity at the mentioned condition. However, the PILs is higher stable, hydrophobic, and easier to handle and separate from the reaction than the ILs form.[41]

1.3 Integration of COFs and ILs

From the advantages of porous material especially COF materials and ILs as mentioned above, in the past few years, ILs has been applied with the porous materials in form of composite materials or so-called hybrid materials. In 2016, Tarnacka *et al*. reported the polymerization of monomeric of 1-butyl-3-vinyl imidazolium bis(trifluoromethanesulfonyl)imide ([bvim][NTf$_2$]) forming a polymer, poly[bvim][NTf$_2$], which were later intercalated into the pore of a nanoporous uniaxial alumina. The conductivity and charge transfer of the modified materials were analyzed. The results indicated that the conductivity and charge transfer of poly[bvimNTf$_2$] is higher and more effective than that of monomeric form and also better than the polymeric products obtained from the bulk solution method.[42] Moreover, the early work of COFs in host-guest application has shed some light on the recent work developed by Gao *et al.* in 2017. The successful intercalation of ionic liquids (ILs), namely 1-ethyl-3-methylimidazolium bis(trifluoromethyl sulfonyl) imide ([Emim][NTf$_2$]), inside the pores of a 3D COF-320, (Figure 1.15) was reported. The incorporated samples were prepared by mixing the COF-320 material with [Emim][NTf$_2$] using a physical grinding method with the ratio of the COF to ILs of 1:0.25, 1:1 and 1:2, denoted as 25%IL@COF-320, 100%IL@COF-320 and 200%IL@COF-320, respectively. The final products were obtained after subsequent heating the hybrid materials at 90 °C overnight. The desired products were analyzed using powder XRD, N$_2$ adsorption and desorption, IR, differential scanning

calorimetry (DSC) and solid-state ^{19}F-NMR techniques. The DSC curves indicated the solidified IL occupying inside the pores of COF-320. Furthermore, the 200%IL@COF-320 showed the signals of similar phase behavior to the bulk IL revealing the excess IL located outside the pores of COF materials. These materials were expected to be used in gas separation or catalysis reaction.[43]
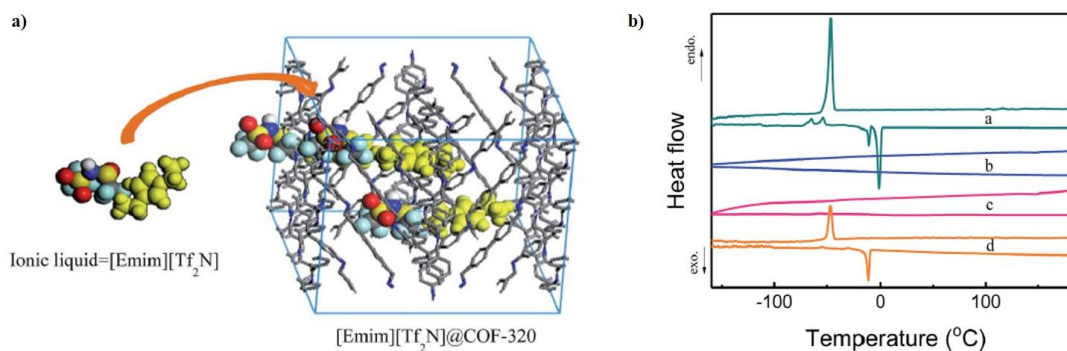
Figure 1.15 Graphical representation of 1-ethyl-3-methylimidazolium bis(tri fluoromethylsulfonyl)imide [Emim][NTf$_2$]) intercalation into the pores of COF-320 and b) the DSC curves of (a) bulk [Emim][NTf$_2$], (b) 25%IL@ COF-320, (c) 100%IL@COF-320 and (d) 200%IL@COF-320.

To extend the synergistic effect in the catalytic activity mentioned above, the hybrid materials between porous substrate and ILs were integrated to reinforce the effective catalysis in the organic syntheses. In 2016, the COF material named COF-TpBpy anchored with copper (II) ions on the walls were used as Lewis acid active sites encapsulating a polymer of IL named ethyldiphenyl (4-vinylphenyl)phosphonium bromide (PPS) to afford PPS⊂COF-TpBpy-Cu. (Figure 1.16a) The catalytic performance showed the great activity in the cycloaddition reaction of CO_2 to an epichlorohydrin yielding the epoxide product of 95 %, without side products. In comparison, COF-TpBpy-Cu and PPS gave the evidently lower yields (5 and 12 %yield, respectively) confirming the cooperative effect between the Cu ions as Lewis acid active sites and the halide anions of PPS as nucleophiles to feasibly promote the formation of epoxides as shown in the proposed mechanism. (Figure 1.16b) Furthermore, the catalyst still showed the highly efficient performance after ten recycles without any significant change in the product yields.[44]
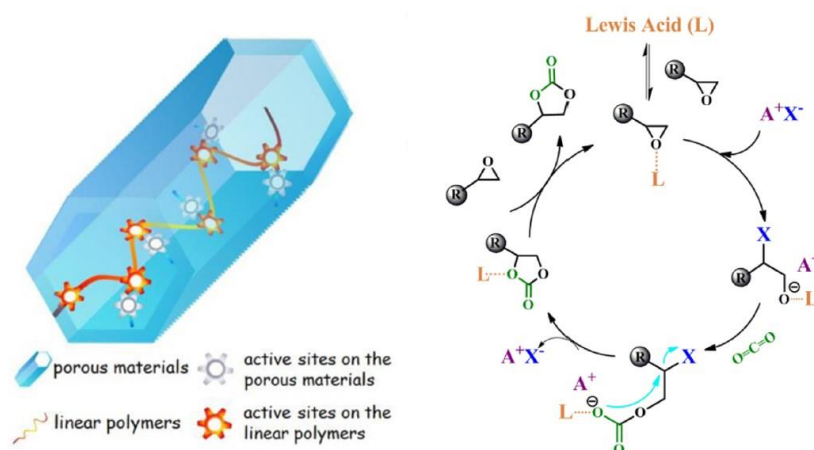
Figure 1.16 The graphical representation of the catalytic material and b) the scheme showed the proposed mechanism of CO_2 addition upon the presence of halide anions.

The other example is the use of a porous MOFs material named MIL-101 cooperating with the occupied PILs, 1-vinyl-3-ethylimidazolium bromide (VEIMBr), inside the pores, denoted as polyIL@MIL-101. (Figure 1.17) The results showed a great catalytic activity and recyclability upon the cycloaddition reaction of CO_2 to an epoxide under mild condition. The synergic effect is also demonstrated in this work, whereby Cr^{3+} ion in the hybrid materials acts as a Lewis acid, whilst Br^- anion of the intercalated PIL behaves as a Lewis base or a nucleophile. Therefore, their catalytic systems required no co-catalyst and a low-pressure CO_2 due to the presence of CO_2 absorbing PIL.[45]
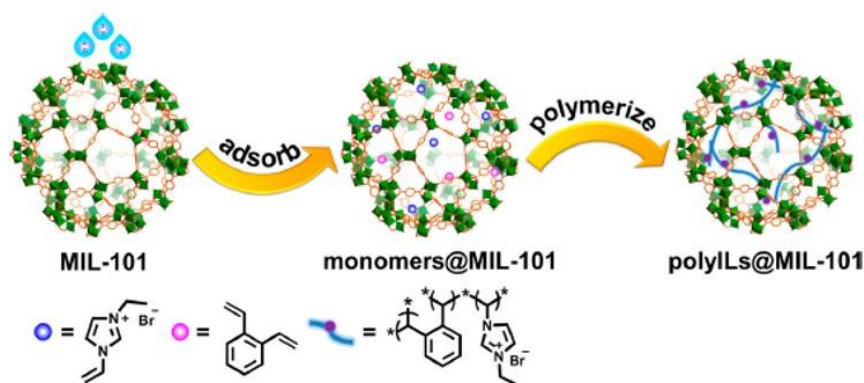
Figure 1.17 Graphical illustration of polyILs@MIL-101 preparation.

1.4 Objectives of this work
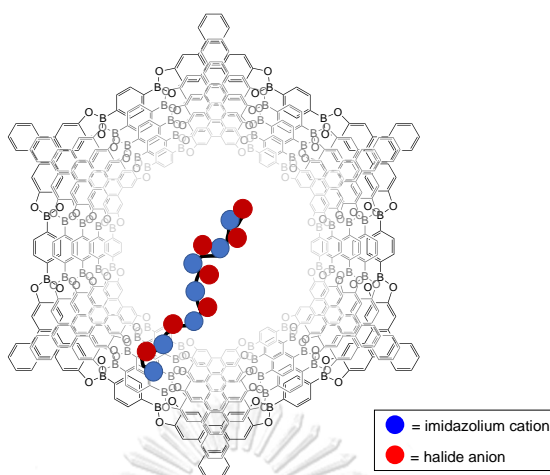
Figure 1.18 Illustration of poly(ionic liquid) infiltrated into borate-ester covalent organic framework.

Herein, we presume new nanoreactors integrating active ILs and PILs intercalated into defined pores of covalent organic frameworks (COFs) as catalysts for CO_2 conversion under mild conditions. (Figure 1.18) In this project, boronate ester-linkage COF is chosen as a host material as it possesses high surface acidic sites; 1,000 folds higher than SBA-15 and 10-50 times higher than MIL-101. The boronate ester COF offers high Lewis acid sites, whilst ionic liquids or poly(ionic liquids) concurrently act as Lewis bases. The intercalation imparts the close proximity of Lewis acids and bases, enhancing the cooperative effect, which is necessary to catalyze the formation of cyclic carbonates and formamides. This concept is rarely explored in literature.

CHAPTER 2

Experimental

2.1 Materials & Instruments

2.1.1 Materials

General manipulations were carried out using standard Schlenk line and glove box techniques under nitrogen atmosphere. Glasswares were dried at 110 °C and cooled under vacuum prior to use. Solvents were dried by stored over molecular sieves for 48 hours before using. All solvents and reagents were obtained from commercial sources (Sigma-Aldrich, TCI, Alfa Aesar and RCI labscan) and used as the received except in some stated procedures. SBA-15 was synthesized according to the previous literatures[46, 47] with an assistant of Dr. Wipark Anutrasakda, Chulalongkorn university using a triblock copolymer, $EO_{20}PO_{70}EO_{20}$ (Pluronic, P123, BASF) and tetraethyl orthosilicate (TEOS, 98 %, Acros). 2,2'-azobisisobutyronitrile (AIBN) was synthesized by Dr. Thanatorn Khotavivattana, Chulalongkorn university. The imine-1 materials received from Professor Dr. Jia Gao, Fudan university, Shanghai, China and stored in a glove box. COF-5[21, 48, 49], TFBP[50], NUS-15[51-53], CAT-B[54], VEIM[Br][55] and VEIM[NTf$_2$][56] were synthesized from the previous literatures with adaptations.

2.1.2 Instruments

Nuclear Magnetic Resonance (NMR): [1]H, ^{13}C, ^{19}F and ^{31}P spectra were recorded using a Bruker AV500 Fourier transform nuclear magnetic resonance spectrometer 500 MHz. and Bruker ultrashield plus (400 MHz.) at ambient temperature using residual deuterated solvent as an internal standard. The chemical shifts were reported in part per million (ppm) unit relative to a residual deuterated solvent as an internal standard. Mestrenova software (version 6.0) was used to process the spectra.

Solid Nuclear Magnetic Resonance (solid-state NMR): ^{13}C NMR resonances were provided using a Bruker Ascend™ 400WD model Fourier transform nuclear magnetic resonance spectrometer (400 MHz.) operating on a pulse technique called cross-polarization/total sideband suppression (CP/TOSS) progress at room

temperature to eliminate the sidebands of the spectrum. The chemical shifts were reported in part per million (ppm) unit and the raw data was manipulated using a Mestrenova software (version 6.0).

Powder X-ray Diffraction (PXRD): PXRD data were recorded on a Rigaku, Dmax 2200/utima$^+$ X-ray powder diffractometer by packing powder on 2x2 cm glass holder with continuous scanning range between $2\theta = 0.7$ to 35 degrees. A monochromator and Cu K_α radiation ($\lambda = 0.1543$ nm) were employed at 40 kV and 30 mA at room temperature.

Fourier-transform infrared spectroscopy (FT-IR): The spectra were collected on a Thermo, NICOLET iS5 infrared spectrometer with iD7 ATR probe operating on OMNIC 9 software (version 9.3.32). The ATR-FTIR mode was used in the range 400 to 4000 cm^{-1} at room temperature.

Surface area analysis: The pore size and surface area of samples were measured at 77 K (cooled with liquid nitrogen) using BEL Japan, inc., BELSORP mini-II nitrogen adsorptometer operating on BELSORP-mini adsorption/desorption data analysis (version 6.3.0.0). Before measurement, the samples were degassed under vacuum at 90 °C for 2 hours using a BELprep II mini vac instrument. The specific surface area was calculated using Brunauer-Emmett-Teller (BET) and t-plot theories.

Thermogravimetry analysis (TGA): The thermal properties of the obtained materials were investigated using a Perkin Elmer Pyris 1 TGA thermogravimetric analyzer with a Pyris software (version 9.0.1.0174). All of samples are operated under the same temperature program which hold on at 70 °C for 1 minute prior to heat from 70 °C to 950 °C with the rate of 20.00 °C/minute.

Elemental analysis (EA): The amount of an inserted IL in the porous material was analyzed using a THERMO (CHNS/O) elemental analyzer on THERMO FLASH 2000 model. The result of the percentages of the nitrogen atoms can be converted to the amount of IL molecules infiltrating in the pores.

Karl Fisher: Trace amounts of water in a solvent was determined by a Karl Fischer titration method on Mettler Toledo DL39 Karl Fisher coulometer model at room temperature.

2.2 Experimental procedure

2.2.1 The synthesis of Porous materials

2.2.1.1 COF-5

Procedure 1: In a glovebox, a schlenk tube was added 2,3,6,7,10,11-hexahydroxy triphenylene (HHTP, 112 mg, 0.35 mmol) and 1,4-phenylenediboronic acid (BDBA, 86 mg, 0.52 mmol). The reactants were added methanol (210 µL) and further added the mixture of 1,4-dioxane/mesitylene with the ratio of 4:1 (43 mL). The mixture was sonicated at room temperature for 10 minutes prior to filtration by 0.45 µm PTFE filters get rid of some insoluble reactants. The solution was heated at 90 °C under a nitrogen atmosphere for 20 hours. After which time, the gray solid was obtained and filtrated from the suspension. The crude product was briefly rinsed with chloroform and dried on a schlenk line (10^{-3} mbars) for 24 hours, giving the product as a gray power with 48 %yield (60.0 mg). The product was stored in glovebox under a nitrogen atmosphere. Solid NMR (400 MHz, ppm): **δ** 146.2 (B-O-$\underline{C}$Ar), 132.8 (-B-CAr-$\underline{C}$), 126.6 (-B-$\underline{C}$Ar), 123.3(Ar$\underline{C}$Ar), 102.7(Ar-$\underline{C}$-Ar). PXRD (2θ, degree, reflection plane); 3.5 (100), 6.0 (110), 9.0 (210), 26.5 (001). ATR FT-IR (wavenumber, cm^{-1}); 540 (br), 613 (s), 655 (s), 729 (s), 794 (br), 832 (s), 849 (s), 1020 (s), 1076 (s), 1160 (s), 1237 (s), 1340 (s), 1395 (s), 1449 (s), 1492 (s), 1522 (s), 1628 (br), 2358 (br), 3285 (br). BET; a_s = 1741 m^2 g^{-1}, v_p = 0.9708 cm^3 g^{-1}, d_p = 2.43 nm.

Procedure 2: HHTP (112 mg, 0.35 mmol) and BDBA (86 mg, 0.52 mmol) were dissolved in a mixture of 2 %methanol/tetrahydrofuran (10.3 mL). The mixture was refluxed under static nitrogen atmosphere for 3 days. As the reaction progress, the addition of tetrahydrofuran was needed to maintain the level of the solvent in the reaction. Over the time, the reaction was cooled to room temperature and a fine suspension was collected by filtration and briefly rinse with tetrahydrofuran. The product was dried under vacuum for 24 hours to give a dark-gray powder.

2.2.2.2 NUS-15

The synthesis of 1,3,5-tris(4-formylphenyl)benzene (TFPB):

In a schlenk tube, 1,3,5-tribromobenzene (TBB, 100 mg, 0.32 mmol), 4-formylphenylboronic acid (FPB, 145 mg, 0.94 mmol) and bis(triphenylphosphine) palladium(II) dichloride (Pd(PPh$_3$)$_2$Cl$_2$, 30 mg, 0.43 mmol) were evacuated and back-filled with nitrogen for 3 times. After which time, tetrahydrofuran (10 mL) and aqueous solution of potassium carbonate (K$_2$CO$_3$, 2 M, 5 mL) were added. The resulting suspension was dominated to 3 times of freeze-pump-thaw cycle. The suspension was refluxed at 90 °C for 24 hours under a nitrogen flow. Once the time had elapsed, the reaction was extracted with dichloromethane (3x20 mL) and the organic phase was collected and washed with water (3x20 mL). The obtained solution was dried over sodium sulfate (Na$_2$SO$_4$). All volatiles were removed under vacuum. The crude product was purified by column chromatography, eluting with pure dichloromethane to 1:1 dichloromethane/ethyl acetate and recrystallized in chloroform/hexane giving a white crystalline powder with 67 %yield (82.4 mg, 0.21 mmol). ^{1}H-NMR (400 MHz, CDCl$_3$, ppm): **δ** 10.11 (s, 3H, −CHO), 8.03 (d, J = 7.6 Hz, 6H, Ar−H), 7.91 (s, 3H, Ar−H), 7.88 (d, J = 8.0 Hz, 6H, Ar−H).

The synthesis of NUS-15:

Procedure 1: In a glass vial, a 1,3,5-tris-(4-formyl phenyl) benzene (TFPB, 136 mg, 0.35 mmol) and a *p*-phenylene diamine (PDA, 56.5 mg, 0.52 mmol) were added mesitylene/ethanol (1:1 v/v, 16 mL). The solution was sonicated for 10 minutes at room temperature. After which time, acetic acid (3 M, 1.6 mL) was slowly added and the vial was left with undisturbed for 3 days at room temperature. The yellow precipitate was collected by filtration and briefly rinsed with tetrahydrofuran and dichloromethane. The obtained powder was activated by Soxhlet extraction with anhydrous methanol at 88 °C for 24 hours. The power product was collected and dried in vacuum oven at 70 °C for 24 hours, giving an orange-yellow power with 89 %yields. (102 mg, 0.15 mmol). The product was characterized using PXRD, FT-IR and BET. BET; a$_s$ = 12.75 m^2 g^{-1}, v$_p$ = 0.03503 cm^3 g^{-1}, d$_p$ = 2.43 nm.

Procedure 2: 1,3,5-tris-(4-formyl phenyl) benzene (TFPB, 136 mg, 0.35 mmol) and a p-phenylene diamine (PDA, 56.5 mg, 0.52 mmol) was mixed in a glass vial and dissolved in the mixture of dioxane/mesitylene (4:1, 12.6 mL). The solution was heated to 70 °C for 3 minutes to assure the dissolving and then cooled to room temperature. After which time, deionized water (2.4 mL) and glacial acetic acid (3.6 mL) were slowly added, respectively. The obtained suspension was sealed and heated to 70 °C for 72 hours. The product was manipulated by filtrate, rinsed with toluene and activated by Soxhlet extraction with anhydrous methanol at 88 °C for 24 hours. Over the time pass by, the powder product was dried under vacuum oven at 70 °C for 24 hours, yielding a yellow powder with 70 %yield (80 mg, 0.12 mmol). The product was characterized using PXRD, FT-IR and BET techniques. BET; a_s = 82.80 m^2 g^{-1}, v_p = 0.2282 cm^3 g^{-1}, d_p = 2.43 nm.

Procedure 3: The vial glass was charged with 1,3,5-tris-(4-formyl phenyl) benzene (TFPB, 391 mg, 1.00 mmol) and a *p*-phenylene diamine (PDA, 162 mg, 1.50 mmol). The reactants were fully dissolved in dioxane/mesitylene (4:1, 40 mL) after sonicated at 25 °C for 30 minutes. Scandium(III) trifluoromethane sulfonate (30 mg, 60 μmol) was added into the solution and briefly sonicated. The suspension solution was obtained after a few minutes passed and left for 30 minutes at room temperature. The orange-yellow powder was collected by filtration and activated by Soxhlet extraction with anhydrous methanol at 88 °C for 24 hours. Over the time pass by, the powder product was dried under vacuum oven at 70 °C for 24 hours to give a yellow powder product with 83 %yield (95 mg, 0.14 mmol). The product was characterized using PXRD, FT-IR and BET techniques. ATR FT-IR (wavenumber, cm^{-1}); 789 (s), 796 (s), 854 (s), 1170 (br), 1210 (s), 1310 (s), 1380 (s), 1570 (s), 1600 (s), 1690. BET; a_s = 126 m^2 g^{-1}, v_p = 0.101 cm^3 g^{-1}, d_p = 2.43 nm.

2.2.2.3 NUS-16

The synthesis of NUS-16:

To a glass vial was charged with 1,3,5-tris(4-aminophenyl) benzene (TAPB, 350 mg, 1.00 mmol) and 4,4'-biphenyl dicarboxylic acid (BPCA, 320 mg, 1.50 mmol). The reactants were fully dissolved in dioxane/mesitylene (4:1, 40 mL) after sonication at 25 °C for 30 minutes. Scandium(III) trifluoro methane sulfonate (30 mg, 60 μmol) was added into the solution and briefly sonicated. The suspension was obtained after a few minutes passed and left for 1 hour at room temperature. The orange powder was collected by filtration and activated by Soxhlet extraction with anhydrous methanol at 88 °C for 24 hours. Over the time pass by, the powder product was dried under vacuum oven at 70 °C for 24 hours to give an orange powder product with 76 %yield (353 mg, 38 mmol). BET; a_s = 45.45 m^2 g^{-1}, v_p = 0.1142 cm^3 g^{-1}, d_p = 2.43 nm.

2.2.2.4 SBA-15

To a solution of pluronic (P123, 1.00 g, mmol) dissolved in millipore water (7.5 g) was added hydrochloric acid (2 M, 30 g) with stirring at room temperature. Afterward, tetraethyl orthosilicate (TEOS, 2.08 g, mmol) was dropped into the mixture followed by a stirring for an hour. After which time, the solution was aged with sturdy stirring at 40 °C for 24 hours at room temperature. The slurry was transferred to a Teflon-lined autoclave for hydrothermally treatment at 100 °C for 48 hours. The product was collected by filtration, washed with deionized water and ethanol and dried under vacuum for 24 hours. A triblock copolymer was removed by calcination method at 550 °C for 5 hours giving a white powder. PXRD (2θ, degree, reflection plane); 0.96 (100), 1.58 (110), 1.80 (200). ATR FT-IR (wavenumber, cm^{-1}); 444 (s), 800.54 (s), 962 (s), 1053 (s), 3402 (br). BET; a_s= 662.0 m^2 g^{-1}, v_p= 1.05 cm^3 g^{-1}, d_p = 8.06 nm.

2.2.2 The synthesis of 1-vinyl-3-ethyl imidazolium derivatives

2.2.2.1 1-vinyl-3-ethyl imidazolium bromide (VEIM[Br])

To a sturdy stirred 1-vinylimidazole (10.0 g, 106 mmol) in a round bottom flask was added bromoethane (19.6 g, 180 mmol) dropwise, all in an iced bath. The reaction

was refluxed at 70 °C for 3 hours. After which time, the reaction was allowed to cool to room temperature and the excess bromoethane was removed under reduced pressure. The obtained solid was re-dissolved in methanol until a clear solution was gained. The methanol solution was slowly dropped into cooled ethyl acetate with sturdy stirring. The product was filtrated and dried under vacuum for 24 hours to obtain an off-white solid product with 54 %yield (11.5 g, 56.7 mmol). ^{1}H-NMR (500 MHz, CDCl$_3$, ppm): **δ** 10.71 (br, 1H, -N=C$\underline{H}$-N-), 7.95 (br, 1H, Im-C$\underline{H}$=CH$_2$), 7.77 (br, 1H, -ImC$\underline{H}$-N$^+$), 7.40 (dd, ^{3}J = 15.8 Hz, ^{1}J = 8.50 Hz, 1H, ImC$\underline{H}$-N-), 5.99 (dd, ^{3}J = 16.0 Hz, ^{1}J = 3.0 Hz, 1H, C$\underline{H}_2$=CH-Im), 5.31 (dd, ^{3}J = 9.0 Hz, ^{1}J = 3.0 Hz, 1H, C$\underline{H}_2$=CH-Im), 4.43 (q, J = 7.5 Hz, 2H, -ImN$^+$-C$\underline{H}_2$-CH$_3$), 1.56 (t, J = 7.5 Hz, 3H, -ImN$^+$-CH$_2$-C$\underline{H}_3$). ^{13}C{H}-NMR (100 MHz, CDCl$_3$, ppm): **δ** 135.3 (s, 1C, -N=$\underline{C}$H-N-), 128.3 (s, 1C, Im-$\underline{C}$H=CH$_2$), 122.8 (s, 1C, -Im$\underline{C}$H-N$^+$), 119.7 (s, 1C, -Im$\underline{C}$H-N-), 109.9 (s, 1C, $\underline{C}$H$_2$=CH-Im), 45.6 (s, 1C, ImN$^+$-$\underline{C}$H$_2$-CH$_3$), 15.60 (s, 1C, ImN$^+$-CH$_2$-$\underline{C}$H$_3$). Solid NMR (400 MHz, ppm): **δ** 134.2 (-N=$\underline{C}$H-N-), 128.3 (CH$_2$=$\underline{C}$H), 126.1 (Im$\underline{C}$H-N$^+$-), 118.7 (Im$\underline{C}$H-N-), 110.6 ($\underline{C}$H$_2$=CH), 45.63 (-ImN$^+$-$\underline{C}$H$_2$-) and 12.08 (-CH$_2$-$\underline{C}$H$_3$). ATR FT-IR (wavenumber, cm^{-1}); 595 (s), 618 (s), 690 (s), 783 (s), 854 (s), 927 (s), 979 (s), 1168 (s), 1185 (s), 1258 (s), 1302 (s), 1330 (s), 1346 (s), 1376 (s), 1417 (s), 1458 (s), 1545 (s), 1581 (s), 1660 (s), 2991 (br), 3057 (br), 3132 (s), 3418 (br).

2.2.2.2 1-vinyl-3-ethyl imidazolium bis(trifluoromethylsulfonyl) amide (VEIM[NTf$_2$])

1-vinyl-3-ethyl imidazolium bromide (VEIM[Br]) (2.48 g, 12.2 mmol) was dissolved in millipore water (6.0 mL). Lithium bis(trifluoromethylsulfonyl) amide (Li[TFSA], 4.42 g, 15.4 mmol) was slowly dropped into the aqueous solution with a vigorous stirring. After a few minutes, a two-phase mixture was observed and left for 4 days at room temperature. The reaction was added by ethyl acetate (20 mL) and washed with millipore water (3x30 mL). The organic phase was collected and evaporated under reduced pressure to obtain a light-yellow oil as a crude product. The oil was dissolved in acetone and dried over magnesium sulfate (MgSO$_4$). All volatiles were removed under vacuum and dried further for 24 hours, giving a product as a clear light-yellow

oil with 76 %yield (3.50 g, 9.2 mmol). ^{1}H-NMR (500 MHz, DMSO-d_6, ppm): **δ** ^{1}H-NMR (500 MHz, CDCl$_3$, ppm): **δ** 9.48 (br, 1H, -N=C$\underline{H}$-N-), 8.17 (br, 1H, Im-C$\underline{H}$=CH$_2$), 7.92 (br, 1H, -ImC$\underline{H}$-N$^+$), 7.28 (dd, ^3J = 15.8 Hz, ^1J = 8.50 Hz, 1H, -ImC$\underline{H}$-N-), 5.95 (dd, ^3J = 15.5 Hz, ^1J = 2.5 Hz, 1H, C$\underline{H}_2$=CH-Im), 5.41 (dd, ^3J = 8.5 Hz, ^1J = 2.0 Hz, 1H, C$\underline{H}_2$=CH-Im), 4.23 (q, J = 7.5 Hz, 2H, -ImN$^+$-C$\underline{H}_2$-CH$_3$), 1.45 (t, J = 7.5 Hz, 3H, -ImN$^+$-CH$_2$-C$\underline{H}_3$). ^{13}C{^{1}H}-NMR (100 MHz, DMSO-d_6, ppm): **δ** 135.0 (s, 1C, -N=$\underline{C}$H-N-), 128.8 (s, 1C, Im-$\underline{C}$H=CH$_2$), 122.8 (s, 1C, -Im$\underline{C}$H-N$^+$), 119.5 (q, 2C, -S-$\underline{C}$F$_3$), 119.1 (s, 1C, -Im$\underline{C}$H-N-), 108.5 (s, 1C, $\underline{C}$H$_2$=CH-Im), 44.6 (s, 1C, -ImN$^+$-$\underline{C}$H$_2$-CH$_3$), 14.50 (s, 1C, -ImN$^+$-CH$_2$-$\underline{C}$H$_3$). ^{31}F{^{1}H}-NMR (471 MHz, DMSO-d_6, ppm): **δ** -80.01 (s, 6F).

2.2.3 The preparation for model studies

2.2.3.1 The synthesis of 2-phenyl-1,3,2-benzodioxaborole (CAT-B)

Phenyl boronic acid (3.00 g, 24.6 mmol) and pyrocatechol (4.00 g, 36.3 mmol) were suspended in dichloromethane (25 mL). Ethyl acetate was added into the suspension until a clear solution was obtained. The solution was filtered to remove any insoluble traces and stirred overnight at room temperature. After which time, the obtained solution was dried over magnesium sulfate (MgSO$_4$). All volatiles were removed under vacuum. The crude product was purified by recrystallization in a solution of hexane/dichloro-methane at and left overnight in refrigerator, giving a product as a white crystalline powder with 54 %yield (2.59 g, 13.2 mmol). ^{1}H-NMR (500 MHz, CDCl$_3$, ppm): **δ** 8.12 (d, J = 7.5 Hz, 2H, -B-ArC$_2\underline{H}$), 7.60 (m, 1H, -B-ArC$_3\underline{H}$), 7.51 (m, 2H, -B-ArC$_4\underline{H}$), 7.34 (m, 2H, -O-ArC$_3\underline{H}$), 7.15 (m, 2H, -O-ArC$_2\underline{H}$). ^{13}C{^{1}H}-NMR (125 MHz, CDCl$_3$, ppm): **δ** 148.7 (s, 2C, -O-Ar$\underline{C}_1$), 135.1 (s, 2C, -B-Ar$\underline{C}_2$), 132.5 (s, 1C, -B-Ar$\underline{C}_1$-), 128.4 (s, 3C, -B-ArC$_3$-$\underline{C}_4$), 123.0 (s, 2C, -O-Ar$\underline{C3}$), 112.7 (s, 2C, -O-Ar$\underline{C}_2$). ^{11}B{^{1}H}-NMR (160 MHz, CDCl$_3$, ppm): **δ** 32.27 (s, 1B).

2.2.3.2 General procedure for NMR-scale reactions for model studies

To an NMR tube (Duran, 1.78x4.95 mm) was added a solution of CAT-B (30 mg, 0.15 mmol, 1 equivalent) in 0.2 mL of suitable deuterated solvent (CDCl$_3$ or DMSO-d_6). Either a solution of VEIM[Br] (121 mg, 0.60 mmol, 4 equivalents) in 0.2

mL of CDCl$_3$ or a solution of VEIM[NTf$_2$] (227 mg, 0.60 mmol, 4 equivalents) in 0.2 mL of DMSO-d_6 was added into the CAT-B solution. After mixing, an NMR measurement was taken immediately. The mixture was then left at room temperature for an hour before an NMR measurement was record again.

2.2.4 General procedure for the synthesis of confined ionic liquids and *in situ* generated poly(ionic liquids) in porous materials

2.2.4.1 1-vinyl-3-ethyl imidazolium derivatives@porous materials

2.2.4.1.1 Vacuum infiltration method

To a schlenk tube was added a porous solid material with the amount started in Table. 2.1. The solid was dried under high vacuum (10^{-3} mbars) over a period of 10 minutes. Once the time had elapsed, a solution of ionic liquid in a suitable solvent was added into the porous solid with a sturdy stirring. The suspension was put under a static vacuum over a period of 24 hours. After which time, the supernatant was filtrated off and the solid material was washed with the same solution for 3 times. **BET:** VEIM[Br]@COF-5; a$_s$ = 170.6 m^2 g^{-1}, v$_p$ = 0.1233 cm^3 g^{-1}, d$_p$ = 2.43 nm., VEIM[Br]@SBA-15; a$_s$ = 350.6 m^2 g^{-1}, v$_p$ = 0.7142 cm^3 g^{-1}, d$_p$ = 7.05 nm., VEIM[Br]@imine-1; a$_s$ = 1128 m^2 g^{-1}, v$_p$ = 0.7376 cm^3 g^{-1}, d$_p$ = 2.43 nm., VEIM[NTf$_2$]@COF-5; a$_s$ = 33.92 m^2 g^{-1}, v$_p$ = 0.09715 cm^3 g^{-1}, d$_p$ = 2.43 nm., VEIM[NTf$_2$]@SBA-15; a$_s$ = 546.3 m^2 g^{-1}, v$_p$ = 0.9583 cm^3 g^{-1}, d$_p$ = 9.23 nm., VEIM[NTf$_2$]@imie-1 a$_s$ = 633.9 m^2 g^{-1}, v$_p$ = 0.4736 cm^3 g^{-1}, d$_p$ = 2.43 nm.

2.2.4.1.2 Grinding method

In a glovebox, COF-5 (100 mg, 0.65 mmol) was mixed with 900 µL of a solution of a 1-vinyl-3-ethyl imidazolium bromide (VEIM[Br], 100 mg, 0.50 mmol) in dried chloroform. The mixture was grinded in an agate mortar for 30 minutes at room temperature until visually dry. The powder was washed with a dried chloroform for 3 times and dried under vacuum for 24 hours. **BET**; VEIM[Br]@COF, $a_s = 517.8$ m^2 g^{-1}, $v_p = 0.2795$ cm^3 g^{-1}, $d_p = 2.43$ nm.

2.2.4.2 poly(1-vinyl-3-ethyl imidazolium) derivatives@porous materials

To a schlenk tube was added a porous solid of COF-5 material with the amount started in Table. 2.1. The solid was dried under high vacuum (10^{-3} mbars) over a period of 10 minutes. Once the time had elapsed, a solution of ionic liquid and AIBN in a suitable solvent were added into the porous solid with a sturdy stirring. The suspension was put under a static vacuum over a period of 24 hours. After which time, the supernatant was filtrated off and the solid material was washed with the same solution for 3 times. The solid was heated at 80 °C under a nitrogen atmosphere for 24 hours to allow an *in-situ* polymerization to take place. The solid material was then characterized with PXRD, FT-IR, BET and TGA. **BET:** polyVEIM[Br]@COF-5; $a_s = 507.3$ m^2 g^{-1}, $v_p = 0.3297$ cm^3 g^{-1}, $d_p = 2.43$ nm.

2.2.5 Catalytic activity studies in cycloaddition.

A high-pressure stainless steel reactor was charged with the VEIM[Br]@COF-5 material (15 mg, 0.03 mmol of Br$^-$ anion) and dried propylene oxide (5 mL, 60 mmol) with a magnetic stirrer. After the pressurizing the reactor with 1 MPa of CO$_2$, the reactor was placed in an oil bath setting at 60 °C and was vigorously stirred for 20 hours. After which time, the reactor was left at room temperature to cool down followed by a slowly releasing of the residue gas. The reaction was filtrated by 0.45 µm of PTFE filter to an NMR tube prior to a monitoring by ^{1}H-NMR technique which could be converted to a yielding of the reaction.

Table 2.1 The number of substrates in the syntheses of infiltration of ionic liquids@porous materials and polymerization of an infiltrated ionic liquid inside the porous material (poly(VEIM[Br]@COF-5).

Samples	Component substrates			
	Porous material	Ionic liquid	AIBN	Solvent
VEIM[Br]@COF-5	COF-5 (80 mg, 0.52 mmol)	VEIM[Br] (350 mg, 1.72 mmol)	-	chloroform 15 mL
VEIM[NTf₂]@COF-5	COF-5 (80 mg, 0.52 mmol)	VEIM[NTf₂] (1.0 mL, ca. 9.55 mmol)	-	tetrahydrofuran (THF) 15 mL
VEIM[Br]@SBA-15	SBA-15 (200 mg, 0.30 mmol)	VEIM[Br] (350 mg, 1.72 mmol)	-	chloroform 15 mL
VEIM[NTf₂]@SBA-15	SBA-15 (200 mg, 0.30 mmol)	VEIM[NTf₂] (1.0 mL, ca. 9.55 mmol)	-	acetone 15 mL
VEIM[Br]@imine-1	imine-1 (50 mg, 0.16 mmol)	VEIM[Br] (350 mg, 1.72 mmol)	-	chloroform/THF (1:1) 15 mL
VEIM[NTf₂]@imine-1	imine-1 (50 mg, 0.16 mmol)	VEIM[NTf₂] (1.0 mL, ca. 9.55 mmol)	-	tetrahydrofuran (THF) 15 mL
polyVEIM[Br]@COF-5	COF-5 (80 mg, 0.52 mmol)	VEIM[Br] (350 mg, 1.72 mmol)	30 mg, (0.18 mmol)	chloroform 15 mL

CHAPTER 3

Results and discussion

3.1 Covalent organic frameworks (COFs) synthesis

3.1.1 COF-5

3.1.1.1 The synthesis of COF-5
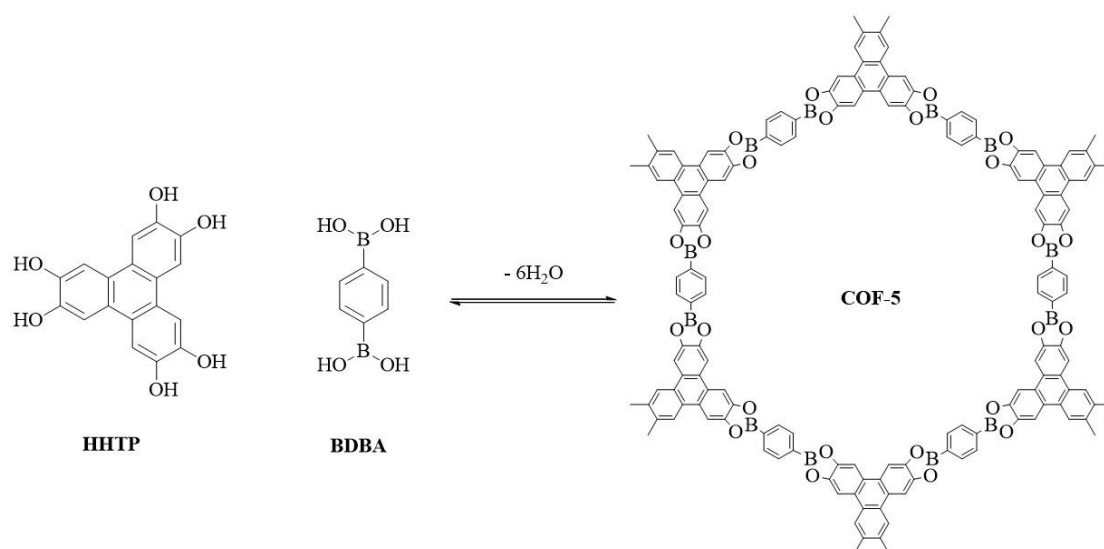
Figure 3.1 The condensation reaction between 2,3,6,7,10,11-hexahydroxy triphenylene (HHTP) and 1,4-phenylenediboronicacid (BDBA) to form COF-5.

COF-5 $(C_9H_4BO_2)_n$ is a crystalline porous material belonging to a pore size of 27 Å, which is first reported in 2005 by Yaghi *et al.*[7] The 2D hexagonal layers are formed *via* a condensation reaction of 2,3,6,7,10,11-hexahydroxytriphenylene (HHTP) and 1,4-phenylenediboronicacid (BDBA) giving a five-membered boronate ester ring connections (Figure 3.1). Each layer is commonly stacked to each other through a π-π stacking interaction forming a 1D channel. The syntheses of COF-5 were reported through various methods such as solvothermal[7, 8], sonochemical method[57], growing on substrate surface[58], conventional heating process[48, 59, 60] and microwave condensation synthesis[61-63] which could give COF-5 products with different crystallinity and surface area as shown in Table 3.1.

Table 3.1 The summary of the reported surface area of COF-5 obtained under different method.

Entry	BDBA (mmol)	HHTP (mmol)	Method	Reaction time (h)	S_{BET} (m^2g^{-1})	ref
1	0.15	0.05	solvothermal	72	1590	7
2	0.52	0.35	conventional heating	20	2000	48
3	1	0.7	sonochemical method	1	1143	57
4	1	0.7	sonochemical method	0.5	1098	57
5	1	0.7	sonochemical method	2	2092	57
6	2	1.7	sonochemical method	1	1268	57
7	1	0.3	sonochemical method	1	842	57
8	0.1	0.7	conventional heating	20	1828	60
9	1.12	0.75	microwave	1	2335	61
10	1.12	0.75	oven heating	72	2282	61
11	1.12	0.75	microwave (closed system)	0.33	2019	62
12	1.12	0.75	microwave (open system)	0.33	2027	62

The conventional heating method is a general synthesis methodology to provide a pure and effective product. materials, which does not require extra instruments. It is a non-complicated method which is easy to control and handle in general laboratories and still provides the powdered crystalline COF material products.[48] Hence, here in, we adapted the previous synthetic reports based on the conventional heating process to synthesize the COF-5 material. The homogeneous[48] and heterogenous reaction[21] were chosen which are different in a preparation of an initial mixture of substrates prior to a heating period. Since the product of the reaction would precipitate during the reaction process, the initial insoluble reactants might be contaminations of the obtained product which are difficult to be removed. Therefore, the solution of fully dissolved reactants in the homogeneous process is important key to obtain the crystalline porous material of COF-5.

To a homogeneous process adapting from the previous report[48] (Table 3.1 entry 2), the reactants were fully dissolved in 1:1 dioxane/mesitylene with small amounts of methanol. The mixture was filtered after sonicating to obtain a dark brown solution. The solution was heated to 90 °C under a static nitrogen atmosphere for 24 hours. After the reaction time, the product was filtered to obtain a gray-powder with a clear greenish brown supernatant. The product was washed by dry chloroform and dried on schlenk line overnight prior to characterization and usage. PXRD spectra of the as-synthesized COF-5 shows a characteristic shape signal at 3.5 degree corresponding to the (100) plane in the COF-5 lattice, along with other signals at 6.0 (110), 9.0 (210) and 26.5 (001) degree (2θ, Cu kα), which are in line with the previous reports[48] (Figure 3.2a). ATR FT-IR data exhibits significant peaks at 1340 cm^{-1} assigned to a characteristic signal of B-O stretching band of the boroxole ring[7], which affirms the boronate-ester linkage formation in COF-5 structure (Figure 3.2b). Besides, the as-synthesized COF-5 powder reveals a pore diameter of 2.43 nm with a reversible type-IV isotherm characterizing the mesoporous material trait (Figure 3.2c) of COF-5 material. BET surface area of ca. 1700 m^2 g^{-1} is higher than the value of some previous reports of COF-5 product obtained by different conditions (Table 3.1). As the COF-5 contains numerous boronate-ester linkages, the acidity of COF-5 is expected. The ammonia temperature-programmed desorption (NH$_3$-TPD) was employed to measure acidity of the COF-5 material. The result shown in Figure 3.2d illustrates the acidic sites of ca. 2500 μmolNH$_3$ m^{-3}, which is higher than an SBA-15[64] and MIL-101[65] for 20 and 10 folds, respectively. Moreover, the COF-5 material indicates a high thermal stability measured by a thermogravimetric analysis (TGA) showing ca. 30% weight loss starting around 600 to 900 °C (*vide infra*).
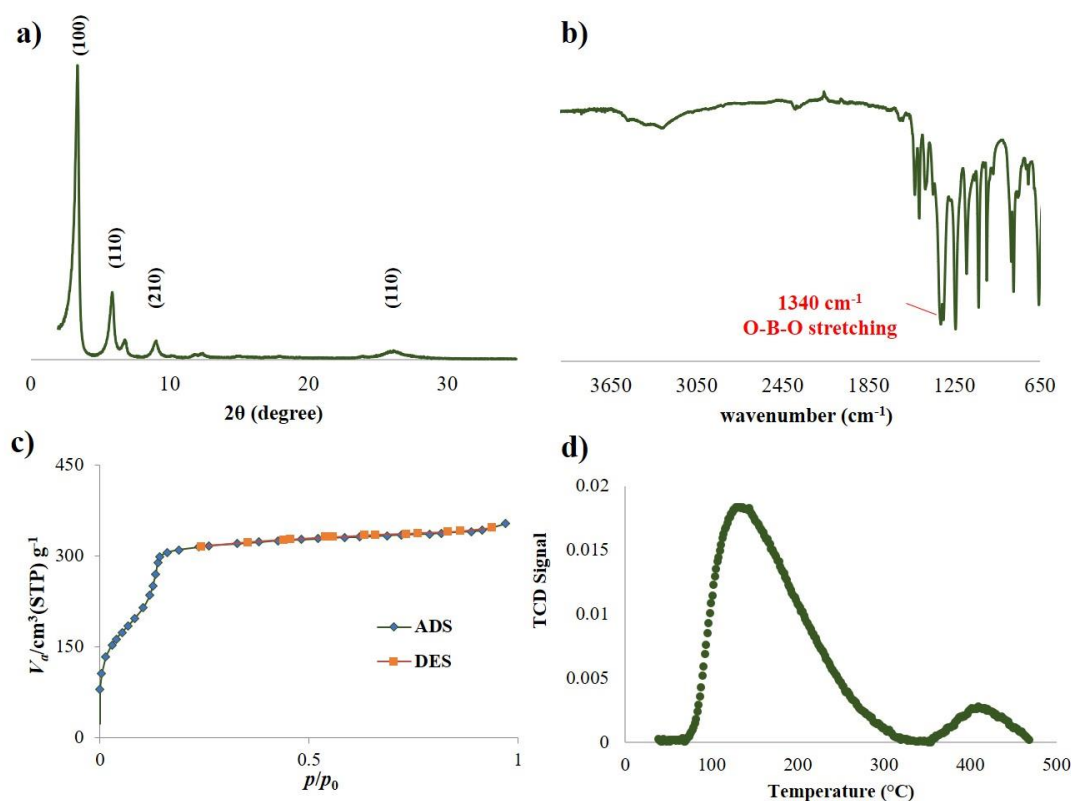
Figure 3.2 The characterization data of COF-5; a) PXRD spectrum, b) FTIR signal in ATR mode, c) N₂ sorption isotherm and d) NH₃-TPD curve.

Aside from the homogeneous method mentioned earlier, the heterogeneous method was also adopted. The reactants were partially dissolved in tetrahydrofuran by vigorous stirring without a displacement of the insoluble substrates. The reaction was refluxed under a nitrogen atmosphere for 72 hours. After which time, negligible dark gray suspended solid was obtained. The PXRD measurement of the product revealed a low intensity pattern signifying low crystallinity of the material. Owing to the marginal production of the low crystalline product, in this work, only the homogeneous methodology was chosen and focused over the heterogeneous one.

3.1.1.2 The hydrolysis study of COF-5

Unavoidable, the hydrolysis of boronate-ester based COFs were reported[21] since 3-coordinated trigonal planar boron atoms with sp^2 hybridization have a vacant sited orbital which is susceptible to a nucleophilic attack. The accessing nucleophile, including moisture in the air, could alter the structure of the COF materials to 4-coordinate tetrahedral boron atom with sp^3 hybridization or even break down the bonding between building units back to the starting reactants. In 2013, Yi Du *et al.* demonstrated the effect of pyridine addition into boron containing COFs named COF-5 and COF-10. The results showed the over loading of pyridine causes the formation of sp^3 hybridized tetrahedral boron atoms changing the 3-coordinate boron to 4-coordinate form. This change in coordination numbers of boron atoms could result in structural strain and eventually the stacking behavior of COF-5.[66] To understand the hydrolysis process, Huifang *et al.* recently reported the study of the hydrolytic process of boronater-ester COFs, especially COF-5, using density functional theory (DFT) calculations. For a brief summary, the hydrolysis of boronate-ester linkages can be described as a two-step reaction as shown in Figure 3.3. The first step is the H_2O molecule reacting with a boron atom in TDPBA ring causing a generation of an intermediate one (INT). For the next step, INT reacts again with another H_2O resulting in the reformation of HHTP and BDBA molecules.[67]
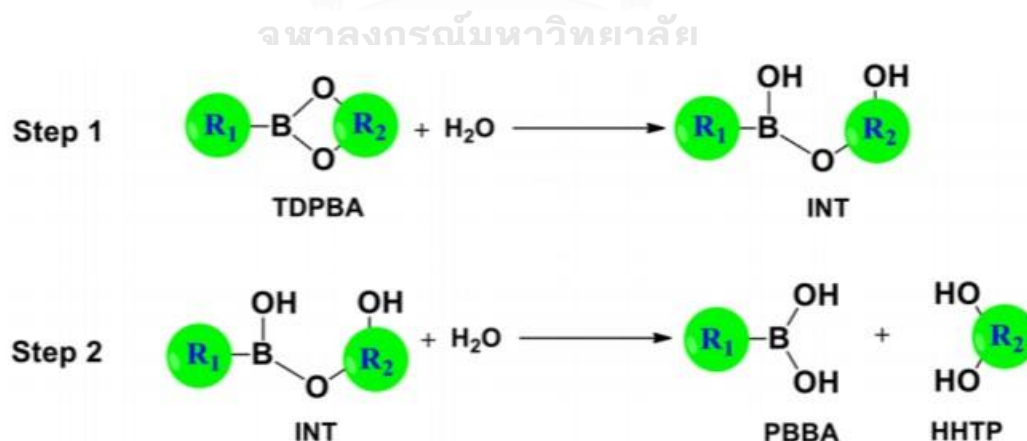
Figure 3.3 The scheme of the hydrolysis reaction of the boronate-ester COF which are represented as the TDPBA molecule.

In this research, the hydrolysis of COF-5 in our bench condition was studied, whereby the COF-5 material was kept at the bench condition (average temperature of 28 °C, 1 bar and humidity of 60-70 %) over the period of 11 days. During the period of time, the crystallinity of the product was constantly measured by PXRD technique. (Figure 3.4). The result shows significant half-intensity decrease of the dominant peak of 2θ of 3.5 (100) degree within 6 days after synthesized and almost 5 times less intense after left at the bench condition within 11 days. The appearing of the signal around 24-27 degree corresponding to the finger print pattern of a HHTP indicate the reformation of the starting material. This phenomenon is in line with the low hydrolytic stability of the boronate-ester linkaged COF materials reported in the previous publication.[21] Hence, in our study, COF-5 had been manipulated under an inert atmosphere of nitrogen and stored in a glovebox.
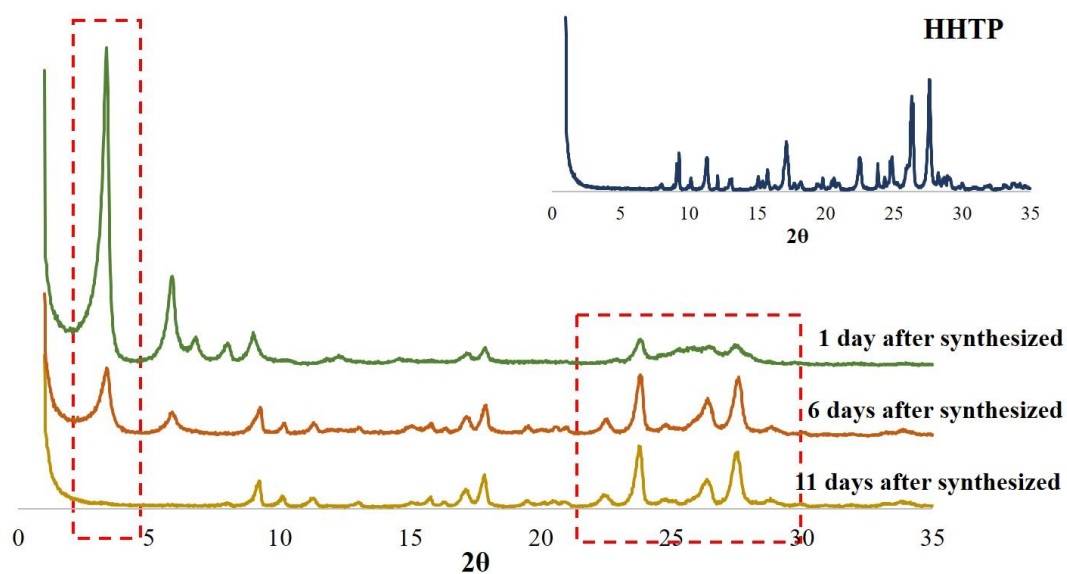
Figure 3.4 PXRD data of the hydrolytic studies of COF-5 under a bench condition.

3.1.2 NUS-15 and NUS-16
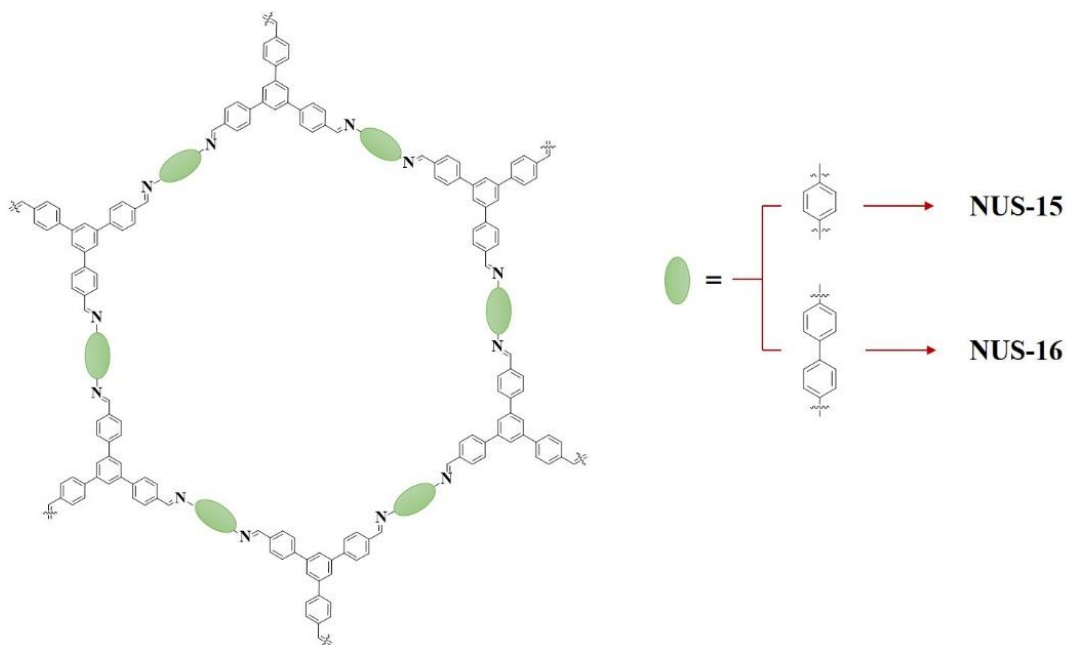
Figure 3.5 The structures of NUS-15 and NUS-16.

In this project, the syntheses of imine-based COFs were also attempted. NUS-15 and NUS-16 (Figure 3.5) are basically representatives of imine-based COFs with a pore size of 34 Å and 47 Å, respectively. Their synthetic methodologies such as drop-casting[68], room temperature solution-suspension process[51], heating method[52] and metal-catalytic reaction.[53] have been reported. Here in, we adapted 3 methodologies, such a room temperature solution-suspension process, heating method and metal-catalytic reaction process, to synthesize the NUS-15. This all the synthetic methodologies gave the product as yellow powders. The characterization using a FT-IR technique reveal a typical stretching band of C=N bonding at a signal of 1620 cm^{-1} while the signal of 1685 cm^{-1} belonging to a C=O stretching of the aldehyde group of starting material is decreased which can confirm the formation of C=N linkages between TFPB and PDA (Figure 3.6).
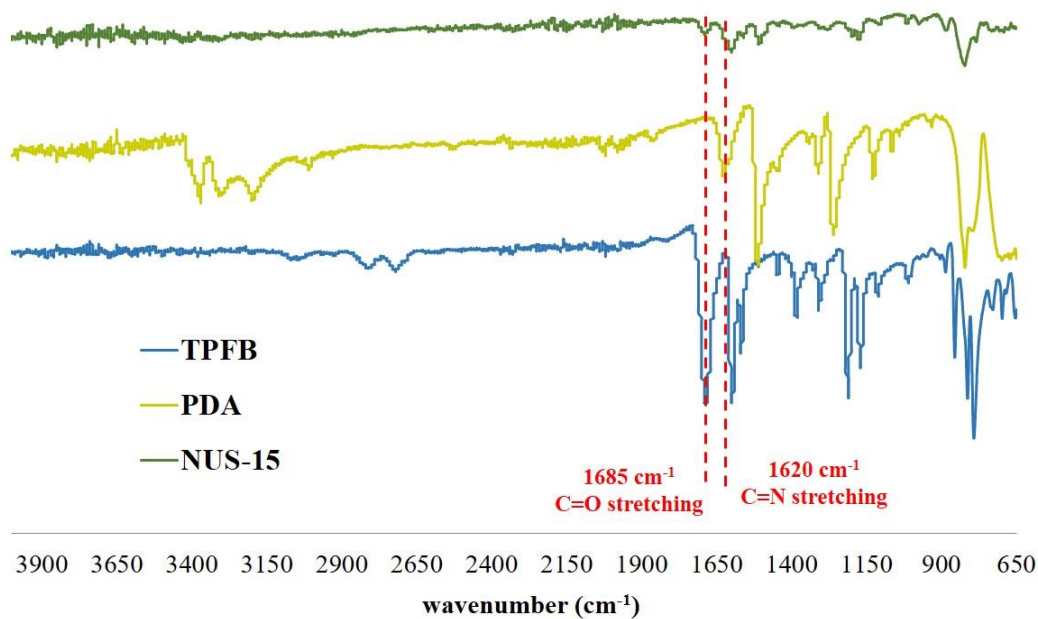
Figure 3.6 FT-IR spectra of NUS-15 (green line) comparing with the starting materials, TPFB (blue line) and PDA (yellow line).

Nevertheless, PXRD data of as-synthesized NUS-15 (Figure A2) shows no significantly signals at 2.9, 5.0, 5.7, 7.5, 10.0 and 25.5 degree which are the reported finger print signals of NUS-15 corresponding to (100), (110), (200), (210) and (220) reflections and an interlayer stacking of the NUS-15 sheets, respectively.[52] Moreover, the NUS-15 powder products exhibit a BET surface area as 12.75-126 m^2 g^{-1}, obviously lower than previous reports of 600-2175 m^2 g^{-1}. These results indicate that the synthesis of NUS-15 could not repeatable at our laboratory condition, which give the low-crystalline product as shown in the PXRD results.

In the case of the synthesis of NUS-16, the metal-catalytic reaction method was employed, whereby a scandium(III) trifluoromethane sulfonate (Sc(III)OTf₃) was used to accelerates the formation reaction between 1,3,5-tris(4-aminophenyl) benzene (TAPB) and 4,4'-biphenyl dicarbaldehyde (BPCA). The characterization result of PXRD technique of as-synthesized NUS-16 show no significant signal instead of the

PXRD pattern reported with broad peak at 2θ of 15-25 degree reported by Song *et al.*[69] Moreover, the surface analysis exhibits a low BET surface area of 20-45 m^2 g^{-1}, which exceedingly lower than a previous report of 1235 m^2 g^{-1}.[53] These data imply the similar information to the case of NUS-15 suggesting unrepeatable of NUS-16 under our laboratory condition. Hence, in this work, we are concentrated on only the boronate-ester based COF, COF-5, as a porous material to emerge the hybrid materials.

3.2 Model studies

As COF-5 consists of sp^2 boron atoms bearing vacant *p*-orbitals which are susceptible to the nucleophilic attack by Lewis base or other strong nucleophiles as mentioned in section 3.1, the use of COF-5 as an infiltrating host with imidazolium based ILs consisting of mild nucleophilic nitrogen atoms and counter anions. In this work, we investigated the effect of guest nucleophilic molecules; 1-vinyl-3-ethylimidazolium bromide (VEIM[Br]), 1-vinyl-3-ethylimidazolium bis(trifluoromethanesulfonyl) imide (VEIM[NTf$_2$]) and also a strong nucleophilic aniline (Figure 3.7) on a modelled compound (2-phenyl-1,3,2-benzodioxaborole, CAT-B) closely resembling to COF-5.
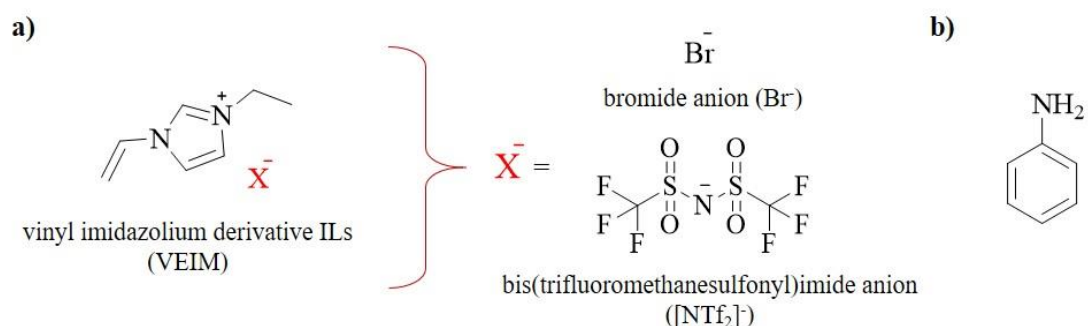
Figure 3.7 The structure of a) ionic liquids: 1-vinyl-3-ethylimidazolium bromide (VEIM[Br]), 1-vinyl-3-ethylimidazolium bis(trifluoromethanesulfonyl) imide (VEIM[NTf₂]) and b) aniline.

The modelled compound was synthesized *via* the coupling reaction between pyrocatechol and phenylboronic acid (Figure 3.8). The reaction was stirred overnight at room temperature and was characterized by ^{1}H-NMR and ^{11}B{^{1}H}-NMR techniques in CDCl$_3$ as shown in Figure 3.9a) and 3.10a), respectively. In this study, the change of coordination numbers of boron atoms in CAT-B was followed by NMR techniques upon the addition of multiple equivalents of 1-vinyl-3-ethylimidazolium bromide (VEIM[Br]), 1-vinyl-3-ethylimidazolium bis(trifluoromethanesulfonyl)imide (VEIM[NTf$_2$]) and aniline. The change was monitored by NMR experiments immediately after mixing and after left standing for 2 hours at room temperature.
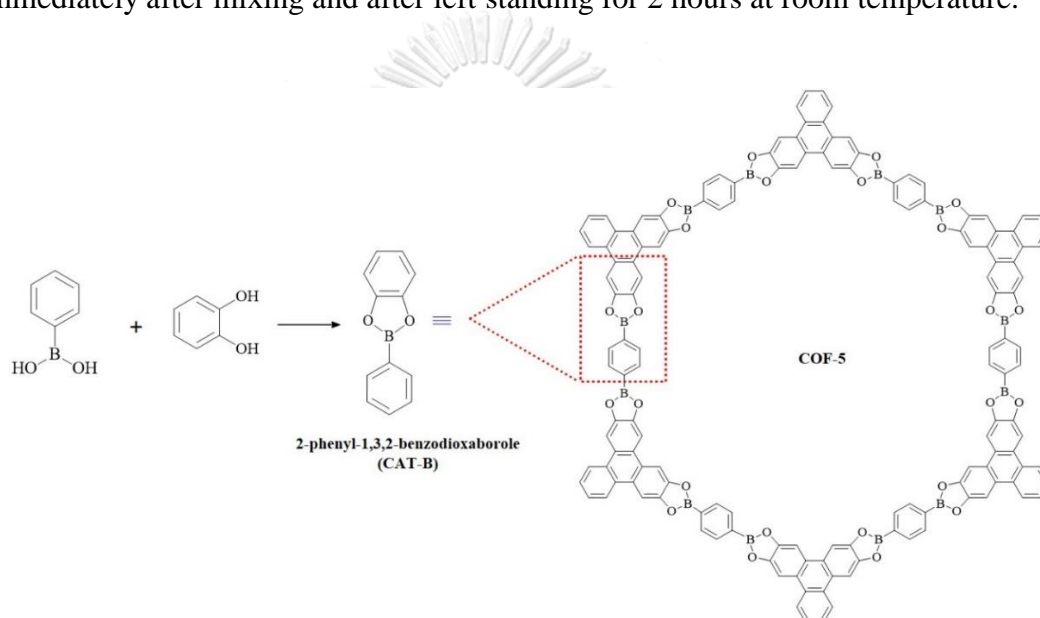
Figure 3.8 The synthesis of the modelled molecule, 2-phenyl-1,3,2-benzo dioxaborole (CAT-B).

The ^{1}H-NMR spectrum of the mixture of CAT-B and 4 equivalents of VEIM[Br] exhibits insignificant change of resonances compared with both the CAT-B and VEIM[Br] spectra. The slight upfield shift of some resonances indicated with the blue and yellow dash lines in Figure 3.9, which could possibly be caused by the change in physical environments. However, these effects are yet precisely identified. Hence, the ^{11}B{^{1}H}-NMR technique was used which could give clear finger print of boron coordination. Normally, the 3-coordinate boron with RB(OR')$_2$, where R and R' are alkyl or aryl groups, functionality gives the resonance signal around 25-35 ppm whereupon the addition of other nucleophiles such as Lewis bases, ligands or

solvents, exhibits the pronounced upfield shift in signal when compared to the 3-coordinate boron as previous reported.[70]
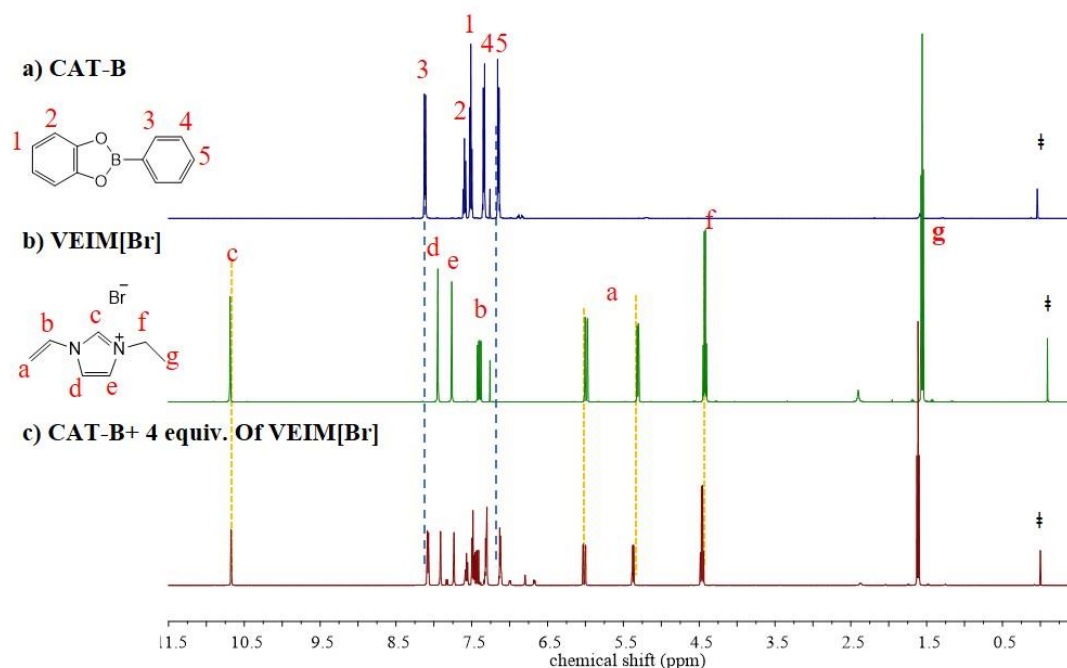
Figure 3.9 ^{1}**H-NMR spectra of a) CAT-B, b) VEIM[Br] and c) the mixture of CAT-B and VEIM[Br]. The dagger signs refer to the TMS residue in deuterated CDCl$_3$.**

In Figure 3.10, the characteristic resonance with a chemical shift of 32 ppm was observed representing a 3-coordinate boron atom, which in the case is RB(OR')$_2$ functionality in CAT-B. The ^{11}B{^{1}H}-NMR spectra showed no change upon the addition of 4 equivalents of VEIM[Br]. This certainly result confirms no Lewis acid base interaction between CAT-B and VEIM[Br] and no structural change of CAT-B compound. Even, after the standing for 2 hours, the NMR results of the mixture solutions remain the same, which confirm the intact structures of CAT-B and VEIM[Br].
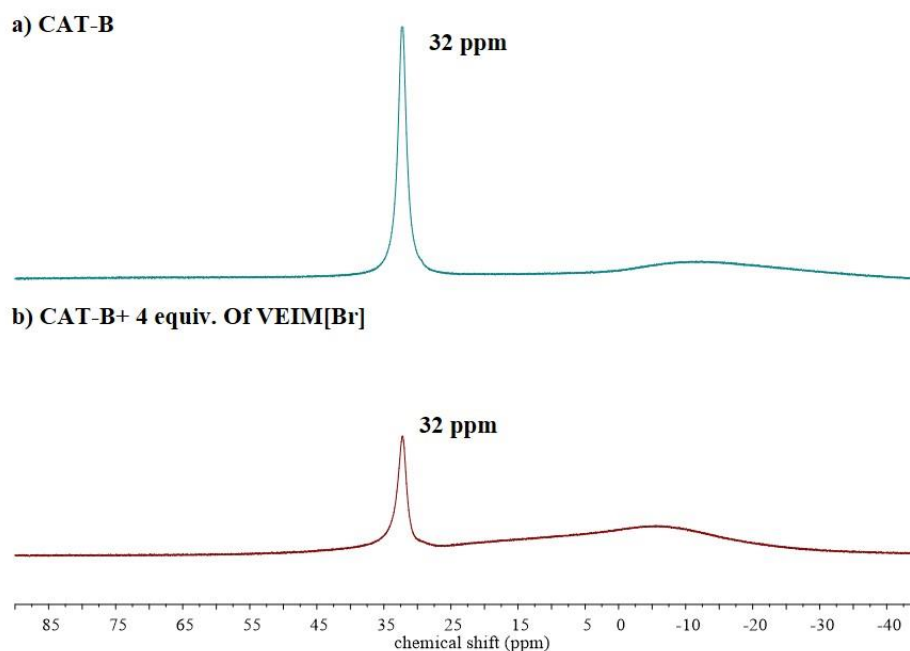
Figure 3.10 ^{11}B-NMR spectra of a) CAT-B and b) the mixture of CAT-B and VEIM[Br] in deuterated CDCl$_3$.

The effect of the more hydrophilic IL, VEIM[NTf$_2$], on CAT-B was explored in a polar coordinating solvent, DMSO-d_6. The ^{1}H-NMR spectrum of CAT-B in DMSO-d_6 provides a different resonance from CAT-B in CDCl$_3$, which shows a one major set of the resonance together with the minor one (Figure 3.11a). A small peak at 7.8 ppm shows an integral of 0.07 relative to the peaks No. **4, 5** in the Figure 3.11a, which can estimate to 6.5 % of a minor set in this solution of CAT-B. Besides, the ^{11}B{^{1}H}-NMR result of CAT-B also shows 2 peaks at 12 and 28 ppm as illustrated in Figure 3.12a(i)) indicating the solution of CAT-B in DMSO-d_6 have 2 different environment of boron atoms consistent with the ^{1}H-NMR result. The signal of 28 ppm corresponding to the 3-coordinated boron in CAT-B as mentioned in another solvent. Whilst, a signal of 12 ppm is probably belonging to (RO)$_2$BR'·DMSO due to the DMSO is a typical strong electron donor through a sulfonyl group (RSO$_2$R') which normally can form complexes with Lewis acids such a boron atom in some compounds as also found in previous reported by Miklos *et al.* in 1991.[71]
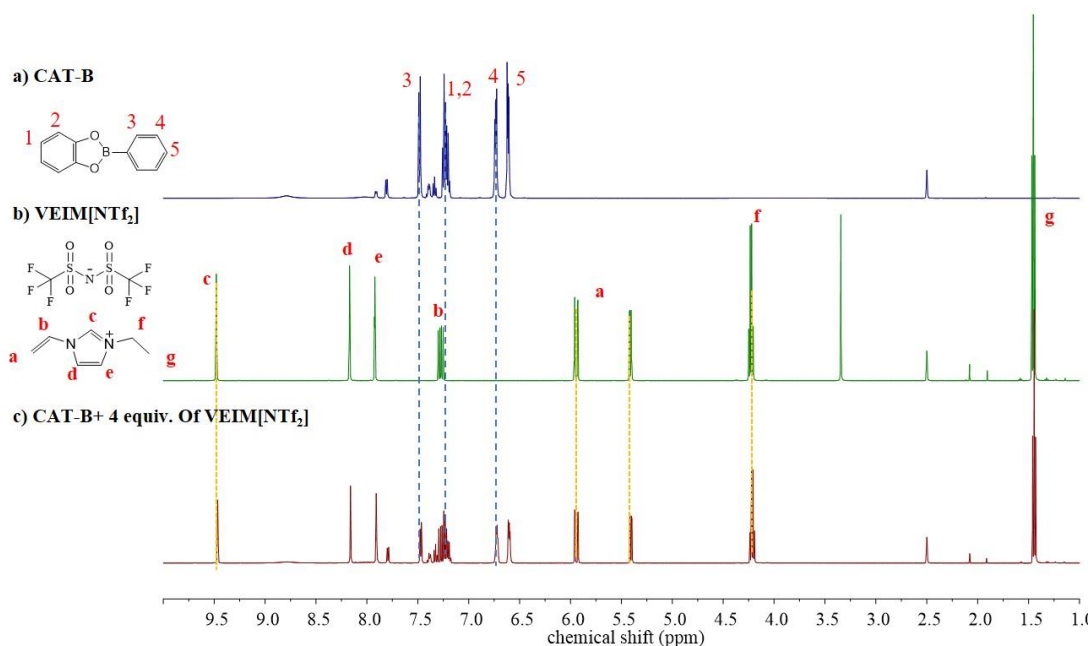
Figure 3.11 ^{1}**H-NMR spectra of a) CAT-B, b) VEIM[NTf₂] and c) the mixture of CAT-B and VEIM[NTf₂] in DMSO-*d₆*.**

For the mixture tube, the ^{1}H-NMR results exhibit the slight shift of chemical shifts with the same resonances which are predictable the major unchanged of CAT-B and VEIM[NTf₂] molecules in mixture solution as shown in Figure 3.11c. However, the small peak at 7.8 was grew out which shows relative integral of 0.14 against the same peaks calculating to 12.3 %. The assumption was assured by ^{11}B{^{1}H}-NMR and ^{19}F{^{1}H}-NMR which could provide the clear signals to understand an interaction between CAT-B and VEIM[NTf₂] in DMSO-*d₆* (Figure 3.12). From ^{11}B{^{1}H}-NMR spectrum, the result still shows 2 resonances of 2 boron species as mentioned above and also the peak of 12 ppm are still a major one. These results imply that the binding on the boron atoms by sulfonyl groups does not only come from the sulfonyl groups of a DMSO-*d₆* but also the sulfonyl groups of anions of VEIM[NTf₂]. However, the minor peak at 7.8 ppm representing an only 12.3 % of boron atoms are a little bit concerned. So, in this research, we are still use the VEIM[NTf₂] to infiltrate into a pore of COF-5 to demonstrate this effect on the actual COF-5 structure.
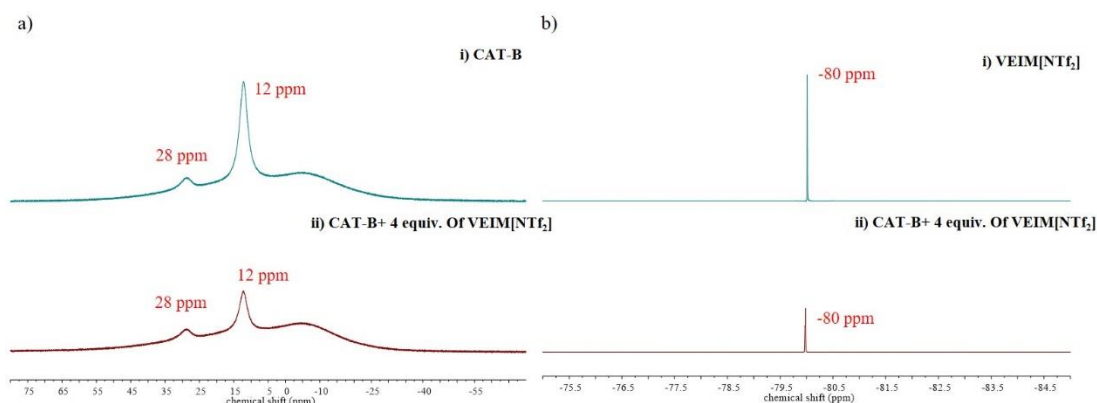
Figure 3.12 a) ^{11}B-NMR spectra of i) CAT-B and ii) the mixture of CAT-B and VEIM[NTf$_2$] and b) ^{19}F-NMR spectra of i) VEIM[NTf$_2$] and ii) the mixture of CAT-B and VEIM[NTf$_2$] in DMSO-d_6.

Furthermore, the stronger nucleophilic base, aniline, was challenged to explore the effect of aniline on CAT-B by mixing 4 equivalents of aniline with CAT-B in deuterated chloroform. The ^{1}H-NMR resonance (Figure A3) of the mixture exhibits insignificant change of resonances comparing with the CAT-B and VEIM[Br] spectra and also no change in ^{11}B{^{1}H}-NMR resonances (Figure A4) as same as the observed results as noted in the previous cases. Even, the 10 equivalents of aniline were added into the CAT-B solution, the results are still similar to what was observed in 4-equivalent addition of aniline showing the nondestructive behavior of coexistence of CAT-B and strong nucleophilic base. Thereby, it could predict the possibility of collaboration between boron containing COFs and nitrogen-containing ILs in term of keeping the structures of COFs material and doped molecules.

3.3 Infiltration of ILs@porous material

The infiltration of guest molecules into the pores of host material can be successfully done through various methods such as drop-casting,[72-74] dipstick,[74] heating,[75] sonication,[76] vacuum infiltration,[42, 77] grinding processes,[45] etc. Here in, we adopted vacuum infiltration and grinding method to primarily demonstrate the infiltration of an IL into the pore of COF-5. Owning to the flexibility and the moisture sensitivity of COF-5, the investigations into the infiltration of IL to the more rigid porous silica and non-moisture sensitive imine-based COF were carried out for comparison purposes. SBA-15 is a rigid mesoporous silica material having parallel hexagonal pores in 2D arrangements as 1D channels through a siloxane linkage (Figure 3.13a).[78] The characteristic PXRD pattern of SBA-15 shows the signals at 2θ of 0.8, 1.8 and 1.9 degree corresponding to the (100), (110) and (200) reflections, respectively (Figure 3.16b).[79] The measured BET surface area was investigated to be 600 m^2 g^{-1} with an average pore size of ca. 8.0 nm. The imine-1 is an imine-based COFs usually known to be less crystallinity than that of the boroxine analogous COF but exhibit higher tolerance to the moisture and other nucleophilic molecules. The PXRD signals of imine-1 at 2θ of 2.76 (100), 4.82 (110), 5.60 (200), 7.42 (210), 9.70 (220) and 25.2 (001) degree were obtained which is a fingerprint pattern of the imine-1 (Figure 3.16c).[80] Furthermore, the BET surface area of 1770 m^2 g^{-1} was obtained using a N_2 adsorption-desorption analysis and also an average pore size of ca. 3.0 nm was evaluated. In this study, the vinyl imidazolium-based IL was used with either bromide anion (Br^-) and bis(trifluoro methanesulfonyl)imide anion (NTf_2^-) as a counter anion. The choices of IL allow the comparative investigation into the effect of sizes, hydrophilicity/hydrophobicity and the infiltrating ability of ILs with different physical states. (VEIM[Br] is a solid and VEIM[NTf$_2$] is a liquid at room temperature). The synthesized hybrid materials are denoted as VEIM[X]@COF-5, VEIM[X]@SBA-15 and VEIM[X]@imine-1, whereby the "X" refers to Br^- or NTf_2^- anion. The infiltrated products are affirmed by the FT-IR, TGA, PXRD and BET techniques and the results are compared with a parental COF-5.
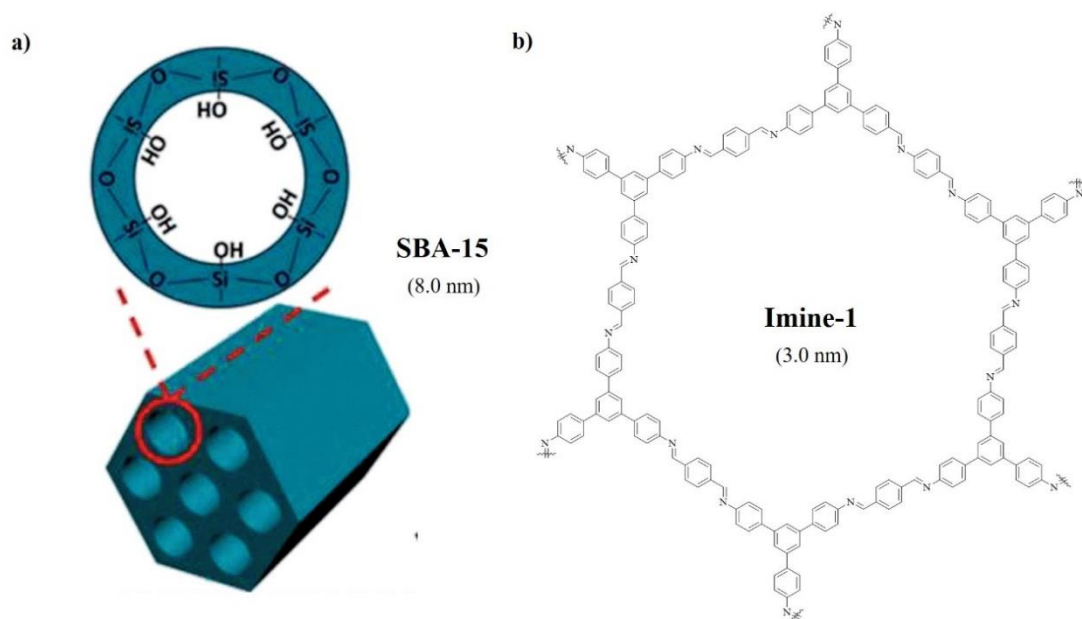
Figure 3.13 The structures of a) SBA-15 and b) imine-1.

3.3.1 Vacuum infiltration method

Recently, a vacuum assisted physical imbibition process was reported by Kumar *et al.* in 2016, whereby the molecules of 1-ethyl-3-methyl imidazolium tetrafluoroborate ([EMIM][BF$_4$]) were filled into the pore of MIL-41.[77] Moreover, in the same year, Tarnacka *et al.* reported about the vacuum infiltration into uniaxial alumina pores with a 1-butyl-3-vinylimidazolium *bis*(trifluoromethanesulfonyl)imide ([bvim][NTf$_2$]) and AIBN *via* the same method prior to the *in-situ* polymerization process.[42] In this research, to synthesize the hybrid materials, a 0.115 M of the solution of IL in an appropriate solvent was added to the porous powder. The mixture was stirred under static vacuum for 24 hours. After which time, the mixture was filtered, and the powder was washed with the previously used solvent to remove the possible leftover IL adhering on the external surface of the porous material. The produce was dried under vacuum for 24 hours prior to characterization.

3.3.1.1 Infiltration of VEIM[Br]

Characterization: FT-IR and solid-state ^{13}C NMR

The successful infiltration of VEIM[Br] into the pores of porous materials (VEIM[Br]@COF-5, VEIM[Br]@SBA-15 and VEIM[Br]@imine-1) was first examined by the FT-IR technique. The IR spectra of all hybrid materials (Figure 3.14) reveal that the majority of the signals correspond to those belong to the host materials. Nevertheless, low intensity signal at the wavenumber of 1660 cm^{-1} was observed in all spectra. The new emerging peak is in the fingerprint region of C=N and well corresponding to the stretching of C=N in the imidazolium ring of IL. These results indicate the coexistence of hosts and VEIM[Br] in hybrid materials. To further elaborate the result discovered by IR analysis. The MAS-^{13}C NMR spectroscopy was utilized to clarify the coexistence of VEIM[Br] and COF-5. MAS-^{13}C NMR spectrum of COF-5 shows the signals in aromatic region at the chemical shifts of 102.6, 123.6, 133.2 and 146.0 ppm related to the different environments of carbon atoms as assigned in Figure 3.15b.[81] While MAS-^{13}C NMR spectrum of VEIM[Br] is in line with that of the liquid $^{13}C\{^1H\}$ NMR spectrum displaying the resonances at the chemical shifts of 12.08, 45.63, 110.6, 118.7, 126.1, 128.3 and 134.2 ppm related to the labelled **g**, **f**, **a**, **e**, **d**, **b** and **c** carbon atoms as shown in Figure 3.15a. The MAS-^{13}C NMR of VEIM[Br]@COF-5 (Figure 3.15c) shows both signals at aromatic and low-intensity signals of aliphatic regions, the latter is well corresponding to the ethyl substituent of VEIM[Br]. Although, both IR and MAS-^{13}C NMR analyses confirm the coexistence of both VEIM[Br] and COF-5, the exact location of IL cannot yet be identified with these techniques. Complimentary techniques such as PXRD, BET, TGA are hence required (*vide infra*).
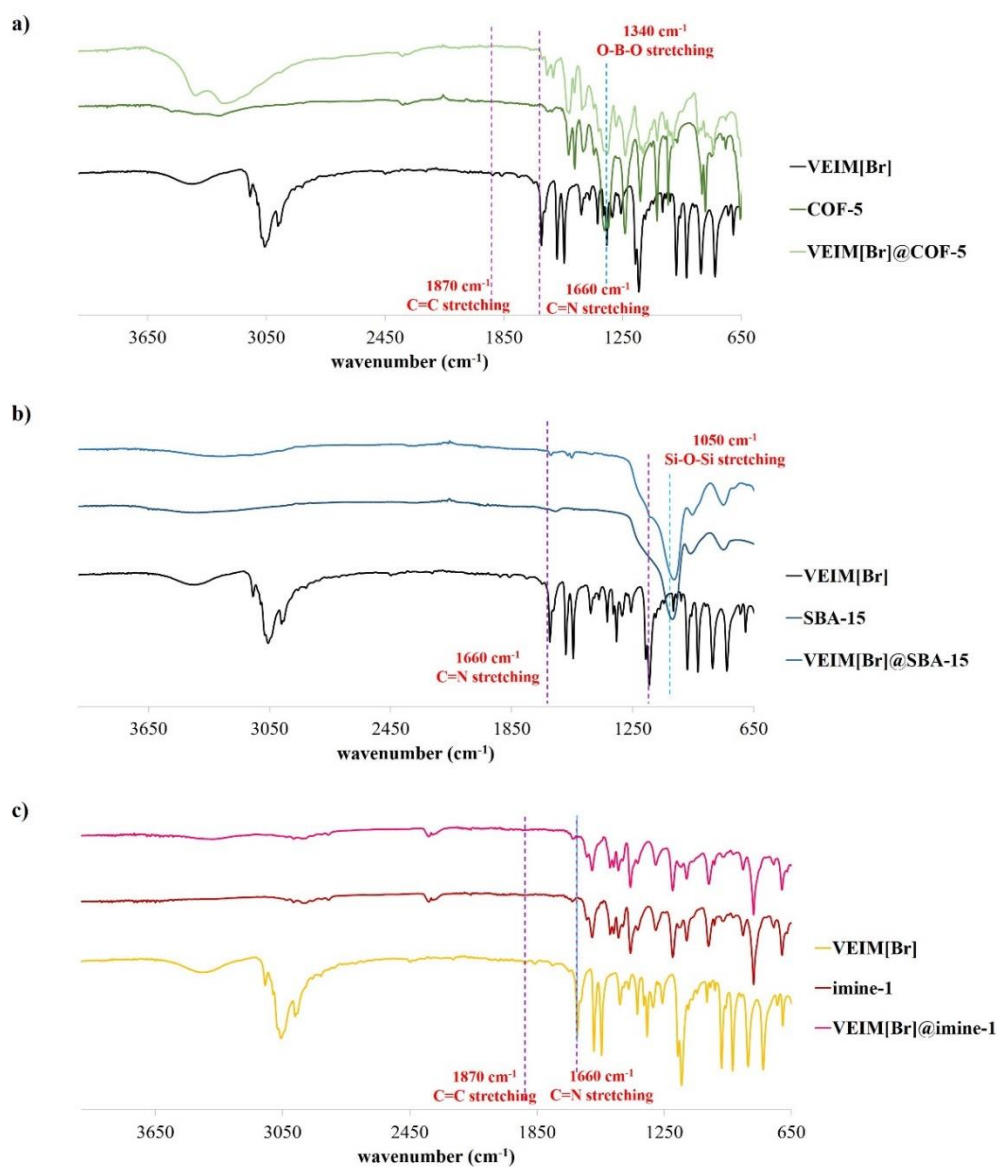
Figure 3.14 The comparison of FTIR data of the infiltrated samples of a) VEIM[Br] and COF-5 series, b) VEIM[Br] and SBA-15 series and c) VEIM[Br] and imine-1 series.
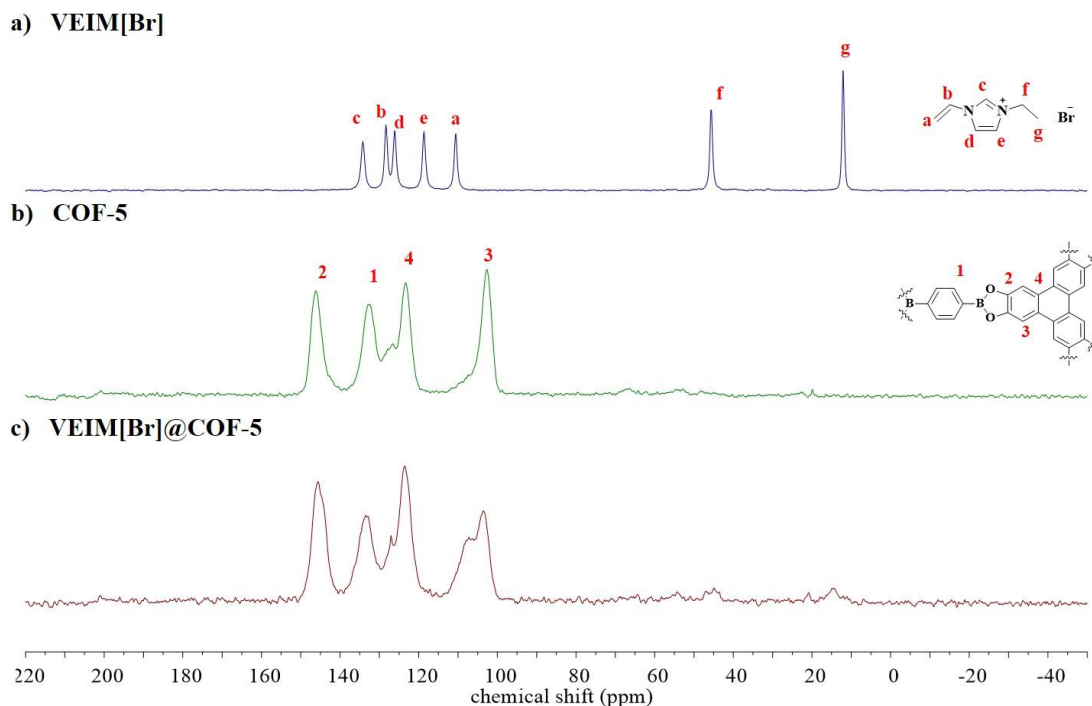
Figure 3.15 The solid-state MAS-^{13}C NMR spectra of a) VEIM[Br], b) COF-5 and c) VEIM[Br]@COF-5.

Characterization: PXRD

PXRD pattern of hybrid materials, VEIM[Br]@COF-5, shows obvious decreases in intensity compared to the parental COF-5, especially the dominant peak at 2θ of 3.5 degree (100) (Figure 3.16). The decreasing trends in signal intensity are observed across all hybrid materials even with the more rigid host – SBA-15 or the moisture-insensitive imine-based COF – imine-1. The decrease in intensity implies the lower crystallinity of the hybrid materials upon the addition of IL. These phenomena are related to the observations made for other infiltration materials such as the encapsulation of an 1-ethyl-3-methylimidazolium bis(trifluoromethylsulfonyl) imide (Emim[NTf$_2$]) inside the pores of a 3D COF-320 or a polyaniline intercalation into a pore of MIL-101.[43, 82] Nevertheless, the crystallinity of the host materials was reduced probably due to the decline in structural orders of the porous materials as the VEIM[Br] molecules are in the porous cavities.

Even though, these IR and XRD results could confirm the occupancy of the ILs in the pores of host materials, but it still cannot precisely identify that the VEIM[Br] molecules are residing within the internal cavities of the porous materials. Therefore, weight loss behavior of IL in the hybrid materials were carried out by TGA technique (*vide infra*).

Figure 3.16 The PXRD spectra show the comparison of the inserted samples of a) VEIM[Br] and COF-5 series, b) VEIM[Br] and SBA-15 series and c) VEIM[Br] and imine-1 series.
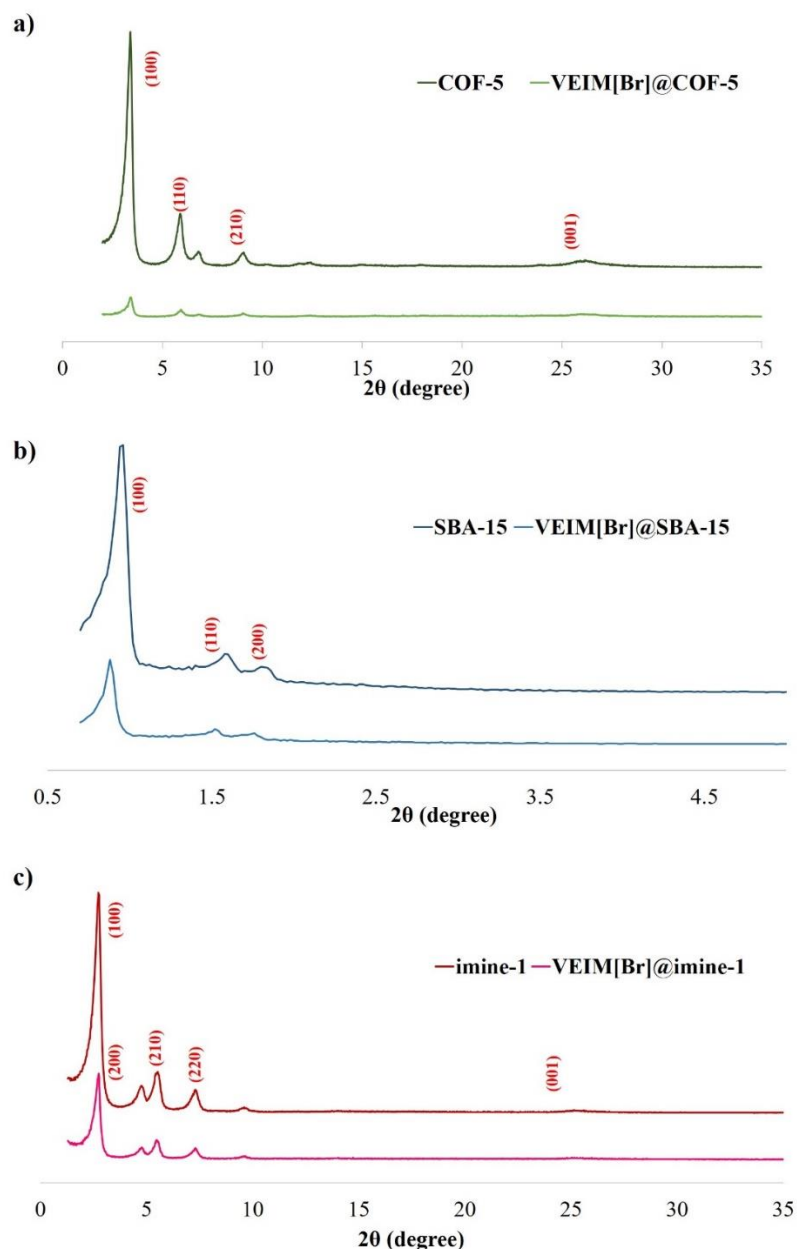
Characterization: TGA

Thermogravimetric analysis (TGA) results for all hybrid materials (Figure 3.17) show weight loss behaviors before 100 °C possibly from the low boiling point solvents and also the moisture in the samples. For the pristine COF-5 and imine-1 (Figure 3.17a (brown-line), b (navy-line)), the TGA profiles imply high thermal stability of both materials. The gradually decomposition starts at the temperature around 600 °C for COF-5 and at the lower temperature of ca. 450 °C for imine-1. It is noteworthy to mentioned that the imine-1 undergoes complete decomposition before 800 °C, whilst this is the case observed in COF-5. The gradual decomposition in the porous layered structures (COF5 and imine-1) could probably be explained by the sliding of the stacking sheets, which possibly be occurred prior to the degradation of each sheet at higher temperature.

The TGA profile of the monomeric VEIM[Br] itself exhibits a shape degradation behavior starting around 300 °C (Figure 3.17 (black-line)) indicating the single environment of VEIM[Br]. In the cases of hybrid materials, the decomposition temperature of infiltrated IL in VEIM[Br]@COF-5 and VEIM[Br]@imine-1 seem slightly higher when compared with the pristine IL. Moreover, it is worth mentioning that the IL degradation in both hybrid materials do not show the single sharp signals, which imply the existence of more than one environment of infiltrated IL inside the pore. The arising environments could be caused by the interaction between IL to the inner surface of pores in confined spaces. This observation is agreeable with a previous report, whereby the confined IL inside the pore of MCM-41 was studied through a dielectric spectroscopic technique indicating charge transport and motional behavior of IL due to the interaction with the inner surface of MCM-41. The report also indicates 2 types of confined IL; the first is the IL forming an interfacial layer on the wall of the host material, and second one is the IL occupied in the core of porous channel.[77]

The quantitative amount of infiltrated ILs inside the porous materials was estimated from the percentage of weight loss in range of 300 to 550 °C for VEIM[Br]@COF-5 and 300-450 °C for VEIM[Br]@imine-1. The results show the value of %weight loss of 20 % of infiltrated VEIM[Br] in COF-5, which is close to a result obtained from an elemental analysis of 24 % of VEIM[Br] in this hybrid material. While, only 10 % of infiltrated IL was estimated in the case of VEIM[Br]@imine-1 powder. These results imply the successful of infiltration of VEIM[Br] into the pore of COF-5 and imine-1 with expected amount of infiltrated IL as seen in the precedent publication.[45]
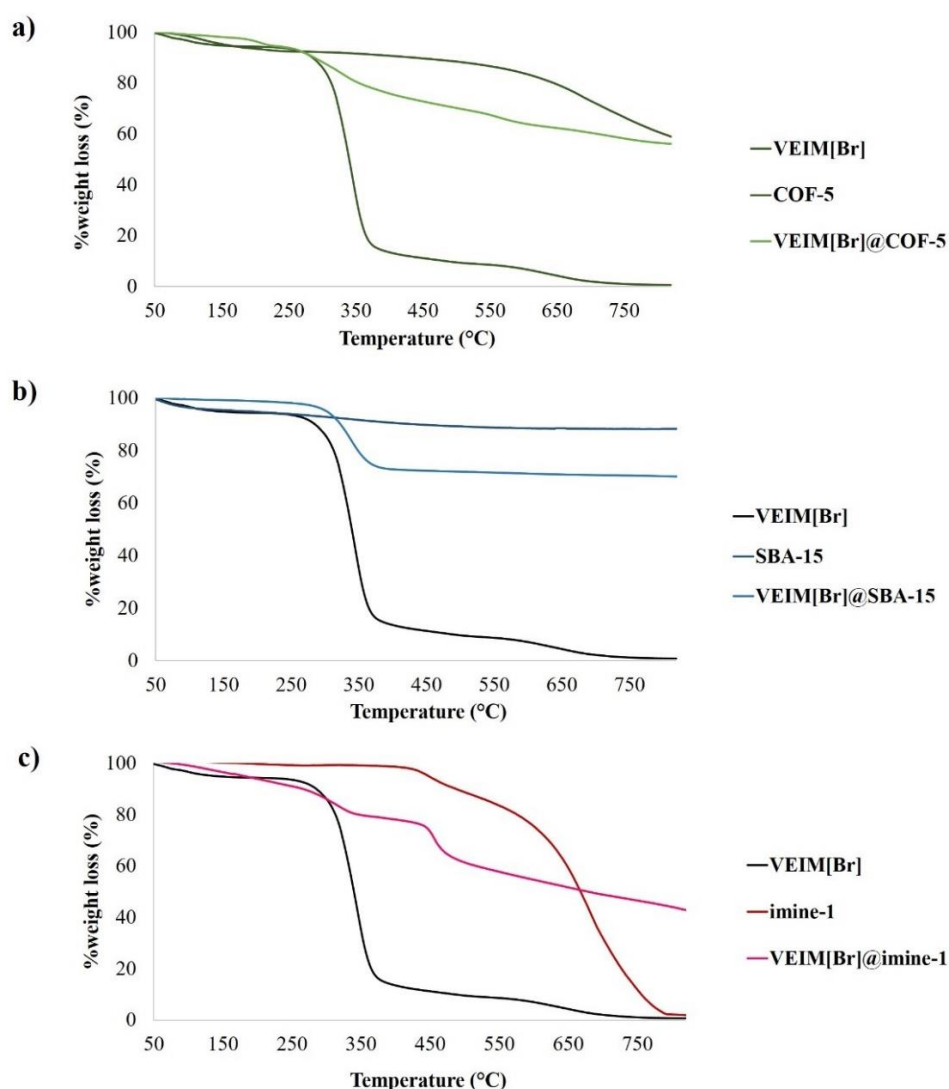
Figure 3.17 TGA profiles of the pristine materials and hybrid materials: a) VEIM[Br] and COF-5 series, b) VEIM[Br] and SBA-15 series and c) VEIM[Br] and imine-1 series.

In the case of VEIM[Br]@SBA-15, TGA result shows a single sharp profile of the decomposition of infiltrated IL around 300-350 °C as seen in pristine VEIM[Br] and no changes are observed after the temperature of 450 °C as the rigid SBA-15 remains unchanged (Figure 3.17b (blue-line)). Moreover, the TGA result of VEIM[Br]@SBA-15 indicates the higher of % loading of VEIM[Br] compared to other hybrid materials mentioned above, which was estimated around 30 %. This percentage is well agreed to the elemental analysis measurement, which was found to be 27 %. This is expected due to larger pore diameter (9.5 nm) of SBA-15. In addition, there is no clear cut between the degradation of IL and the degradation of layered porous materials (COF-5 and imine-1), compared to observation made in VEIM[Br]@SBA-15. This confirms the closer contact between the infiltrated IL and the inner surface of the smaller pores of COF-5 and imine-1 than the corresponding SBA-15. The higher degradation temperature of hybrid material, VEIM[Br]@COF-5 and VEIM[Br]@imine-1, than the parental porous materials were detected. This suggests the higher thermal stability of hybrid material than the sole materials.[45] The differences in degradation temperatures and behaviors suggest the successful infiltration of IL in the porous cavities of the materials.

Characterization: BET

Brunauer-Emmett-Teller (BET) surface area of the infiltrated VEIM[Br]@SBA-15 and VEIM[Br]@imine-1 were measured to be 350.6 and 1128 m^2 g^{-1}, respectively, with reversible type IV isotherm behaviors. The BET surface areas of VEIM[Br]@SBA-15 and VEIM[Br]@imine-1 are around half of those pristine hose materials (Table 3.3). The observation is well in line with an encapsulation of fullerene (PCBM) molecules inside the 1D channels of TT-COF reported by Dogru *et al.* in 2013 and the modification of the wall of 2D ZnPc-COF with fullerene reported by Chen *et al.* in 2014.[26, 75] These decreases in pore volumes of VEIM[Br]@ SBA-15 (from 662.0 to 350.6 m^2 g^{-1}) and VEIM[Br]@imine-1 (from 1767 to 1128 m^2 g^{-1}) together with the previously mentioned analysis results suggest the successful infiltration of VEIM[Br] and hence the VEIM[Br] is be believed to reside within the porous cavities.

Table 3.2 The BET data of the infiltrated and polymerized samples comparing with the pristine materials.

	COF-5	VEIM[Br]@COF-5 Vac. Infl.	VEIM[Br]@COF-5 Grinding	Poly VEIM[Br]@COF-5	VEIM[NTf$_2$]@COF-5	SBA-15	VEIM[Br]@SBA-15	VEIM[NTf$_2$]@SBA-15	imine-1	VEIM[Br]@imine-1	VEIM[NTf$_2$]@imine-1
Surface area (BET) (m^2 g^{-1})	1783	170.6	517.7	507.3	33.92	662.0	350.6	546.3	1767	1128	633.9
Pore volume (cm^3 g^{-1})	0.9708	0.1233	0.2795	0.3297	0.09715	1.048	0.7142	0.9583	1.257	0.7376	0.4736
Mean pore diameter (nm)	2.177	2.891	2.159	2.600	11.46	6.335	8.148	7.017	2.846	2.617	2.988
Popular pore diameter (nm)	2.43	2.43	2.43	2.43	2.43	8.06	7.05	9.23	2.43	2.43	2.43
Total surface (t-plot) (m^2 g^{-1})	1741	170.8	518.0	609.0	44.11	668.4	437.0	594.2	1848	1189	636.2
External surface (t-plot) (m^2 g^{-1})	56.99	15.66	26.49	33.78	42.59	45.86	46.46	56.17	119.3	47.40	57.38
Internal surface (t-plot) (m^2 g^{-1})	1684	155.1	491.5	575.2	1.520	622.6	390.5	538.1	1729	1141	578.8

The observation made for VEIM[Br]@COF-5 shows slight difference to the others two porous materials. Whereby, only 10 % of the original pore volume and surface area was obtained after vacuum infiltration (from 1700 m^2 g^{-1} to 170 m^2 g^{-1}). This brought about the concern over the degradation by hydrolysis due to the presence of water in solvent used in the vacuum infiltration method. Thus, a control experiment was carried out to investigate the possible cause.

Control experiment was carried out whereby the COF-5 powder was stirred in chloroform (used after received), which include 2 %weight of amount of water (measured by Karl Fisher method) under the same condition as the vacuum infiltration method. The PXRD result still showing the clear finger print signal of COF-5 (Figure 3.18a) at 2θ of 3.5(100), 6.0 (110), 9.0 (210) and 26.5 (001) degree without the new signals of HHTP and BDBA as mentioned in the hydrolysis section. Meanwhile, the BET surface area shows the insignificant decrease from ca. 1700 m^2 g^{-1} to ca. 1500 m^2 g^{-1} with a reversible type-IV isotherm behavior (Figure 3.18b). So, these results confirm that all the decline of the signals is not caused by the hydrolysis of COF-5 due to the moisture in solvent but by the residing ILs inside the pores.
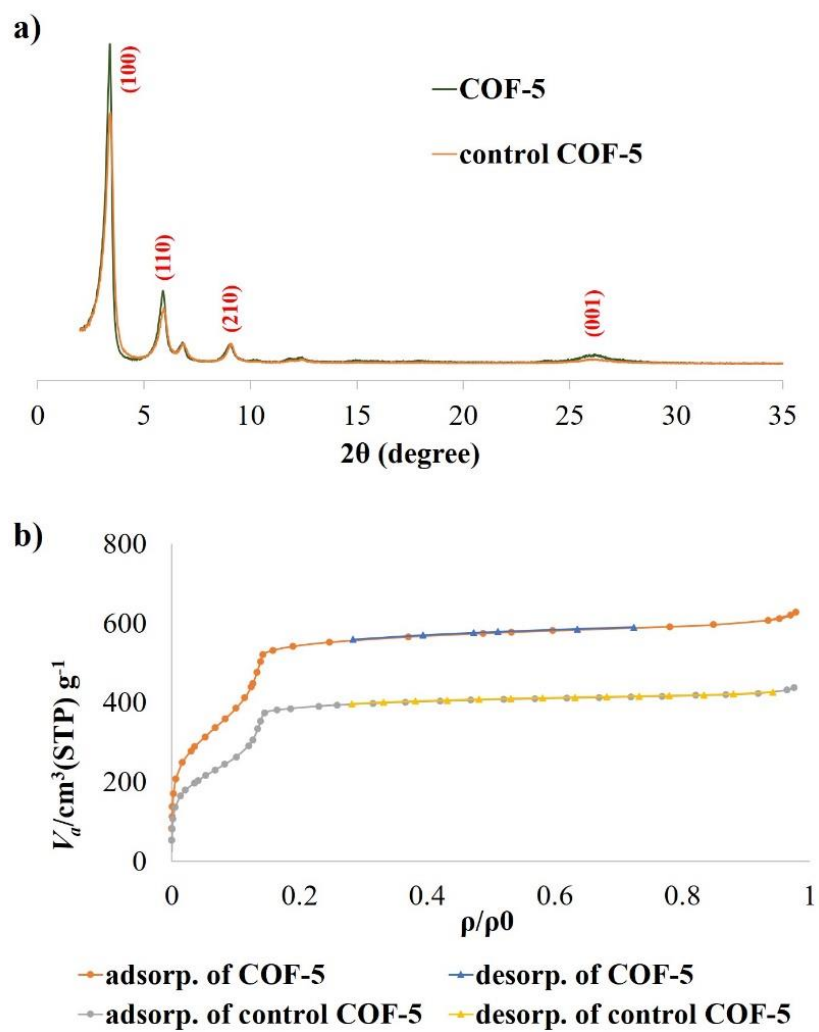
Figure 3.18 The comparison data between the as-synthesized COF-5 and the soaked COF-5 in chloroform for 24 hours: a) PXRD spectra and b) N$_2$ adsorption-desorption isotherms.

3.3.1.2 Infiltration of VEIM[NTf₂]

From the preliminary results of the model studies mentioned in section 3.2, the VEIM[NTf$_2$] show some interactions with boron atoms in boroxine linkages resulting in the additional small signal in ^{11}B-NMR spectrum at the chemical shift of 12 ppm corresponding to the formation of (RO)$_2$BR'·SO$_2$R$_2$ (R and R' refer to alkyl or aryl groups). Nevertheless, the infiltration of VEIM[NTf$_2$] into the pore of porous materials was still attempted. In this research, a 0.64 M solution of VEIM[NTf$_2$] in suitable solvent (stated in table 2.1) was added into the porous materials and the procedure was manipulated according to the section 3.3.1.1. The infiltrated products were denoted as VEIM[NTf$_2$]@COF-5, VEIM[NTf$_2$]@SBA-15 and VEIM[NTf$_2$]@imine-1.

FT-IR results of all hybrid materials of VEIM[NTf$_2$] (Figure A6) shows the majority of the signals belonging to the host materials. The signals with the wavenumbers of ca. 1350 cm^{-1} and 1660 cm^{-1} corresponding to the stretching of S=O bond in bis(trifluoromethylsulfonyl) imide cation of IL and the stretching of C=N bond of an imidazolium moiety of the IL, respectively, are expected in the IR spectra of VEIM[NTf$_2$]@COF-5, VEIM[NTf$_2$]@SBA-15 and VEIM[NTf$_2$]@imine-1. Unlike the observations meet with VEIM[Br], no expected signals can be evaluated. The success of infiltration is hence questionable in this case.

The PXRD pattern of VIEM[NTf$_2$]@COF-5 and VIEM[NTf$_2$]@imine-1 (Figure A7) indicate that the two hybrid materials are amorphous, whilst the decrease in intensity of PXRD peak was observed in VEIM[NTf$_2$]@SBA-15. For the BET results, the characteristic behavior of a non-porous amorphous material is obtained in VEIM[NTf$_2$]@COF-5, whereby the almost decrease of surface area and type II isotherm were observed compared with a sole COF-5 (from 1780 m^2 g^{-1} to 33.92 m^2 g^{-1}) (Table 3.2). While the BET result of VEIM[NTf$_2$]@imine-1 indicates that the VEIM[NTf$_2$]@imine-1 should be an amorphous porous material because the type IV isotherm was obtained, which is a characteristic isotherm of the porous materials. Moreover, the BET data of VEIM[NTf$_2$]@imine-1 also shows the value of surface area of 633.9 m^2 g^{-1} and pore volume of 0.4736 cm^3 g^{-1}, which confirms a porous material of VEIM[NTf$_2$]@imine-1. Nevertheless, the TGA profiles of

VEIM[NTf$_2$]@COF-5 and VEIM[NTf$_2$]@imine-1 indicate the low-temperature decompositions (270 °C and 70 °C, respectively) of deconstructed hybrid materials. The deconstruction of these two hybrid materials could be originated from the Lewis acid-base interactions of the sulfone moieties of NTf$_2^-$ anions to the boroxine linkages in COF-5 or the nucleophiles addition of the sulfone moieties of NTf$_2^-$ anions to the imine linkages (Figure 3.19). While crystallinity of SBA-15 is retained, however, due to a small decrease of surface area and pore volume of VEIM[NTf$_2$]@SBA-15 compared to the pristine one (from $S_a = 662.0$ m^{2}g^{-1}, $V_p = 1.048$ cm^3 g^{-1} to $S_a = 546.3$ m^{2}g^{-1}, $V_p = 0.958$ cm^3 g^{-1}). This suggests a small portion of infiltrated IL being successfully incurred. This agrees well with the TGA result, whereby the profile shows only 10 %wt of IL being detected. Of which the infiltrated amount of VEIM[NTf$_2$] in VEIM[NTf$_2$]@SBA-15 is noticeably less than the corresponding amount of VEIM[Br] in the same host material. This infers that the states of IL may affect the infiltrating capacity of ILs. In this case, the liquidified VEIM[NTf$_2$] and the larger pore size of SBA-15 (9.0 nm) than other two materials (2.7 and 3.0 nm) might possibly be leached out under the condition of the vacuum filtration method.

Even though, those results indicate the unsuccessfully infiltration of VEIM[NTf$_2$] into pores of porous materials, but some further specific techniques such as computational studies, dynamic activity, *etc* are still required to obtain deep information to explain the coexistence between porous materials and ILs. Therefore, in this research, we mainly focus on a using of an infiltrate VEIM[Br] in porous materials.

3.3.2 Grinding process

To avoid the use of excessive of solvent and high equivalent of IL, which risks the hydrolysis of COF-5. The grinding method was attempted whereby the 900 µL of dried chloroform and 1 equivalent of IL were used. The grinding method are used in previous reports[43, 45] to infiltrate the IL molecules into the pore of porous material, which are rely on the physical force to enter the IL into the pore cavities. To optimize the formation and physical properties of VEIM[Br]@COF-5, the grinding method was introduced. The mixture of COF-5 powder and 5.6 M solution of VEIM[Br] in dried chloroform was grinded in an agate mortar until visually dried. After the manipulation, the as-synthesized VEIM[Br] was characterized by PXRD technique, surface analysis, TGA and elemental analysis. PXRD spectrum of VEIM[Br]@COF-5 reveals the visually decrease of the signal intensity (Figure 3.19a). It is noteworthy that new small signals emerge in the range of about 15-30 degree, which are presumed to be the signals of VEIM[Br] in its solid state as mentioned in the previous report.[43] Figure 3.19b shows the N_2 adsorption-desorption isotherm of the as-synthesized VEIM[Br]@COF-5 from the grinding method indicating type-II isotherm of non-porous material. The BET surface area suggests a very low surface are of 80 m^2 g^-1. TGA profile illustrates the shape decomposition of 40 % of weight loss of VEIM[Br] in the hybrid materials whilst the elemental analysis indicates 60 %. All the analysis results point towards the presence of VEIM[Br] on the external surface area of host materials.
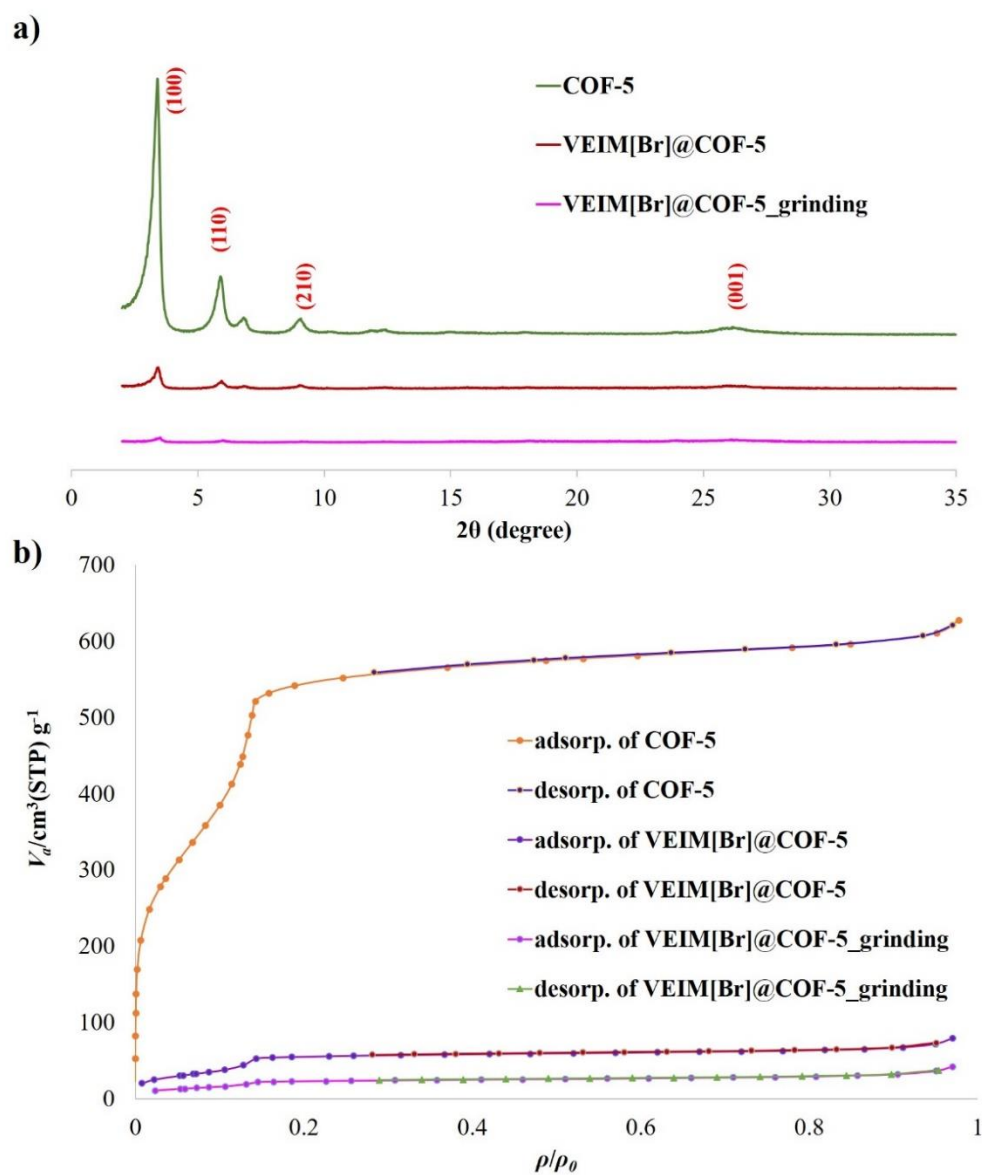
Figure 3.19 The comparison data between the VEIM[Br]@COF-5 products from a vacuum infiltration method and grinding process; a) PXRD spectra and b) N_2 adsorption-desorption isotherms.

As a consequence, the hybrid product was washed with dried dichloromethane 3 times to remove the excess VEIM[Br] adhering on the external surface. The PXRD of the washed product (Figure 3.20a (blue line)) shows an increase of intensity at 2θ of 3.5 (100) degree comparing to the anterior one, which could imply the renewal of its crystallinity by elimination of excess IL. Moreover, the BET surface area reveals a higher value of the BET surface area of 518 m^2 g^{-1} when compared to the as-synthesized product and also to the hybrid product derived from the vacuum infiltration method as mentioned in section 3.1 (170 m^2 g^{-1}). In addition, the TGA profile (Figure 3.20b) shows 20 %wt of VEIM[Br] in the hybrid material product, which was equally found in the product obtained from the vacuum infiltration method.
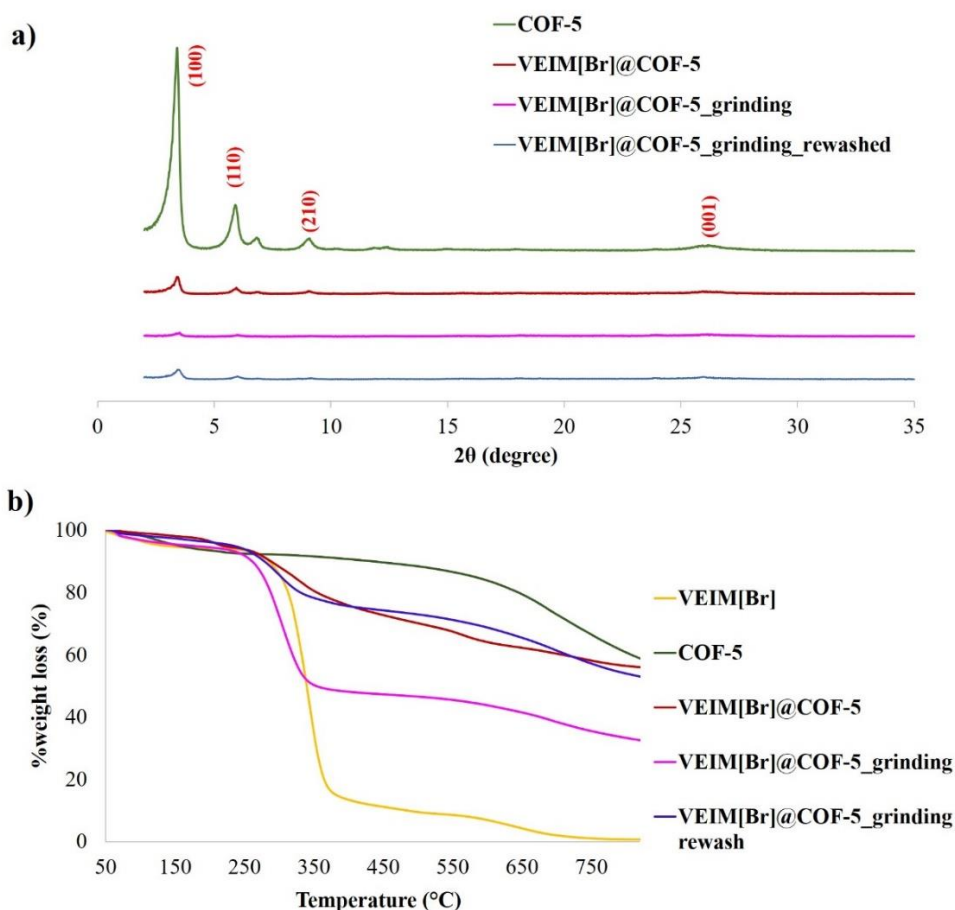
Figure 3.20 The comparison data between the VEIM[Br]@COF-5 products from a vacuum infiltration method, grinding method and after rewashed with dried CH₂Cl₂; a) PXRD spectra and b) TGA profiles.

3.4 *In situ* infiltrated ILs polymerization

In 2008, Uemura *et al.* demonstrated the use of nanochannel of porous coordination polymers (PCP) as a templating host to generate *in-situ* polymer chains of styrene, methyl methacrylate, and vinyl acetate with specific molecular weight and stereoregularity.[83, 84] Nevertheless, to obtain the isolated polymers, the porous material have to be destroyed. Therefore, we are attended to explore the properties of the hybrid materials between porous materials and poly(ionic liquids) (PILs). From the results of infiltrating materials, VEIM[Br]@COF-5 exhibits the good information of the successful infiltration *via* a vacuum infiltration method, so we extended this material into the *in-situ* polymerization experiment.

In the past studies, the *in-situ* polymerization was done in such a condition that allow liquidiflied mixture of monomer and radical initiator. For example, the *in-situ* polymerization of an acrylonitrile inside the pore of mesoporous organosilica and the carbonaceous nanostructured material had to be dissolved in distilled acrylonitrile prior to the polymerization process.[85] However, the *in-situ* polymerization in our work was thought to be done using a solvent-free condition, thus we applied the melting of the IL to its liquidified state instead of the use of solvent.[42, 45, 86] The polymerization was initiated by radical initiator using 2,2'-azobisisobutyronitrile (AIBN). Moreover, as known in literature reports, IL can be undergone by phase transition of solid crystalline material, crystalline liquid and isotopic liquid. For the previous report, a 1-butyl-3-methylimidazolium bromide (BMIM[Br]) resembling to our VEIM[Br], was found the melting temperature onset of 78 °C and the glassy transition of -65 °C. At those point, the (BMIM[Br]) are in transition states between solid to liquid and liquid to glassy solid, respectively.[87] Therefore, we explored the *in-situ* polymerization of VEIM[Br] in COF structure by using the higher temperature than the phase transition of solid to liquid state (more than 78 °C). The experiment was carried out whereby the VEIM[Br] and AIBN were first synthesized *via* a vacuum infiltration method. The obtained infiltrated material, VEIM[Br]+AIBN@COF-5 was heated at 80 °C for 24 hours in solvent-free condition under an inert atmosphere of nitrogen to obtain the polymerized hybrid material, so called polyVEIM[Br]@COF-5. polyVEIM[Br]@COF-5 will be further use as a heterogeneous catalyst for cycloaddition reaction of CO_2 with epoxide.

For the characterization, PXRD result of polyVEIM[Br]@COF-5 indicates the slight increase of signal comparing to the infiltrated one (Figure 3.21a), which is assumed as caused by the higher ordered-alignment of PILs along the 1D-channel of COF-5. In the same way, the BET internal surface area of polyVEIM[Br]@COF-5 was increased to be 575 m^2 g^{-1} (from 155 m^2 g^{-1} of VEIM[Br]@COF-5, Table. 3.2), which is agreeable with the assumption as mentioned above. The TGA data of the polymerized sample (Figure 3.21b) displays a similar behavior of decomposition temperature profile to an infiltrated product, VEIM[Br]@COF-5. Anyway, IR spectrum of polyVEIM[Br]@COF-5 shows no obvious changing of the signals comparing with the result of infiltrated product (Figure 3.21d), which imply that the polymerization of VEIM[Br] in all of porous materials do not cause any structural damaging.

The attempt to confirm the successful formation of *in-situ* polymerization of VEIM[Br] was proceeded by using the differential scanning calorimetry technique (DSC). The differences in glass transition temperature (T_g) and melting temperature (T_m) allow the differentiation between the monomeric and polymeric VEIM[Br]. Nevertheless, no T_g and T_m signals were detected by DSC measurement. The other possibility to ensure the formation the formation of *in-situ* generated polymer is to destroy the COF framework by using acidic or basic condition and isolate the infiltrated polymeric IL of which can be measured by gel permeation chromatography (GPC) and matrix assisted laser desorption/ionization with time of flight mass spectrometry (MALDI-TOF-MS). Due to the limitation of accessibility to the water-column of GPC, the investigation shall be done a further study. At this point, although polyVEIM[Br] is thought to be generated, however the successful formation is still doubtful.
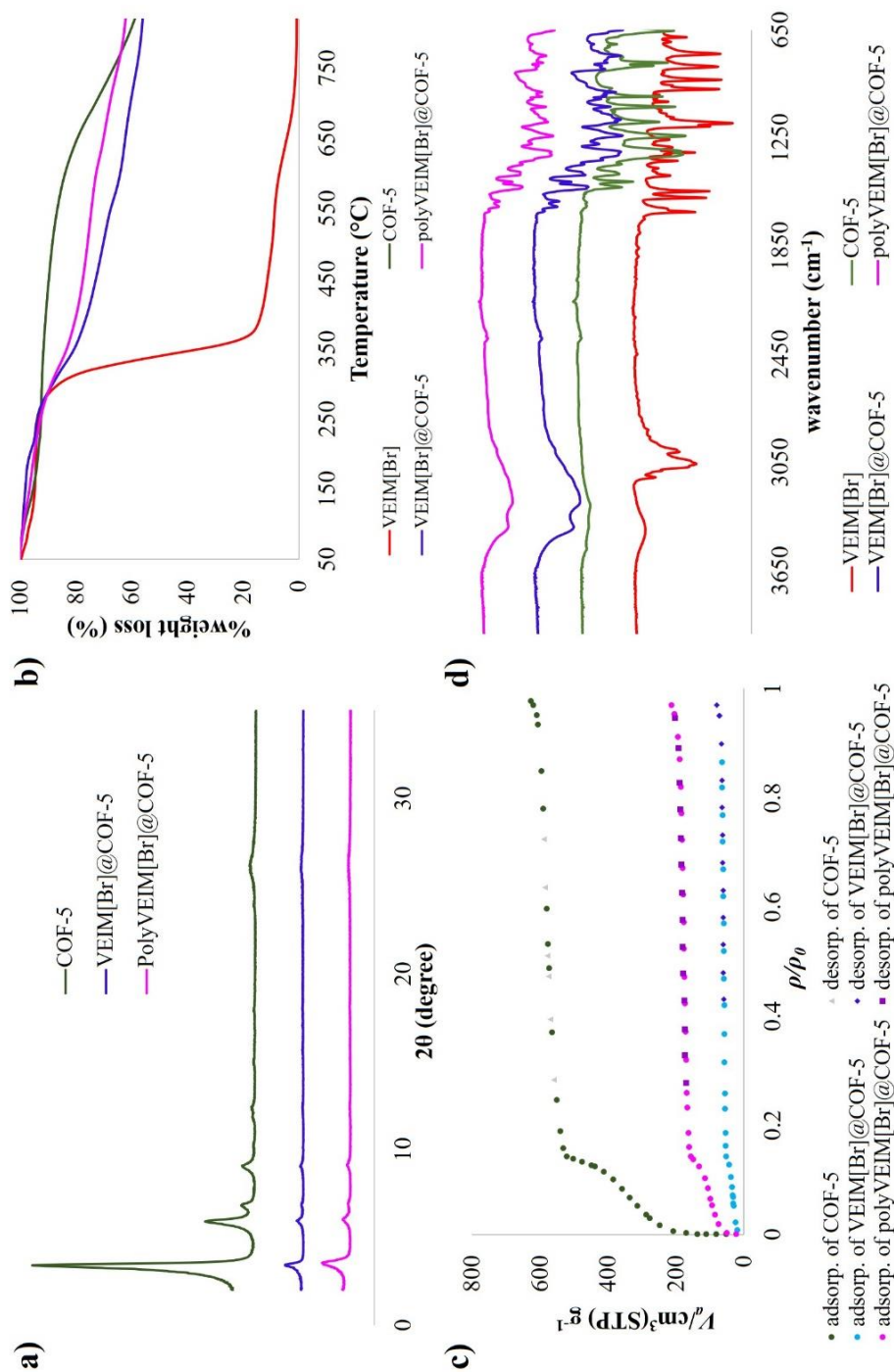
Figure 3.21 The characterization results of polyVEIM[Br]@COF-5 compared to the sole materials and VEIM[Br]: a) PXRD spectra, b)TGA profile, c) N₂ adsorption-desorption isotherm and d) FT-IR spectra.

3.5 Applications: Catalytic activity for CO_2 addition reaction

Recently, it is witnessed that the synergistic effect has play an important role effectively catalyzing the cycloaddition of CO_2 and epoxides. The synergistic effect in these reactions is a concurrence of a Lewis acid site and a Lewis base site to accelerate the reaction. The development of MOF[45, 65, 88] and COF[41, 44, 89, 90] as Lewis acidic hosts in the reaction has been continuously reported. In this work, the hybrid material of VEIM[Br]@COF-5 is composed of boroxine linkages and bromide ions, which act as Lewis acid sites and Lewis base sites, respectively. Moreover, from an ammonium temperature-programmed desorption (NH_3-TPD), the result indicates the high surface acidic sites to 1,000 folds higher than SBA-15 and 10-50 times higher than MIL-101. Therefore, this hybrid material is expected to perform as a catalyst in the cycloaddition reaction between CO_2 and epoxides.

Here in, the catalytic activity performance of VEIM[Br]@COF-5 upon the cycloaddition of CO_2 was preliminary demonstrated using propylene oxide as a substrate with an adapted condition from a previous report.[44] Under 10 MPa of CO_2 pressure in a high-pressure reactor, propylene oxide (5 mL, 60 mmol) and catalyst (15 mg, 0.03 mmol of Br^-) were heated at 60 °C for 20 hours in neat. After the reaction, the heterogeneous catalyst was filtrated to leave the clear filtrate. This affirms that the VEIM[Br]@COF-5 behaves as a heterogeneous catalyst as expected. ^{1}H-NMR spectrum of the filtrate shows the resonance of the propylene oxide at 4.83, 4.53, 4.00 and 1.48 ppm corresponding the assigned protons as shown in Figure 3.22, together with characteristic resonances of a cyclic carbonate product, 4-methyl-1,3-dioxolan-2-one. The integration data shows a ratio of the product to the reactant in the reaction solution of 0.04:1 (4% yield, TON = 64, TOF = 3.2). These results indicate that the hybrid material can act as the catalyst in this reaction, but the catalyzing condition will to be optimized.
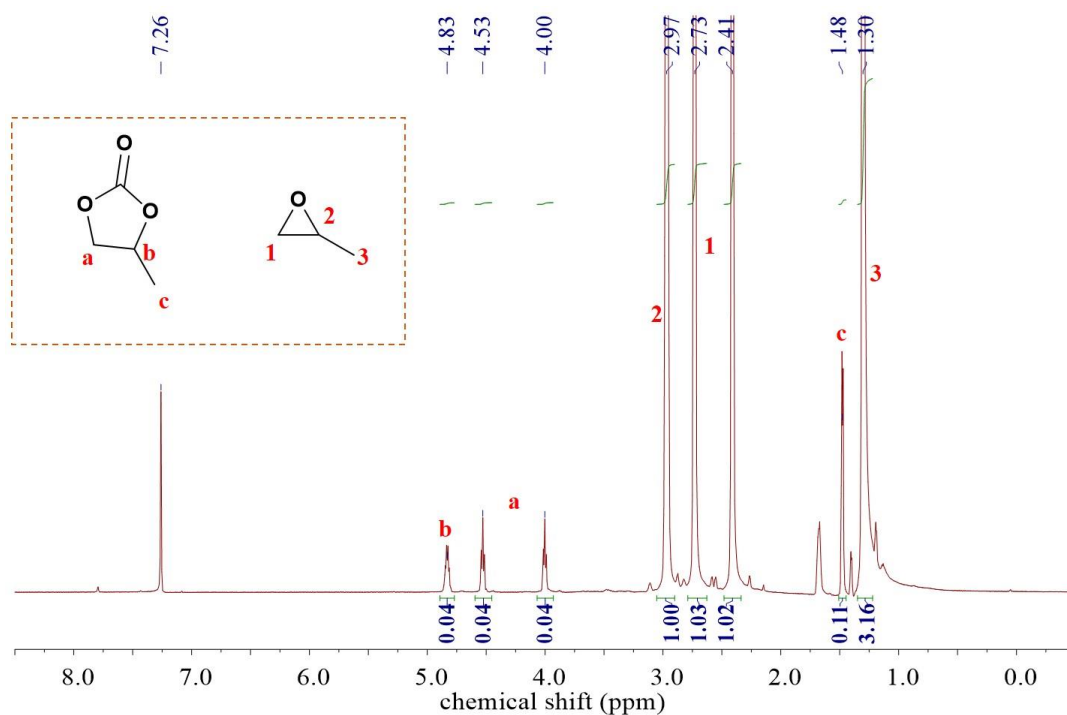
Figure 3.22 The ^{1}H-NMR spectrum of a supernatant obtained after the cycloaddition reaction of CO$_2$ on propylene oxide.

For the proposed mechanism as shown in Figure 3.23, the boroxine linkage in COF-5 acts as a Lewis acidic site activating the propylene oxide to become more prone to nucleophilic attack (intermediate I). Afterward, the less sterically hindered carbon atom of epoxide is attacked by the bromide anion to ring-open the epoxide to form an intermediate II. The intermediate subsequently inserts into the molecule of carbon dioxide forming a carbonate ester anion (intermediate III). Finally, the ring-closure of the intermediate IV takes place under a thermodynamic driven force giving a 5-membered ring cyclic carbonate and concurrently regenerating bromide anion to enter the new catalytic cycle.
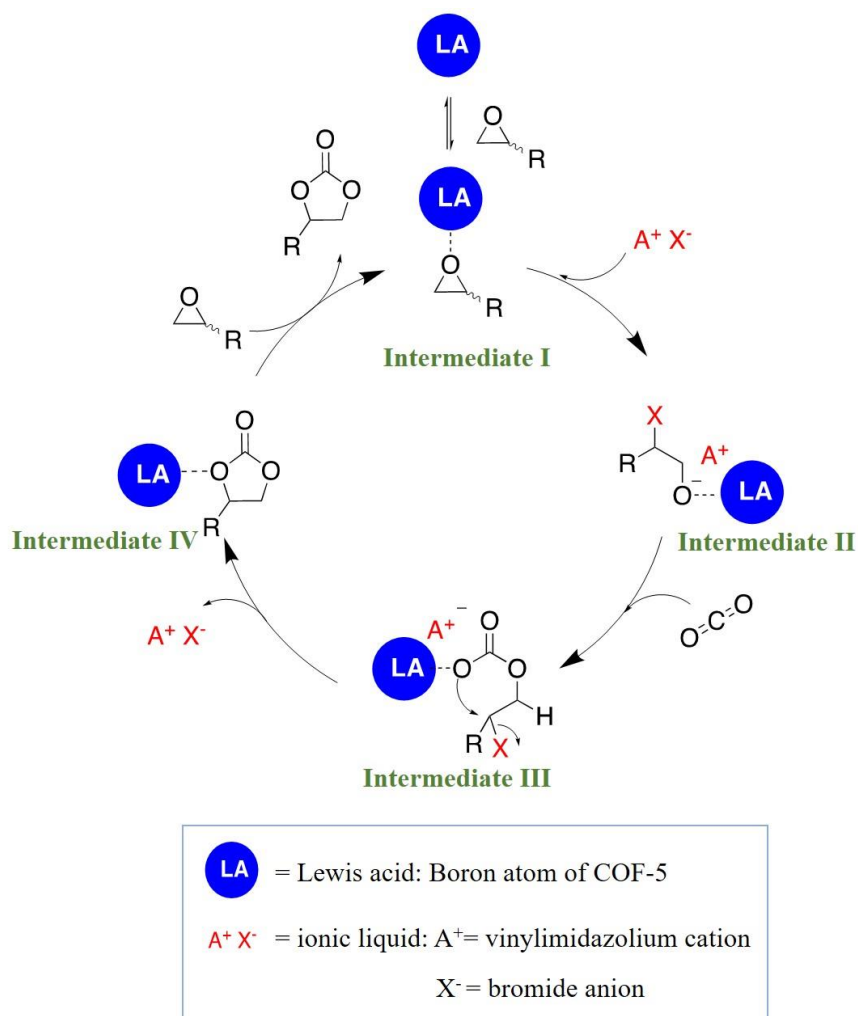
Figure 3.23 The proposed mechanism of a catalytic activity of VEIM[Br]@COF-5 in the cycloaddition reaction of CO₂ to a propylene oxide.

CHAPTER 4
Conclusion

In summary, we have successfully synthesized the boroxine-based COFs named COF-5 *via* a conventional heating of homogeneous condensation reaction. The as-synthesized COF-5 was manipulated and stored under an inert atmosphere due to the hydrolysis of COF-5. The ^{1}H-NMR results of model studies indicate no drastic interactions between the model compound (CAT-B) and vinylimidazolium-base ILs which imply the possibility of coexistence of that materials. To the infiltration, the novel hybrid materials, VEIM[Br]@COF-5, VEIM[Br]@SBA-15 and VEIM[Br]@imine-1 were successfully prepared *via* a vacuum infiltration method under a mild condition. The infiltrated materials exhibit the decreasing of an intensity in PXRD signals and also BET surface area comparing with the pristine host materials. These results indicate the occupying of IL molecules inside the cavities of porous material without a disruption on the matrix structure. Moreover, the *in-situ* polymerization of VEIM[Br]@COF-5 was attempted using a thermal radical initiator (AIBN) to yield a polyVEIM[Br]@COF-5 powder, of which the significant increase of PXRD signal and BET surface were observed. These imply the higher ordered-alignment of polymeric forms of VEIM[Br] along the 1D-channel of COF-5. However, the infiltration of VEIM[NTf$_2$] into porous cavities is still dubious of which a further detailed study has been carried out. Moreover, the new hybrid material, VEIM[Br]@COF-5 was attempted to use as a heterogeneous catalyst in a cycloaddition of CO$_2$ with propylene oxide. The result shows turnover number (TON) and turnover frequency (TOF) within 20 hours of 64 and 3.2 per hour, respectively, which calculated from the conversion ratio between the reactant and product by ^{1}H-NMR technique. Even through, the hybrid material is not yet be a highly effective catalyst, but it has shed some light on the further development of new hybrid materials.

APPENDIX
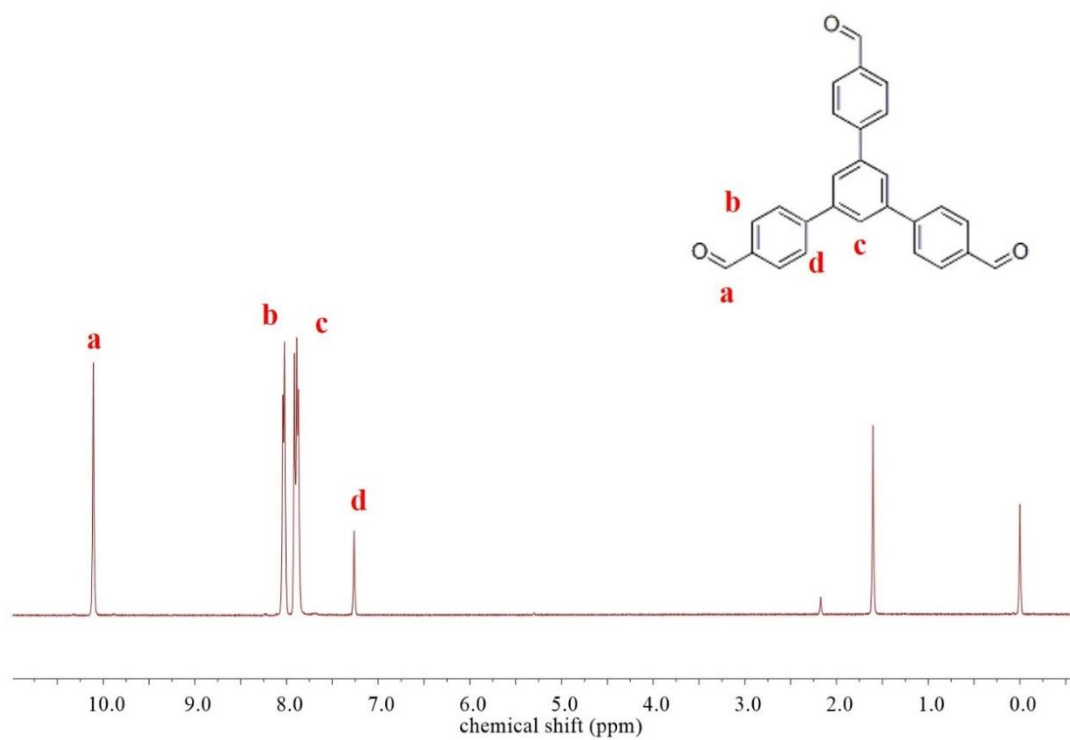
Figure A1 ^{1}H-NMR of 1,3,5-tris(4-formylphenyl)benzene (TPBA) in CDCl$_3$.
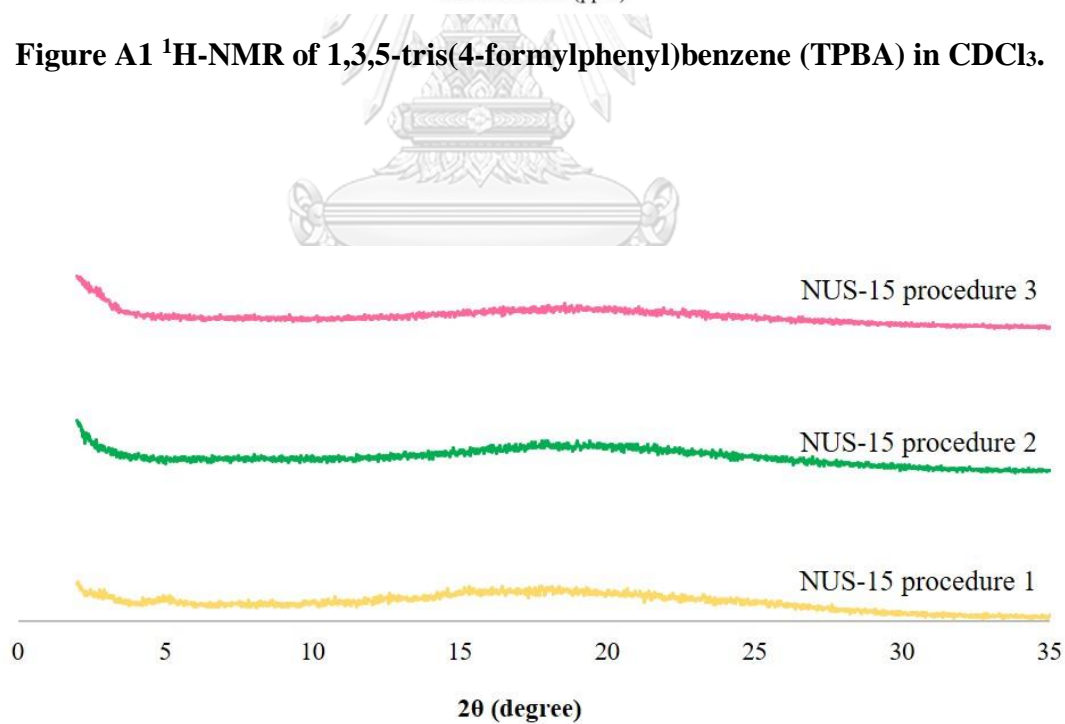
Figure A2 PXRD results of as-synthesized NUS-15.
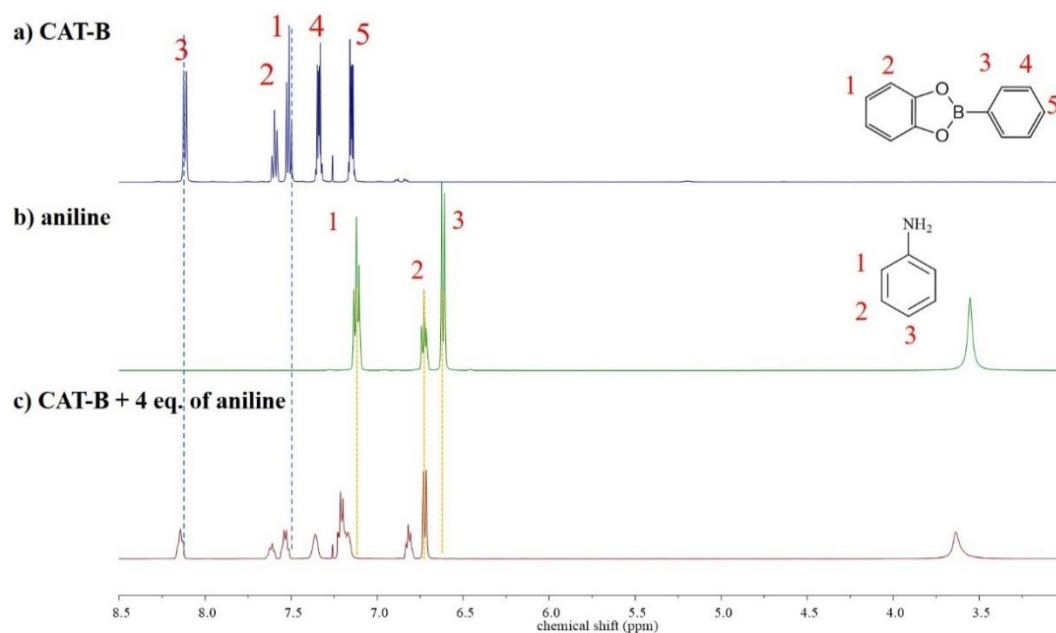
Figure A3 ¹H-NMR spectra of a) CAT-B, b) aniline and c) the mixture of CAT-B and aniline in deuterated CDCl₃.

Figure A4 ¹¹B-NMR spectra of a) CAT-B and b) the mixture of CAT-B and aniline in deuterated CDCl₃.

Figure A3 ^{1}H-NMR spectra of a) CAT-B, b) aniline and c) the mixture of CAT-B and aniline in deuterated CDCl₃.
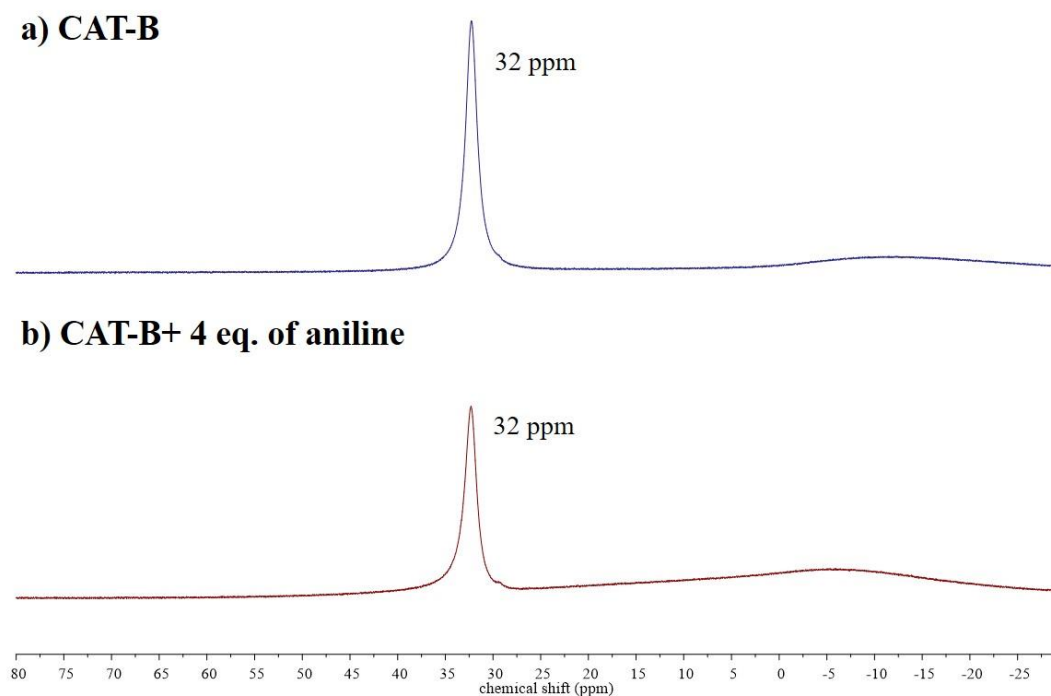
Figure A4 ^{11}B-NMR spectra of a) CAT-B and b) the mixture of CAT-B and aniline in deuterated CDCl₃.
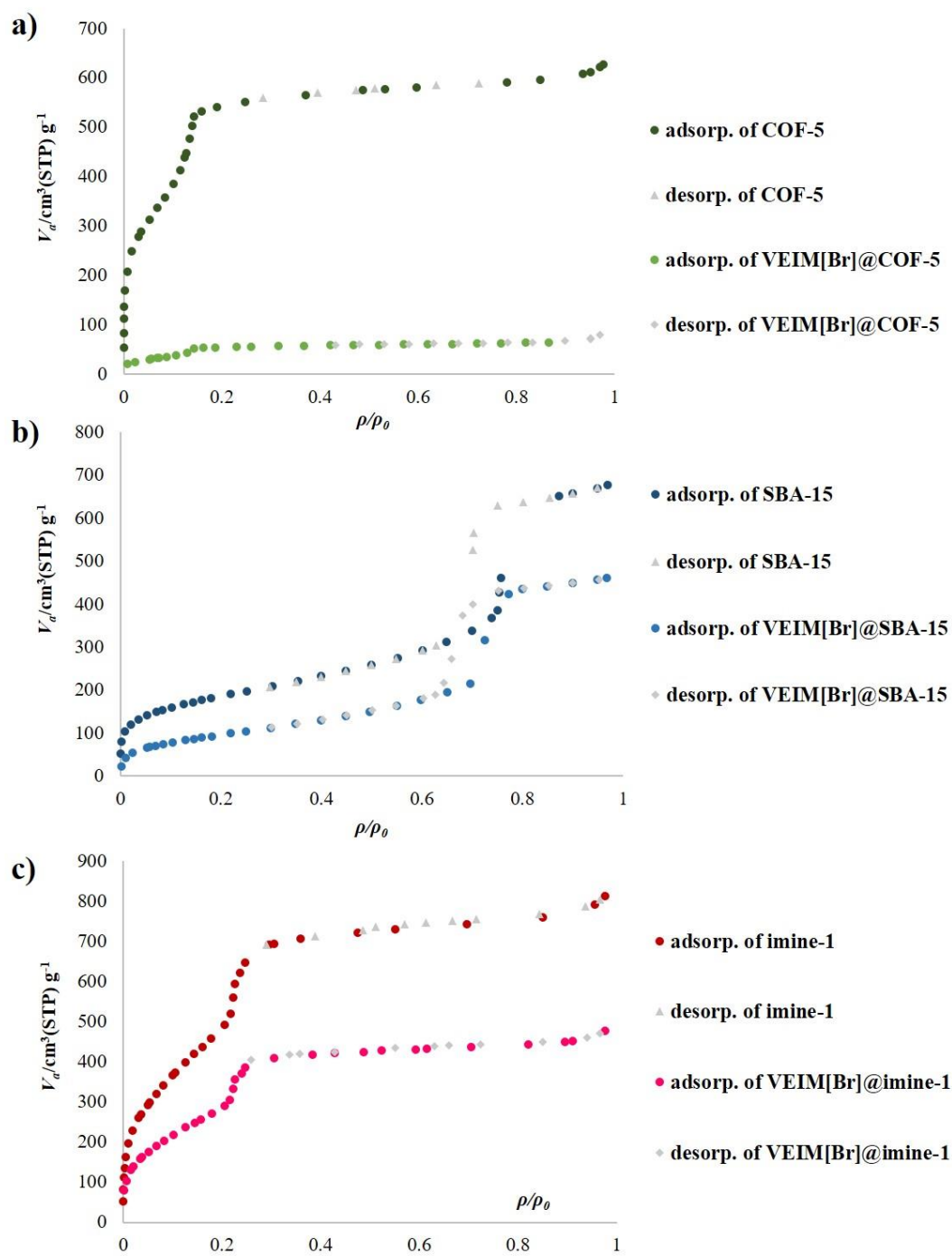
Figure A5 N$_2$ adsorption-desorption isotherm of infiltrated materials of VEIM[Br]: a) COF-5 series, b) SBA-15 series and c) imine-1 series.
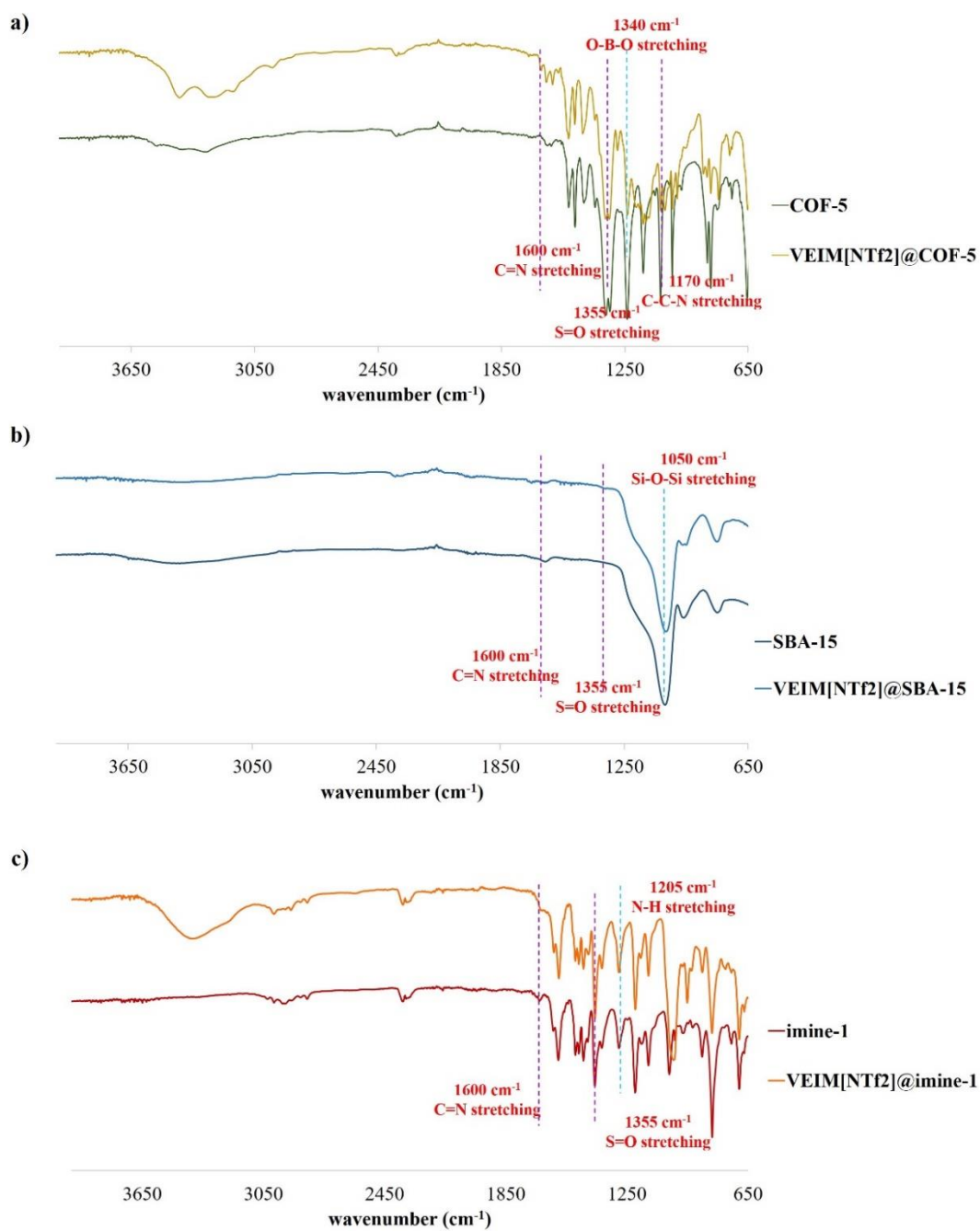
Figure A6 The comparison of FTIR data of the inserted samples of a) VEIM[NTf$_2$] and COF-5 series, b) VEIM[NTf$_2$] and SBA-15 series and c) VEIM[NTf$_2$] and imine-1 series.
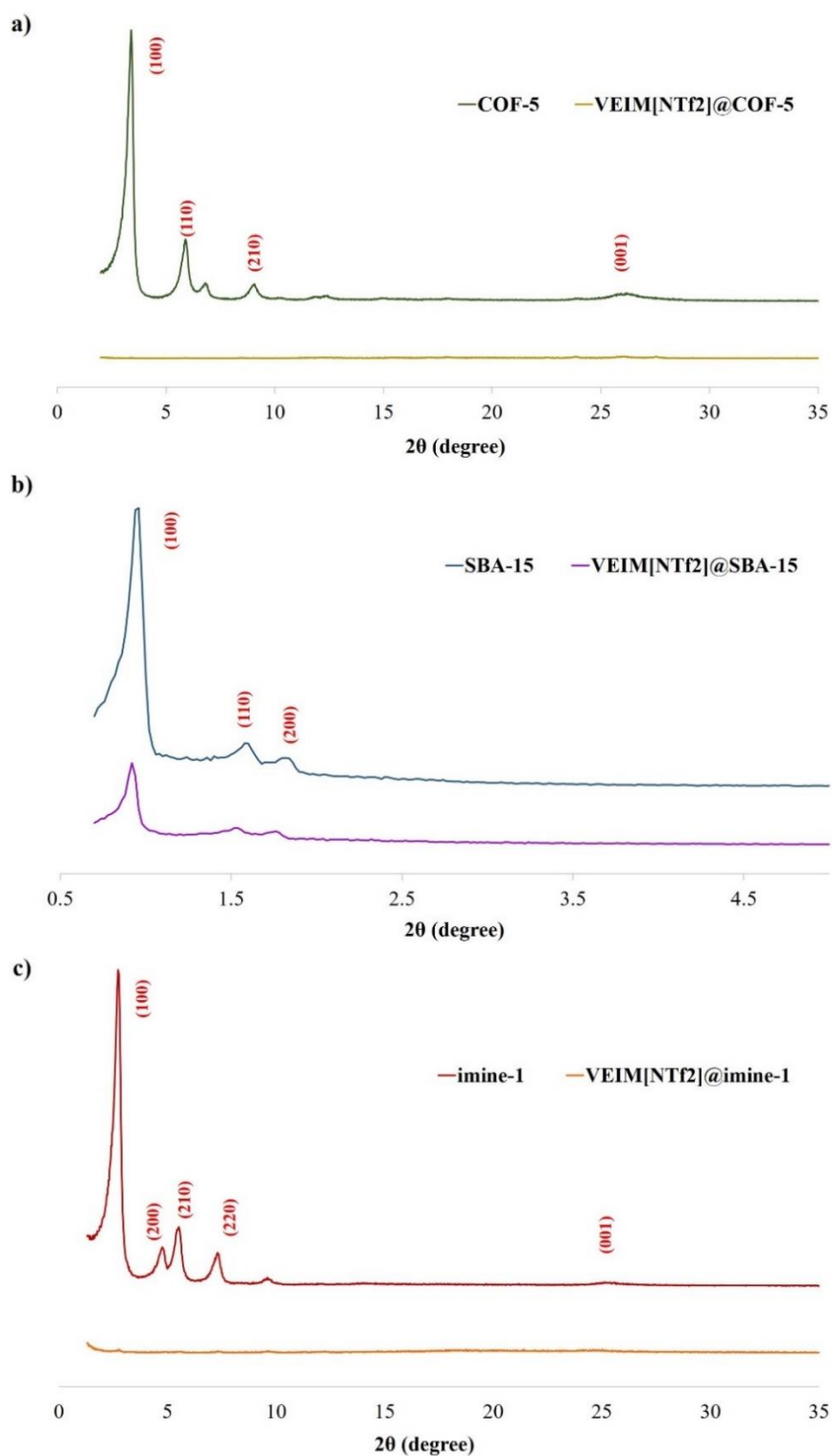
Figure A7 The PXRD spectra show the comparison of the inserted samples of a) VEIM[NTf$_2$] and COF-5 series, b) VEIM[NTf$_2$] and SBA-15 series and c) VEIM[NTf$_2$] and imine-1 series.
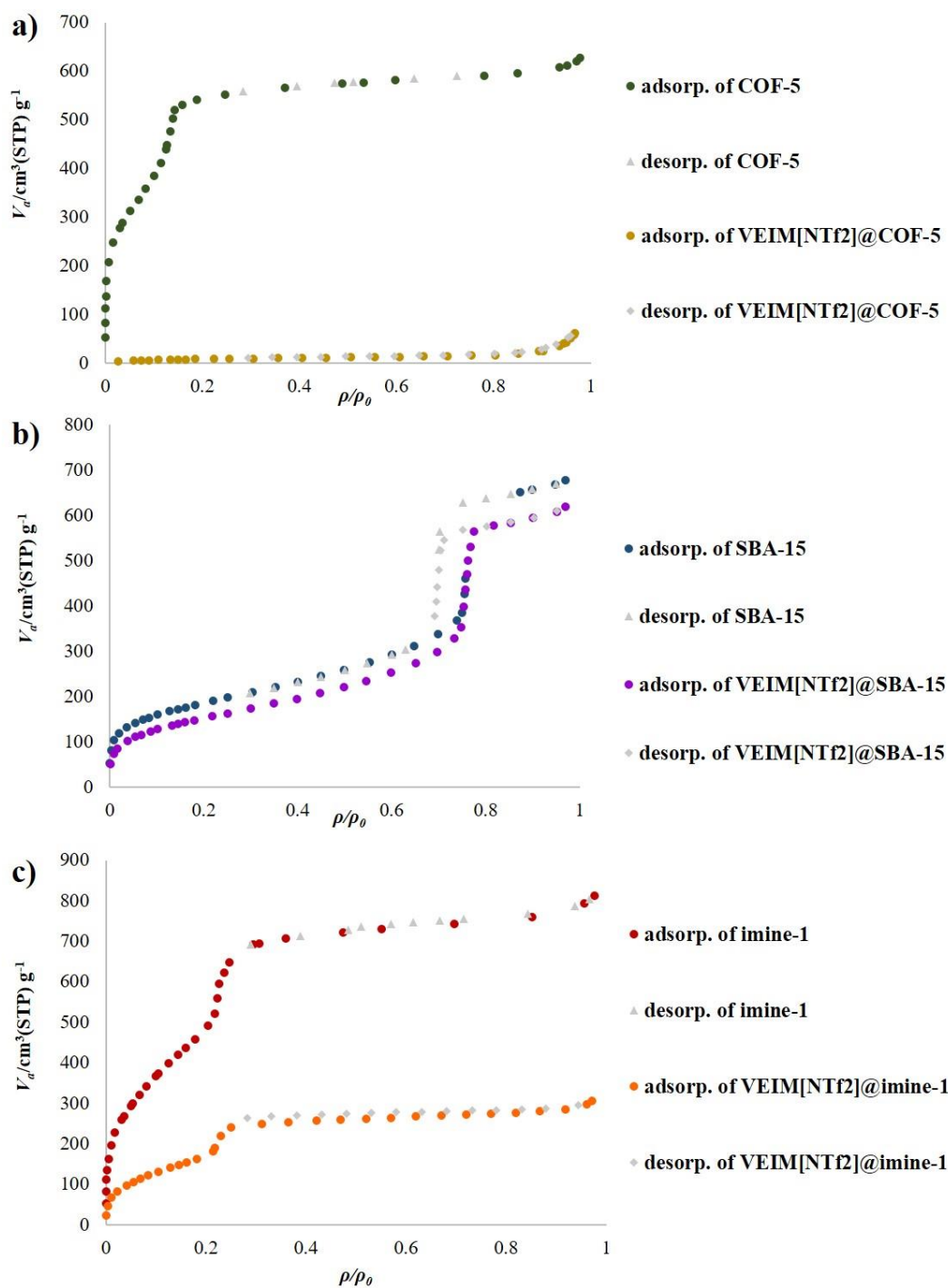
Figure A8 N₂ adsorption-desorption isotherm of infiltrated materials of VEIM[NTf₂]: a) COF-5 series, b) SBA-15 series and c) imine-1 series.
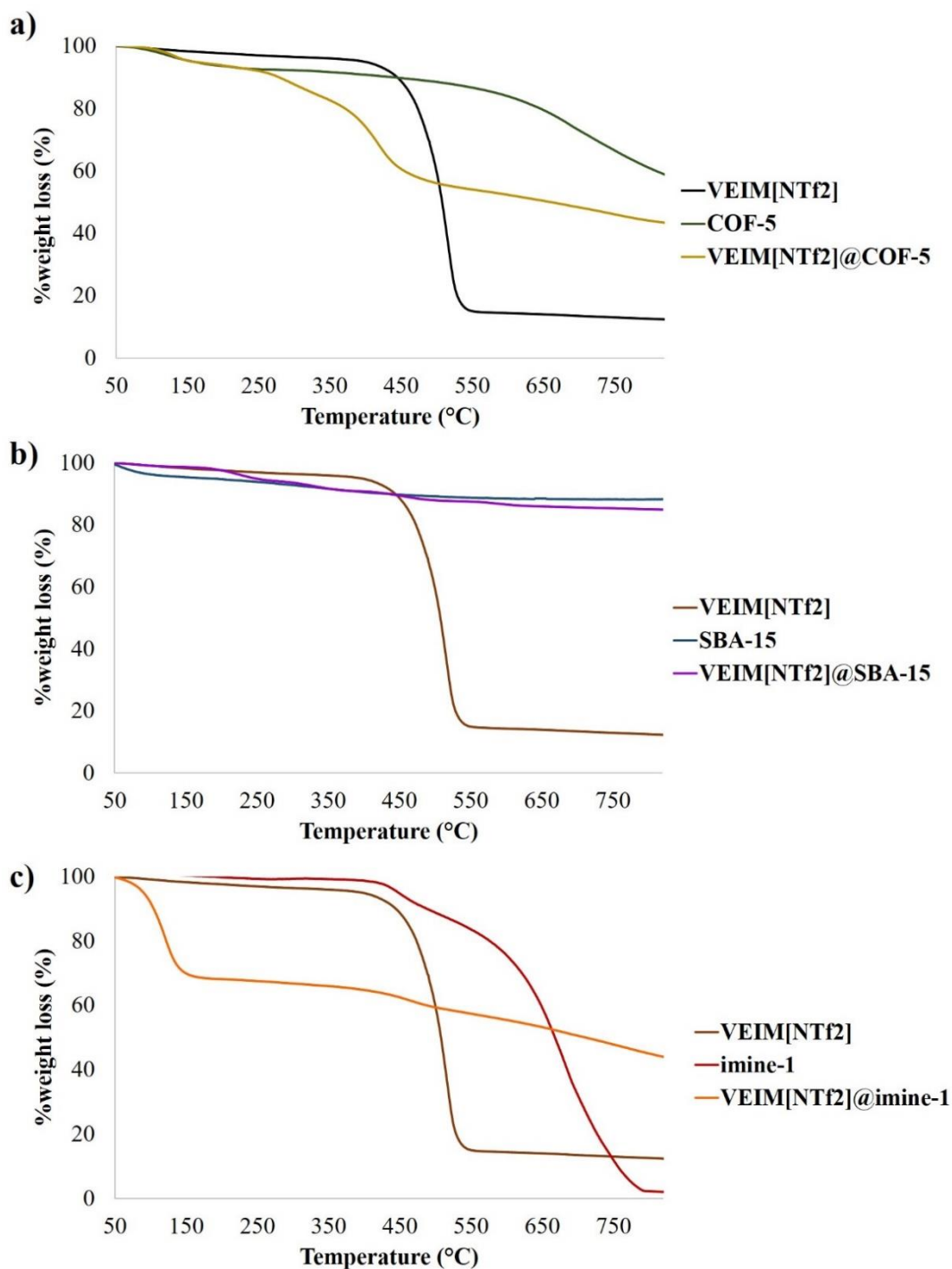
Figure A9 TGA profiles of the pristine materials and hybrid materials: a) VEIM[NTf$_2$] and COF-5 series, b) VEIM[NTf$_2$] and SBA-15 series and c) VEIM[NTf$_2$] and imine-1 series.

REFERENCES

[1]   Slater, A.G., and Cooper, A.I. Function-led design of new porous materials. Science 348 (2015).

[2]   Zdravkov, B., Čermák, J., Šefara, M., and Janků, J. Pore classification in the characterization of porous materials: A perspective. Open Chemistry 5 (2007).

[3]   P. A. Wright. Chapter 1 Introduction in Microporous Framework Solids, Royal Society of Chemistry, Cambridge, 1 (2008).

[4]   Bacakova, L., Vandrovcova, M., Kopova, I., and Jirka, I. Applications of zeolites in biotechnology and medicine – a review. Biomaterials Science 6 (2018).

[5]   Zhou, H.-C., Long, J.R., and Yaghi, O.M. Introduction to Metal–Organic Frameworks. Chemical Reviews 112 (2012).

[6]   Huang, N., Wang, P., and Jiang, D. Covalent organic frameworks: a materials platform for structural and functional designs. Nature Reviews Materials 1 (2016).

[7]   Côté, A.P., Benin, A.I., Ockwig, N.W., Keeffe, M., Matzger, A.J., and Yaghi, O.M. Porous, Crystalline, Covalent Organic Frameworks. Science 310 (2005).

[8]   Furukawa, H., and Yaghi, O.M. Storage of Hydrogen, Methane, and Carbon Dioxide in Highly Porous Covalent Organic Frameworks for Clean Energy Applications. Journal of the American Chemical Society 131 (2009).

[9]   Peng, Y., et al. Synthesis of a Sulfonated Two-Dimensional Covalent Organic Framework as an Efficient Solid Acid Catalyst for Biobased Chemical Conversion. ChemSusChem 8 (2015).

[10]   Zhang, Y., and Ying, J.Y. Main-Chain Organic Frameworks with Advanced Catalytic Functionalities. ACS Catalysis 5 (2015).

[11]   Fan, Q., Gottfried, J.M., and Zhu, J. Surface-catalyzed C-C covalent coupling strategies toward the synthesis of low-dimensional carbon-based nanostructures. Accounts of Chemical Research 48 (2015).

[12]   Ding, S.Y., et al. Thioether-Based Fluorescent Covalent Organic Framework for Selective Detection and Facile Removal of Mercury(II). Journal of the American Chemical Society 138 (2016).

[13] Bao, T., Tang, P., Kong, D., Mao, Z., and Chen, Z. Polydopamine-supported immobilization of covalent-organic framework-5 in capillary as stationary phase for electrochromatographic separation. <u>Journal of Chromatography A</u> 1445 (2016).

[14] Ma, L., Wang, S., Feng, X., and Wang, B. Recent advances of covalent organic frameworks in electronic and optical applications. <u>Chinese Chemical Letters</u> (2016).

[15] Wan, S., Guo, J., Kim, J., Ihee, H., and Jiang, D. A Photoconductive Covalent Organic Framework: Self-Condensed Arene Cubes Composed of Eclipsed 2D Polypyrene Sheets for Photocurrent Generation. <u>Angewandte Chemie International Edition</u> 48 (2009).

[16] El-Kaderi, H.M., *et al*. Designed Synthesis of 3D Covalent Organic Frameworks. <u>Science</u> 316 (2007).

[17] Uribe-Romo, F.J., Hunt, J.R., Furukawa, H., Klöck, C., O'Keeffe, M., and Yaghi, O.M. A Crystalline Imine-Linked 3-D Porous Covalent Organic Framework. <u>Journal of the American Chemical Society</u> 131 (2009).

[18] Ding, S.-Y., and Wang, W. Covalent organic frameworks (COFs): from design to applications. <u>Chemical Society Reviews</u> 42 (2013).

[19] Ding, S.-Y., *et al*. Construction of Covalent Organic Framework for Catalysis: Pd/COF-LZU1 in Suzuki–Miyaura Coupling Reaction. <u>Journal of the American Chemical Society</u> 133 (2011).

[20] Kuhn, P., Antonietti, M., and Thomas, A. Porous, Covalent Triazine-Based Frameworks Prepared by Ionothermal Synthesis. <u>Angewandte Chemie International Edition</u> 47 (2008).

[21] Lanni, L.M., Tilford, R.W., Bharathy, M., and Lavigne, J.J. Enhanced Hydrolytic Stability of Self-Assembling Alkylated Two-Dimensional Covalent Organic Frameworks. <u>Journal of the American Chemical Society</u> 133 (2011).

[22] Nagai, A., *et al*. Pore surface engineering in covalent organic frameworks. <u>Nature Communications</u> 2 (2011).

[23] Bunck, D.N., and Dichtel, W.R. Postsynthetic functionalization of 3D covalent organic frameworks. <u>Chemical communications (Cambridge, England)</u> 49

(2013).

[24]   Guo, J., *et al*. Conjugated organic framework with three-dimensionally ordered stable structure and delocalized pi clouds. Nature Communications 4 (2013).

[25]   Wan, S., Guo, J., Kim, J., Ihee, H., and Jiang, D. A Belt-Shaped, Blue Luminescent, and Semiconducting Covalent Organic Framework. Angewandte Chemie International Edition 47 (2008).

[26]   Dogru, M., *et al*. A Photoconductive Thienothiophene-Based Covalent Organic Framework Showing Charge Transfer Towards Included Fullerene. Angewandte Chemie International Edition 52 (2013).

[27]   Zhi, Y., *et al*. Covalent organic frameworks: efficient, metal-free, heterogeneous organocatalysts for chemical fixation of CO_2 under mild conditions. Journal of Materials Chemistry A 6 (2018).

[28]   Zhang, S., Zhang, J., Zhang, Y., and Deng, Y. Nanoconfined Ionic Liquids. Chemical Reviews 117 (2017).

[29]   Khazaei, A., *et al*. {[MIM-NO2]C(NO2)3} a unique nano ionic liquid: application to the synthesis of novel Biginelli-type compounds. RSC Advances 6 (2016).

[30]   Ye, Y.-S., Rick, J., and Hwang, B.-J. Ionic liquid polymer electrolytes. Journal of Materials Chemistry A 1(2013).

[31]   Ueno, K., Tokuda, H., and Watanabe, M. Ionicity in ionic liquids: correlation with ionic structure and physicochemical properties. Physical Chemistry Chemical Physics 12 (2010).

[32]   Jain, N., Kumar, A., Chauhan, S., and Chauhan, S.M.S. Chemical and biochemical transformations in ionic liquids. Tetrahedron 61 (2005).

[33]   Wishart, J.F. Energy applications of ionic liquids. Energy & Environmental Science 2 (2009).

[34]   Lewandowski, A., and Świderska-Mocek, A. Ionic liquids as electrolytes for Li-ion batteries—An overview of electrochemical studies. Journal of Power Sources 194 (2009).

[35]   Galiński, M., Lewandowski, A., and Stępniak, I. Ionic liquids as electrolytes. Electrochimica Acta 51 (2006).

[36] van de Ven, E., Chairuna, A., Merle, G., Benito, S.P., Borneman, Z., and Nijmeijer, K. Ionic liquid doped polybenzimidazole membranes for high temperature Proton Exchange Membrane fuel cell applications. Journal of Power Sources 222 (2013).

[37] Hao, L., *et al*. Imidazolium-Based Ionic Liquids Catalyzed Formylation of Amines Using Carbon Dioxide and Phenylsilane at Room Temperature. ACS Catalysis 5 (2015).

[38] Yuan, J., and Antonietti, M. Poly(ionic liquid)s: Polymers expanding classical property profiles. Polymer 52 (2011).

[39] Cordella, D., *et al*. All Poly(ionic liquid)-Based Block Copolymers by Sequential Controlled Radical Copolymerization of Vinylimidazolium Monomers. Macromolecules 48 (2015).

[40] Cordella, D., *et al*. Direct Route to Well-Defined Poly(ionic liquid)s by Controlled Radical Polymerization in Water. ACS Macro Letters 3 (2014).

[41] Ghazali-Esfahani, S., *et al.* Cycloaddition of CO2 to epoxides catalyzed by imidazolium-based polymeric ionic liquids. Green Chemistry 15 (2013).

[42] Tarnacka, M., *et al*. Polymerization of Monomeric Ionic Liquid Confined within Uniaxial Alumina Pores as a New Way of Obtaining Materials with Enhanced Conductivity. ACS Applied Materials & Interfaces 8 (2016).

[43] Xin, Y., Wang, C., Wang, Y., Sun, J., and Gao, Y. Encapsulation of an ionic liquid into the nanopores of a 3D covalent organic framework. RSC Advances 7 (2017).

[44] Sun, Q., Aguila, B., Perman, J., Nguyen, N., and Ma, S. Flexibility Matters: Cooperative Active Sites in Covalent Organic Framework and Threaded Ionic Polymer. Journal of the American Chemical Society 138 (2016).

[45] Ding, M., and Jiang, H.-L. Incorporation of Imidazolium-Based Poly(ionic liquid)s into a Metal–Organic Framework for CO2 Capture and Conversion. ACS Catalysis 8 (2018).

[46] El Mourabit, S., Guillot, M., Toquer, G., Cambedouzou, J., Goettmann, F., and Grandjean, A. Stability of mesoporous silica under acidic conditions. RSC Advances 2 (2012).

[47] Zhao, D., *et al.* Triblock Copolymer Syntheses of Mesoporous Silica with Periodic 50 to 300 Angstrom Pores. Science 279 (1998).

[48] Smith, B.J., and Dichtel, W.R. Mechanistic Studies of Two-Dimensional Covalent Organic Frameworks Rapidly Polymerized from Initially Homogenous Conditions. Journal of the American Chemical Society 136 (2014).

[49] Tilford, R.W., Gemmill, W.R., zur Loye, H.-C., and Lavigne, J.J. Facile Synthesis of a Highly Crystalline, Covalently Linked Porous Boronate Network. Chemistry of Materials 18 (2006).

[50] Zhao, Y.-C., Zhang, L.-M., Wang, T., and Han, B.-H. Microporous organic polymers with acetal linkages: synthesis, characterization, and gas sorption properties. Polymer Chemistry 5 (2014).

[51] Peng, Y., *et al.* Room Temperature Batch and Continuous Flow Synthesis of Water-Stable Covalent Organic Frameworks (COFs). Chemistry of Materials 28 (2016).

[52] Smith, B.J., Overholts, A.C., Hwang, N., and Dichtel, W.R. Insight into the crystallization of amorphous imine-linked polymer networks to 2D covalent organic frameworks. Chemical communications (Cambridge, England) 52 (2016).

[53] Matsumoto, M., *et al.* Rapid, Low Temperature Formation of Imine-Linked Covalent Organic Frameworks Catalyzed by Metal Triflates. Journal of the American Chemical Society (2017).

[54] Smith, M.K., and Northrop, B.H. Vibrational Properties of Boroxine Anhydride and Boronate Ester Materials: Model Systems for the Diagnostic Characterization of Covalent Organic Frameworks. Chemistry of Materials 26 (2014).

[55] Yang, J., Hua, Z., Wang, T., Wu, B., Liu, G., and Zhang, G. Counterion-Specific Protein Adsorption on Polyelectrolyte Brushes. Langmuir 31 (2015).

[56] Nakamura, K., Saiwaki, T., Fukao, K., and Inoue, T. Viscoelastic Behavior of the Polymerized Ionic Liquid Poly(1-ethyl-3-vinylimidazolium bis(trifluoromethanesulfonylimide)). Macromolecules 44 (2011).

[57] Yang, S.-T., Kim, J., Cho, H.-Y., Kim, S., and Ahn, W.-S. Facile synthesis of

covalent organic frameworks COF-1 and COF-5 by sonochemical method. RSC Advances 2 (2012).

[58] Zwaneveld, N.A.A., *et al.* Organized Formation of 2D Extended Covalent Organic Frameworks at Surfaces. Journal of the American Chemical Society 130 (2008).

[59] Medina, D.D., *et al.* Room temperature synthesis of covalent-organic framework films through vapor-assisted conversion. Journal of the American Chemical Society 137 (2015).

[60] Huang, Y.-B., Pachfule, P., Sun, J.-K., and Xu, Q. From covalent–organic frameworks to hierarchically porous B-doped carbons: a molten-salt approach. Journal of Materials Chemistry A 4 (2016).

[61] Ritchie, L.K., Trewin, A., Reguera-Galan, A., Hasell, T., and Cooper, A.I. Synthesis of COF-5 using microwave irradiation and conventional solvothermal routes. Microporous and Mesoporous Materials 132 (2010).

[62] Neil L. Campbell, Rob Clowes, K., L., Ritchie, and Andrew I. Coope. Rapid Microwave Synthesis and Purification of Porous Covalent Organic Frameworks. Chemistry of Materials (2009).

[63] Calik, M., *et al.* From Highly Crystalline to Outer Surface-Functionalized Covalent Organic Frameworks—A Modulation Approach. Journal of the American Chemical Society 138 (2016).

[64] Gómez-Cazalilla, M., Mérida-Robles, J.M., Gurbani, A., Rodríguez-Castellón, E., and Jiménez-López, A. Characterization and acidic properties of Al-SBA-15 materials prepared by post-synthesis alumination of a low-cost ordered mesoporous silica. Journal of Solid State Chemistry 180 (2007).

[65] Lee, Y.-R., Chung, Y.-M., and Ahn, W.-S. A new site-isolated acid–base bifunctional metal–organic framework for one-pot tandem reaction. RSC Advances 4 (2014).

[66] Du, Y., *et al.* The effects of pyridine on the structure of B-COFs and the underlying mechanism. Journal of Materials Chemistry A (2013).

[67] Li, H., Li, H., Dai, Q., Li, H., and Brédas, J.-L. Hydrolytic Stability of Boronate Ester-Linked Covalent Organic Frameworks. Advanced Theory and Simulations

1 (2018).

[68] Liu, X.H., *et al.* On-surface synthesis of single-layered two-dimensional covalent organic frameworks *via* solid-vapor interface reactions. Journal of the American Chemical Society 135 (2013).

[69] Song, F., Zhang, H., Wang, D.-G., Chen, T., Yang, S., and Kuang, G.-C. Imine-linked porous organic polymers showing mesoporous microspheres architectures with tunable surface roughness. Journal of Polymer Science Part A: Polymer Chemistry 56 (2017).

[70] Böser, R., Haufe, L.C., Freytag, M., Jones, P.G., Hörner, G., and Frank, R. Completing the series of boron-nucleophilic cyanoborates: boryl anions of type NHC–B(CN)$_2$ $^-$. Chemical Science 8 (2017): 6274-6280.

[71] Zsuga, M., Kelen, T., and Borbély, J. Investigation of the mechanism of living cationic polymerization of isobutylene by ^{11}B NMR spectroscopy. Polymer Bulletin 26 (1991): 417-422.

[72] Sun, J., Zhou, X., and Lei, S. Host-guest architectures with a surface confined imine covalent organic framework as two-dimensional host networks. Chemical communications (Cambridge, England) 52 (2016).

[73] Liu, C., Zhang, W., Zeng, Q., and Lei, S. A Photoresponsive Surface Covalent Organic Framework: Surface-Confined Synthesis, Isomerization, and Controlled Guest Capture and Release. Chemistry 22 (2016).

[74] Cui, D., MacLeod, J.M., Ebrahimi, M., Perepichka, D.F., and Rosei, F. Solution and air stable host/guest architectures from a single layer covalent organic framework. Chemical communications (Cambridge, England) 51 (2015).

[75] Chen, L., *et al.* Photoelectric covalent organic frameworks: converting open lattices into ordered donor-acceptor heterojunctions. Journal of the American Chemical Society 136 (2014).

[76] Pachfule, P., Panda, M.K., Kandambeth, S., Shivaprasad, S.M., Díaz, D.D., and Banerjee, R. Multifunctional and robust covalent organic framework–nanoparticle hybrids. Journal of Materials Chemistry A 2 (2014).

[77] Tripathi, A.K., and Singh, R.K. Interface and core relaxation dynamics of IL molecules in nanopores of ordered mesoporous MCM-41: a dielectric

spectroscopy study. <u>RSC Advances</u> 6 (2016).

[78] dos Santos, S.M.L., Nogueira, K.A.B., de Souza Gama, M., Lima, J.D.F., da Silva Júnior, I.J., and de Azevedo, D.C.S. Synthesis and characterization of ordered mesoporous silica (SBA-15 and SBA-16) for adsorption of biomolecules. <u>Microporous and Mesoporous Materials</u> 180 (2013).

[79] García, J.C., *et al.* Selective adsorption of nitrogen compounds using silica-based mesoporous materials as a pretreatment for deep hydrodesulfurization. <u>Catalysis Today</u> 305 (2017).

[80] Xu, H., Gao, J., and Jiang, D. Stable, crystalline, porous, covalent organic frameworks as a platform for chiral organocatalysts. <u>Nature Chemistry</u> 7 (2015).

[81] Du, Y., *et al.* Experimental and computational studies of pyridine-assisted post-synthesis modified air stable covalent-organic frameworks. <u>Chemical communications (Cambridge, England)</u> 48 (2012).

[82] Aliev, S.B., Samsonenko, D.G., Maksimovskiy, E.A., Fedorovskaya, E.O., Sapchenko, S.A., and Fedin, V.P. Polyaniline-intercalated MIL-101: selective CO2 sorption and supercapacitor properties. <u>New Journal of Chemistry</u> 40 (2016).

[83] Uemura, T., Ono, Y., Kitagawa, K., and Kitagawa, S. Radical Polymerization of Vinyl Monomers in Porous Coordination Polymers: Nanochannel Size Effects on Reactivity, Molecular Weight, and Stereostructure. <u>Macromolecules</u> 41 (2008).

[84] Distefano, G., *et al.* Highly ordered alignment of a vinyl polymer by host-guest cross-polymerization. <u>Nature Chemistry</u> 5 (2013).

[85] Comotti, A., Bracco, S., Beretta, M., Perego, J., Gemmi, M., and Sozzani, P. Confined Polymerization in Highly Ordered Mesoporous Organosilicas. <u>Chemistry</u> 21 (2015).

[86] Uemura, T., Hiramatsu, D., Kubota, Y., Takata, M., and Kitagawa, S. Topotactic Linear Radical Polymerization of Divinylbenzenes in Porous Coordination Polymers. <u>Angewandte Chemie International Edition</u> 46 (2007).

[87] Efimova, A., Hubrig, G., and Schmidt, P. Thermal stability and crystallization behavior of imidazolium halide ionic liquids. <u>Thermochimica Acta</u> 573 (2013).

[88]   Sun, Y., *et al*. Facile Approach to Graft Ionic Liquid into MOF for Improving the Efficiency of CO_2 Chemical Fixation. <u>ACS Applied Materials & Interfaces</u> 10 (2018).

[89]   Dong, B., *et al.* Immobilization of ionic liquids to covalent organic frameworks for catalyzing the formylation of amines with CO_2 and phenylsilane. <u>Chemical communications (Cambridge, England)</u> 52 (2016).

[90]   Saptal, V., Shinde, D.B., Banerjee, R., and Bhanage, B.M. State-of-the-art catechol porphyrin COF catalyst for chemical fixation of carbon dioxide *via* cyclic carbonates and oxazolidinones. <u>Catalysis Science & Technology</u> 6 (2016).

VITA

NAME	RANIDA MALIYAEM
DATE OF BIRTH	23 September 1992
PLACE OF BIRTH	Bangkok, Thailand
INSTITUTIONS ATTENDED	Bachelor Degree of Science in Chemistry, Silpakorn University, Sanamchan campus, Nakhonpathom, Thailand. Master Degree of Science in Inorganic Chemistry, Chulalongkorn University, Bangkok, Thailand.
HOME ADDRESS	Samut Sakhon, Thailand
PUBLICATION	Poster presentation and proceeding, "HYBRID MATERIALS FROM COVALENT ORGANIC FRAMEWORKS AND IONIC LIQUIDS", were participated in the 24th PPC symposium on petroleum, petrochemicals, and polymers and The 9th research symposium on petrochemical and materials technology, June 5, 2018, Mandarin hotel, Bangkok, Thailand.

จุฬาลงกรณ์มหาวิทยาลัย
CHULALONGKORN UNIVERSITY